PRESSURE DROP ACROSS WOVEN SCREENS UNDER UNIFORM AND NONUNIFORM FLOW CONDITIONS

Final Report - Contract NAS8-28736

Prepared by:

Mike Ludewig
Satoaki Omori
Ganti L. Rao
School of Graduate Studies and Research
The University of Alabama in Huntsville
Huntsville, Alabama 35807

Prepared for:
George C. Marshall Space Flight Center
National Aeronautics and Space Administration
Marshall Space Flight Center, Alabama 35812

October 1974

(NASA-CR-120559) PRESSURE DROP ACROSS WOVEN SCREENS UNDER UNIFORM AND NONUNIFORM FLOW CONDITIONS Final Report (Alabama Univ., Huntsville.) 143 p HC $5.75 CSCL 20D G3/34
N75-14067
Unclas 06454

PRESSURE DROP ACROSS WOVEN SCREENS UNDER UNIFORM AND NONUNIFORM FLOW CONDITIONS

Final Report - Contract NAS8-28736

Prepared by:

Mike Ludewig
Satoaki Omori
Ganti L. Rao
School of Graduate Studies and Research
The University of Alabama in Huntsville
Huntsville, Alabama 35807

Prepared for:
George C. Marshall Space Flight Center
National Aeronautics and Space Administration
Marshall Space Flight Center, Alabama 35812

October 1974

TABLE OF CONTENTS

ACKNOWLEDGEMENT

The authors wish to acknolwedge Mr. Steve Allums, of NASA/Marshall Space Flight Center, for his helpful discussions and interest shown in the study. We would also like to acknowledge the help of Mr. Ramesh Shangvi, a laboratory assistant, and to Mrs. Carol Holladay for the typing of this manuscript.

DEFINITION OF SYMBOLS

Symbol	Definition	Units
a	surface area to unit volume ratio of screen wire (defined in Ref. 2)	cm^{-1}
A	area	cm^2
A'	actual area open to flow, $A\varepsilon$	cm^2
A_1, A_2	empirically determined constants (defined in Ref. 4)	dimensionless
A_c	constant, $A_1L/D_a{}^2g_c$ (defined in Ref. 4)	cm^{-1}
B	screen thickness (defined in Ref. 2)	cm
B_c	constant, A_2L/D_ag_c (defined in Ref. 4)	dimensionless
D	depth of channel	cm
D_a	characteristic pore size	cm
D_h	hydraulic radius (defined in Ref. 9)	cm
Eu	Euler number, $2\Delta p/\rho V^2$	dimensionless
f	friction factor $\Delta p g_c \varepsilon^2 D/TB\rho V^2$ (defined in Ref. 2)	dimensionless
F	parameter, $fH/4D_h$ (defined in Ref. 9)	dimensionless
g	acceleration due to gravity	cm/sec^2
g_c	conversion constant, e.g., $32.174 \frac{lb_m ft}{lb_f sec^2}$	depends on system of units used
H	channel length (defined in Ref. 9)	cm
K	constant, $2LA_1/D_a$ (defined in Ref. 8)	dimensionless
K_o	screen parameter, $\Delta p/V$	$gm/cm^2 sec$
L	channel width (definition in Ref. 9)	cm

Symbol	Definition	Units
O_p	fraction of area open to flow (defined in Ref. 1)	dimensionless
Δp	screen pressure drop	$gm/cm.sec^2$
Q	mass flow rate (defined in Ref. 9)	gm/sec
Q´	volumetric flow rate	cm^3/sec
Re	Reynolds number, $\frac{\rho V}{\mu a^2 D}$ (defined in Ref. 2)	dimensionless
Re_a	Reynolds number, $D_a V\rho/\mu$	dimensionless
S	solidity, $1 - O_p$ (defined in Ref.1)	dimensionless
T	tortuosity factor (defined in Ref. 2)	dimensionless
u	fluid velocity in x-direction	cm/sec
V	screen approach velocity $\frac{Q'}{A}$	cm/sec
V_e	entering screen velocity, $\frac{Q'}{A\varepsilon}$	cm/sec
x,y	Cartesian-coordinate distances	cm
Z	length, X/H (defined in Ref. 9)	dimensionless
α	viscous coefficient (defined in Ref. 2)	dimensionless
β	inertial coefficient (defined in Ref. 2)	dimensionless
ε	screen void fraction (defined in Ref. 2)	dimensionless
η	constant	dimensionless
μ	fluid viscosity	centipose
ν	fluid kinematic viscosity	cm^2/sec
ρ	fluid density	gm/cm^3
ϕ	parameter, $2QH/D^2LK_o$ (defined in Ref. 9)	dimensionless

Symbol	Definition
–	denotes average value when placed above symbol, e.g. $\bar{V}$ is average velocity
*	denotes dimensionless quantity, e.g. V* is the dimensionless velocity.
GDCD	Convair Division of General Dynamics
MDAC	McDonnell Douglas Astronautics Company
NRSD	North American Rockwell Space Division

CHAPTER I

INTRODUCTION

The purpose of the present investigation is to gather experimental pressure drop and velocity data for woven screens.

Previous investigators have presented correlations for predicting pressure drop across woven screens. All correlations presented to date have been developed from "pipe flow" (i.e., circular) configurations and data taken in those experiments. The present experimental investigation uses a rectangular channel configuration.

The report is divided into two major sections and an Appendix A and B.

Section I presents experimental data taken for three dutch twill screens (50 x 250, 200 x 600, and 325 x 2300) and two square weave screens (200 x 200, and 325 x 325) using tap water as the test liquid. Pressure drop measurements were made at four locations in a rectangular channel 8.89 cm long. In every case, no variation (for a given screen) in pressure drop at the four locations was measured. The data is presented as $\dot{\Delta p}$ versus $\overline{V}_e$ where $\overline{V}_e$ is the average entering velocity and is calculated by dividing the volumetric flow rate by the screen area open to flow. Existing data have been based upon an average approach velocity (volumetric flow rate divided by total screen area).

Section II presents experimental data for a 50 x 250 dutch twill screen using water in a modified experimental apparatus. The channel length is extended to a length of 29.16 cm to study the effect of pressure drop variation as a function of Z (dimensionless length along the screen).

Channel depth is made variable in order to study its effect upon pressure drop. Basic data is presented as Δp versus Z.

The equations of continuity and momentum for the present experimental model are presented in Appendix A. Also included in Appendix B, is a computer program listing of an extension of a McDonnell Douglas theoretical model and data from that computer program.

SECTION 1

PREDICTION OF PRESSURE DROP ACROSS WOVEN SCREENS

1-1 Previous Investigations

Several investigators have attempted to obtain empirical or analytical relations between the screen pressure drop and velocity. The correlations are based upon an average approach velocity normal to the screen (i.e., the volumetric flow rate divided by the total screen area) and screen parameters. The empirical equations below are predominant in the literature.

$$f = \frac{\alpha}{Re} + \beta \tag{1-1}$$

where f is the friction factor defined by $\dfrac{\Delta p \, g_c \, \varepsilon^2 \, D}{T \, B \, \rho \, \bar{V}^2}$

Re is the Reynolds number defined by $\dfrac{\rho \bar{V}}{\mu a^2 D}$

α, β are constants determined experimentally

$$Eu = \frac{2 \Delta p}{\rho \bar{V}^2} \tag{1-2}$$

where Eu is the Euler number and is defined in the following manner for square weave and dutch twill screens

$$Eu = \left[\frac{1 - O_p}{O_p}\right]^2 = \left[\frac{S}{1-S}\right]^2 \text{ for square weave screens.} \tag{1-3}$$

Equation (1-3) is the Hoerner equation (Ref. 1) where O_p is the fraction of area open to flow and S is the solidity.

$$Eu = \frac{\partial L}{D_a} \left[\frac{A_1}{Re_a} + A_2 \right] \text{for dutch twill screens} \tag{1-4}$$

where

L is the thickness of the screen

D_a is the characteristic pore size

A_1, A_2 are constants determined experimentally

Re_a is the Reynolds number based on D_a and defined as $D_a\bar{V}\rho/\mu$.

Equation (1-1) was developed by Armour and Cannon (Ref. 2) who modeled screens as a collection of submerged objects with surface area to unit volume ratio "a" for laminar flow and as a bundle of tubes of diameter D for turbulent flow. Pressure drop data for the flow of gaseous nitrogen and helium through plain square, full twill, fourdrinier, plain dutch, and dutch twill screens were used to derive coefficients of $\alpha = 8.61$ and $\beta = 0.52$. An illustration of the types of screens is shown in Figure (1-1).

Other investigators have arranged their data in the form of the Armour-Cannon correlation. McDonnell Douglas Astronautics Corporation (MDAC), using GN_2 and He as test fluids, presented data on three dutch twill screens as shown in Figure (1-2) (Ref. 3)*. Their data points for the friction factor, f, were lower than the Armour Cannon correlation (generally by a factor of 2 for each Reynolds number; however, the correlation was successful in aligning the data points for the three dutch twill screens.

* Ref. 3, Fig. 33, p. 76.

General Dynamics Convair Division (GDCD) tested the following six dutch twill screens in 1969 (Ref. 4):

- 80 x 700
- 165 x 800
- 150 x 700
- 30 x 250
- 50 x 250
- 20 x 250

using GH_2 and GN_2 as test fluids. They compared the results of those tests with previous test data taken in 1968 on three other dutch twill screens and one square weave screen (Ref. 5):

- 200 x 1400
- 165 x 1400 (Dutch Screen)
- 200 x 600
- 20 x 20 (Square Screen)

using GHe, LH_2, GH_2, LH_2, GN_2, tap water, and distilled water as test fluids. Their results of friction factor, f, as shown in Figure (1-3)* were also below the Armour-Cannon correlation, and they found that the data could best be represented by the equation;

$$f = \frac{2.49}{Re} + 0.3 \qquad (1\text{-}5)$$

Some of the most recent work in measurements of pressure drop across

*Ref. 4, Fig. 217, p. 2-12.

woven screens has been performed by Martin-Marietta of Denver (Ref. 6) using four dutch twill screens:

- 375 x 2300
- 325 x 2300
- 250 x 1370
- 200 x 1400

with GN_2 as a test fluid. Their resulting data, as shown in Figure (1-4)*, lie above the Armour-Cannon correlation for Reynolds number less than 10^{-2} and between the Armour-Cannon correlation and the MDAC test data for Reynolds number in the range $10^{-2} < Re < 1.0$.

Information in the paragraphs above is summarized in Table I-1 and Figure (1-5).

*Ref. 6, Figure II-38, p. II-60.

Equations (1-2) and (1-4) were developed by GDCD (Ref. 7) after examination of their data arranged in the form $f = \alpha/Re + \beta$. They noticed that considerable error could arise in attempting to use a single correlation for all screens. GDCD, therefore, proposed that the most accurate way to arrange the data was as follows:

$$\Delta p = \frac{A_1 L \mu}{D_a^2 g_c} V + \frac{A_2 L \rho}{D_a g_c} V^2 \tag{1-6}$$

where Δp is the pressure drop across the screen

μ is the fluid molecular viscosity

ρ is the fluid density

g_c is the conversion constant needed if the "American engineering system" is used $\left(= 32.174 \frac{\text{lbm. ft.}}{\text{lb}_f \text{ sec}^2}\right)$

V is the screen approach velocity

D_a, L, A_1, A_2 are as defined in equation (1-4).

Equation (1-6) is merely a rearrangement of Equation (1-4) using the definition $Eu = 2g_c\Delta p/\rho V^2$ and $Re_a = \rho V D_a/\mu$. Equation (1-6) may be further simplified in the following manner:

$$\Delta p = A_c \mu V + B_c \rho V^2$$

where $A_c = \dfrac{A_1 L}{D_a^2 g_c}$ and $B_c = \dfrac{A_2 L}{D_a g_c}$ * (1-7)

GDCD presents values of A_c, B_c, A_1, and A_2 in Table 2-2 of Reference 7. Values of the solidity S for square weave screen are presented in Table 2-3 of the same reference. It must be pointed out, however, that there

*A_c and B_c are referred to as A and B in Reference 7.

is a discrepancy in this data, as either A_1 or A_2 are not dimensionless or A_c and B_c are not in the units given in their paper. Tables 1-2 and 1-3* summarizes the values of A_c, B_c, A_1, A_2 and S.

North American Rockwell (Ref. 8) presented data for eleven screen materials, in the form given for equation (1-4) using liquid heptane as the test fluid. Over the range of Reynolds number tested, though, they found that their data could best be arranged by deleting the second term containing A_2 in equation (1-4). Letting $K = 2LA_1/D_a$, the equation $Eu = K/Re$ is obtained. Values of A and K are presented in Figure 1-6 †.

1-2 Experimental Equipment and Procedure

Experiments were conducted on 200 x 200 and 325 x 325 square weave screens and 50 x 250, 200 x 600, and 325 x 2300 dutch twill screens using tap water as the test fluid. A schematic drawing of the first experimental apparatus is shown in Figure 1-7, and the screen/channel assembly in Figures 1-8 , 1-9 and 1-10 .

The experimental assembly consisted of the following pieces of equipment:

(1) A centrifugal pump capable of producing outputs from 40 cc/sec to over 400 cc/sec.

(2) A filter system capable of 5 micron filtration. This was used to remove impurities from the tap water and to act as a "buffer" to dampen the pulsating output characteristic of a centrifugal pump.

---

*Ref. 7, Table 2-2 and 2-3, p. 2-14.
†Ref. 8, Figure 4.5, 4.4-2, p.

(3) A rotameter, as shown in Figure 1-11, calibrated with tap water over the range of 30 cc/sec to 150 cc/sec.

(4) A screen/channel assembly as shown in Figure 1-9, in which the screens listed above were set in place at location A. The channel itself was a standard 10.6 cm x 4.2 cm (4" x 1.647") channel size. A plexiglass tank, B, which was divided into two sections, sat on top of the channel, C , and inside screen mounting brackets, D, which were attached to the outside of the channel section (lower mounting bracket) and to the outside of the plexiglass tank (upper mounting bracket). Water flow was introduced into one side of the plexiglass tank which contained an overflow tube, E, and then overflowed into the second section of the tank, which was directly over the screen. The second section of the tank contained a flow straightener, F, parallel to the screen. The tank thus served two purposes -- the first section acted as a calming region for the inlet flow while maintaining a constant liquid head by means of the overflow tube, and the second section directed the flow perpendicular to the screen. Four sets of pressure taps were located in the screen mounting brackets directly above and below the screen.

(5) A manifold system, shown in Figure 1-12, consisting of four three-way stopcocks connected to a single outlet tube. With this system, it was possible to close off three sets of pressure taps, and by rotating the remaining, open stopcock between its two openings, to measure the pressure above and below the screen. In a similar manner (after closing the first

stopcock), each of the other stopcocks could be opened, one at a time, and pressure differentials could be measured at each of the other locations quickly and with sustained accuracy.

(6) An inclined tube manometer, shown in Figure 1-13, with a 0 to 4 inch scale was used. The test fluid itself was used as the manometer fluid.

(7) Other pieces of equipment (as shown in Fig. 1-7), including a water tank to furnish a liquid head for the pump, valves to regulate output and control liquid height in the tank above screen, and a 0^{o} to $40^{o}C$ thermometer graduated in tenths to measure the temperature of the water at steady state.

The procedure for an experimental measurement was as follows: A volumetric flow rate was chosen by adjusting the pump outlet control valve (see Figure 1-7). The pump was allowed to run at this output until steady state was achieved. Steady state was indicated by the constant temperature of the water, constant output of the pump as indicated by the rotameter, constant liquid head above the screen as measured by a ruler fixed to the side of the tank (this height was the same for all screen tested) and no fluxion (i.e., the same reading) in pressure drop across the screen. Once steady state was achieved, the pressure differential at the four locations was recorded. A new, lower volumetric flow rate was then chosen, and the above procedure repeated.

The upper volumetric flow rate was limited by the amount of flow a given screen would pass, while maintaining a constant fixed height above the screen with the outlet control valve wide open. Increasing the flow rate beyond that limit merely increased the liquid head above the screen to such a point that it would eventually overflow the tank.

The lower volumetric flow limit was fixed at the point at which the smallest scale pressure differential could be read (0.254 mm of water).

1-3 Experimental Results and Discussion

Pressure drop versus volumetric flow rate data were collected over the range of 40 cc/sec to 130 cc/sec for the five screens under test. In every case, no variation in pressure drop across the screen was measured at any of the four locations. Thus the local entering velocity and the average entering velocity were the same. An average entering velocity, $\bar{V}_e$ was calculated from the following relationship:

$$\bar{V}_e = \frac{Q'}{A'} = \frac{Q'}{A\varepsilon}^{*} \qquad (1-8)$$

where

Q' is the volumetric flow rate

A' is the actual area open to flow

A is the total screen area

ε is the screen void fraction.

The data collected during the test runs for the five screens are presented in Figures 1-14 through 1-17. It was found that the pressure drop Δp, was proportional to the average entering velocity, $\bar{V}_e$, in the present flow configuration (rectangular). Flow fields of previous investigators were in straight tubes or channels with screens pendicular to the flow

*Note that the present work at UAH uses V_e, which denotes a entering velocity, while previous investigations use V, which denotes a approach velocity. Thus $V_e = \frac{V}{\varepsilon}$.

direction.

Correlations of the present data against previous investigations have been made.

Figure 1-18 is a comparison of the present data for square weave screens with the Hoerner equation, $Eu = \left[\frac{S}{1-S}\right]^2$. Values of the solidity, S, were taken as 0.70 and 0.66 for the 325 x 325 and 200 x 200 mesh screens, respectively. The equation Eu = 5.44 represents the 325 x 325 mesh screen and Eu = 3.77 represents the 200 x 200 mesh screen. The experimental data, for both screens, lie below the Hoerner equation at high velocities and above the equation at the lower velocities. For the lower velocities, the slope of the Hoerner equation and that of the present data is nearly identical.

A comparison of the present data, for the three dutch twill screens tested, against equation (1-4), was not possibly due to the discrepancy (as mentioned previously) of the units of A_c and B_c or the values of A_1 and A_2 (given in Table 1-2 of this report). A comparison of the data for the 50 x 250 dutch twill screen with the North American Rockwell value of A_1 was not possible because they tested a plain dutch screen.

Present data (with the entering velocity changed to approach velocity for comparison with previous investigators) for the 50 x 250 and 325 x 2300 dutch twill screens are shown compared to works by previous investigators over the same Reynolds number range in Figure 1-19. No value of "a" was available in the literature for the 200 x 600 screen. Screen parameters such as ε, B, etc., available in the literature vary from source to source - those used in all calculations made for this report are given in Table 1-4.

The presently obtained plots are lower than any previously reported and are not linear. Two possible reasons are:

(1) Geometric; i.e., the present experimental apparatus is rectangular while previous investigations were "straight pipe flow" configurations. The Reynolds number as defined by Armour-Cannon and GDCD does not take into account the channel diameter (or hydraulic diameter in the case of a non-circular configuration) but rather a characteristic screen pore diameter D_a. Thus, Re, as defined, is independent of the type of geometric configuration, but it is doubtful that this is actually true.

(2) Previous data were obtained from gas flow analysis while the present experiment used water as the test fluid. For a gas such as GN_2, the kinematic viscosity is an order of magnitude larger than water, thereby shifting the Reynolds number of water to the right (i.e. $(Re)\ H_2O > (Re)\ GN_2$). Also for a gas, the friction factor would be less than that for water for the same Reynolds number. Thus, the present data viewed in light of previous gas data would

shift up and to the right, the exact magnitude being impossible to predict without simultaneous experimental comparison between gases and liquids.

The present data for the 50 x 250 and 325 x 2300 dutch twill screens present a different tendency from former investigations - an increase in the friction factor with increasing Reynolds number up to a certain Reynolds number for both screens. At low velocities, the pressure drop for a fluid such as water is extremely low; thus, the relationship between Δp and V causes the friction factor to rise for low V ($f \propto \Delta p/V^2$) and fall for high V. It can be considered that previous data for gases would show this tendency if velocities were low enough to obtain the small pressure differences measured in the present case. If the data are analyzed only in the region where f decreases for increasing Re, equation (1-1) satisfactorily aligns the present data points for the two dutch twill screens.

1-4 Recommendations for Future Work

Examination of the experimental results suggests two additional areas of study:

(1) Because of the geometric configuration of the present experimental apparatus, it is impossible for a given screen to obtain data over a wide Reynolds number range, as has been done in the previous "straight pipe-flow" experiments. With the exception of a very limited Reynolds number range, this prevents comparison of liquid data with a correlation of the form $f = \alpha/Re + \beta$, which can be applied to a gas flow. It is required, therefore, that fluids such as water and heptane should be used in "straight pipe-flow" apparatus with the dutch twill screens tested in this experiment

in order to compare the previous gas data with measured values of liquid. The result would be the extension of the Reynolds number range of liquids over that of formerly tested gases. It would allow comparison of the present data with MDAC (Ref.3) and GDCD (Ref.4) test data, and, finally, a comparison could be obtained for the same screens in different geometric configurations (i.e., rectangular and circular).

(2) For velocities, V_e, used in the present experiment (approximately $1 \rightarrow 5$ cm/sec), each dutch twill screen has a Reynolds number range of less than 10. New dutch twill screens could be chosen to cover Reynolds number range different from those tested in the present case [50 x 250, Re $0.6 \rightarrow 3$, 325 x 2300, Re $0.03 \rightarrow 0.06$]. This would accomplish three objectives:

- It would allow the "holes" in Reynolds number to be covered, thus providing a correlation of liquids which would be indicative of the whole Reynolds number range anticipated.
- It would furnish additional or new data on many dutch twill screens.
- It would allow a more complete correlation with previously collected gas data.

In addition, more experience would be gained in the improved design and use of rectangular-channel screen assemblies.

SECTION 2

VARIATION OF PRESSURE DROP ACROSS WOVEN SCREEN

2-1 Theoretical Analysis of Effect of Nonuniform Flow, McDonnell Douglas

Previous investigators have developed correlations to predict pressure drop across woven screens as a function of a uniform and average approach velocity (volumetric flow rate divided by screen area). However, the division of a fluid stream into parts by means of a screen is accompanied by pressure changes owing to friction and the change of fluid momentum. As a result, the pressure drop is not constant along a screen and may be considerably higher than that predicted by an equation based on an average approach velocity.

McDonnell Douglas (Ref. 9, Appendix A) considered the channel configuration shown in Figure 2-1.* The following equations were presented:

Continuity
$$V = D \frac{d_u}{d_x} \tag{2-1}$$

where V is the velocity normal to the screen

D is the channel depth

u is the velocity in the x-direction

Momentum
$$\frac{dp}{dx} + f \frac{\rho}{2D_h} u^2 + 2\rho u \frac{du}{dx} + \rho g = 0 \tag{2-2}$$

where p is the static pressure

f is the friction factor defined by Darcy's equation

D_h is the hydraulic radius

g is the acceleration due to gravity

ρ is the fluid density.

*Ref. 9, Fig. A-1, p. 92.

The flow loss through the screen was assumed to be

$$K_oV = p_o - \rho gx - p \tag{2-3}$$

where K_o is determined experimentally. Equation (2-3) is applicable for low velocity and in terms of the Armour-Cannon correlation is valid where $8.6/Re \gg 0.52$ (β, an inertial resistance coefficient, defined in equation (1-1), is negligible).

With the following boundary conditions and definitions, the three equations above are non-dimensionalized

B.C. (1) at $x = -H$ $u = 0$ (2-4)

B.C. (2) at $x = 0$ $Q = \rho LDu$ (2-5)

where H is the channel length

L is the channel width

Q is the mass flow rate

$$u^* = \frac{u}{u_{max}} = \frac{\rho uDL}{Q} \tag{2-6}$$

$$V^* = \frac{V}{V_{avg}} = \frac{\rho VLH}{Q} \tag{2-7}$$

$$Z = \frac{x + H}{H} \tag{2-8}$$

$$\Delta p^* = \frac{p_o - p}{\Delta p_{avg}} = \frac{(p_o - p)\ \rho LH}{K_oQ} \tag{2-9}$$

where the terms which contain asterisks are dimensionless and Z is the dimensionless length.

The three basic equations (2-1, 2-2, 2-3) become

$$V^* = \frac{du^*}{dZ} = \Delta p^* - \frac{\rho^2 LH^2 g}{K_o Q}(Z-1) \quad (2\text{-}10)$$

$$\frac{d(\Delta p^*)}{dZ} - \frac{fQH^2}{2D_h D^2 LK_o} u^{*2} - \frac{\rho^2 LH^2 g}{K_o Q} = \frac{2QH}{D^2 LK_o} u^* \frac{du^*}{dz} \quad (2\text{-}11)$$

which are combined into a single nonlinear equation

$$\frac{d^2u^*}{dZ^2} - F\,\phi\,u^{*2} - \phi\,u^* \frac{du^*}{dZ} = 0 \quad (2\text{-}12)$$

where $F = fH/4D_h$ and $\phi = 2QH/D^2LK_o$.

The boundary conditions are written as follows:

B.C.(1) at $Z = 0$ $u^* = 0$ (2-13)

B.C.(2) at $Z = 1$ $u^* = 1$ (2-14)

Equation (2-12), with the assumption that $F = 0$, is solved by McDonnell Douglas. The results are presented in Figure 2-2* as a plot of V^* versus ϕ. The figure shows that V^* at the ends of the channel begins to differ significantly from 1.0 at values of ϕ greater than 1.0. In other words, V is not the average approach velocity for $\phi > 1$ (for $\phi<1$, $V^* = \frac{V}{V_{avg}} \sim 1.0$).

2-2 Extension of McDonnell Douglas Analysis of Effect of Nonuniform Flow

McDonnell Douglas solved equation (2-12) with the assumption that $F = 0$. It was felt that the solution for equation (2-12) would be different by including a treatment of F, especially in the case of small channel depth, D, or high volumetric flow rate Q' (corresponding to high velocities V).

*Ref. 9, Fig. A-3, p. 98.

A computer program employing an implicit finite difference technique of Crank-Nicholson type was developed to solve equation (2-12) in this study. The computer program listing is included in Appendix B. The results of the calculations are shown in Figures 2-3 and 2-4 as plots of V* versus Ø at Z = 0 and Z = 1 with the friction factor in the x-direction, F , as a parameter. Other plots of V* versus Ø and V* versus Z with F as an independent parameter are presented in Appendix B.

A comparison of Figure 2-2 with Figures 2-3 and 2-4 reveals the fact that the effect of F is negligible in the range $F \leq 1.0$ and may be neglected as originally proposed by McDonnell Douglas.

2-3 Experimental Apparatus and Procedure

The experimental apparatus previously discussed in Section I-2 and illustrated in Figures 1-7 through 1-13 was modified to investigate the effect of nonuniform flow (nonuniform flow means that the local entering velocity, V_e, varies along the screen because of the accelerating effect of the velocity u which is parallel to the screen). The following changes were made:

(1) The channel length, H, was increased from the initial length of 8.89 cm to a new length of 29.16 cm.

(2) The channel depth was variable by the insertion of plexiglass spacers which reduced the depths of the channel from an original depth of 3.5 cm to new depths of 2.85 cm and 2.2 cm.

(3) A total of fourteen sets of pressure taps were located at the following positions where the origin x = 0 corresponds to the end of the

channel as shown in Figure 2-5.

Location	Distance x, cm	Dimensionless Distance $Z = \frac{x}{H}$
1	0.28	0.0096
2	1.79	0.06
3	5.95	0.20
4	9.08	0.31
5	10.69	0.37
6	12.32	0.42
7	13.97	0.48
8	15.53	0.53
9	19.56	0.67
10	21.17	0.73
11	22.76	0.78
12	24.37	0.84
13	27.18	0.93
14	28.67	0.98

(4) A new rotameter calibrated with water over a range of 100 cc/sec to 400 cc/sec was installed to allow higher volumetric flow rates Q'. This resulted in obtaining the same average entering velocity range, $\overline{V}_e$, in the modified set up as in the original experimental apparatus.

(5) A larger outlet was provided at the end of the channel to accommodate the higher volumetric flow rates.

All other pieces of equipment shown schematically in Figure 1-7 were retained. A photograph of the modified screen/channel assembly appears in Figure 2-6.

The experimental procedure used in the modified set-up was the same as described in section 1-2 with the following exceptions:

(1) Pressure drop measurements across the screen were taken over a volumetric flow rate range of 100 cc/sec to 400 cc/sec instead of 30 cc/sec to 150 cc/sec.

(2) Each volumetric flow rate chosen was repeated four times in order to measure the pressure drop at the fourteen locations (only four locations at a time could be measured with the manifold system shown in Figure 1-12).

2-4 Experimental Results

Data were taken for a 50 x 250 dutch twill screen using tap water in the modified experimental apparatus discussed in Section II-3. The volumetric flow rate, Q', was varied from 400 cc/sec to 100 cc/sec. The depth of the channel, D, was changed from 3.5 cm to new depths of 2.85 cm and 2.2 cm. The pressure drop across the screen was measured at the fourteen locations.

Figure 2-7 presents the pressure drop as a function of volumetric flow rate at the two ends of the channel ($Z = 0.01$ and $Z = 0.98$) for depths of 3.5 cm, 2.85 cm, and 2.2 cm. The effect of the channel depth, D, on the pressure drop, Δp, is considerable. At $Z = 0.98$ the channel depth plays a significant role in increasing the pressure drop for high volumetric flow rates (which induces the higher velocity u). At $Z = 0.01$ where the velocity u is almost negligible, the smaller channel depth reduces the pressure drop in contrast to the result at $Z = 0.98$.

Figure 2-8 presents the same pressure drop data, as in Figure 2-7, plotted against the average entering velocity $\overline{V}_e$. The average entering velocity is calculated from $\overline{V}_e = Q'/A\varepsilon$ where ε is the screen void fraction. Since the average entering velocity and the local entering velocity are not identical, Figure 2-7 is a more accurate representation of the data than Figure 2-8.

Figures 2-9 through 2-21 present the pressure drop as a function of the dimensionless length, Z, for different volumetric flow rates at depths of 3.5 cm and 2.2 cm.

Analysis of the data of Figures 2-7 through 2-21 yield the following:

(1) The average entering velocity, $\overline{V}_e$ and the local entering velocity, V_e, are considerably different at the higher volumetric flow rates ($Q' > 200 cm^3/sec$) and extreme end ($Z = 0.98$) of the channel. In terms of the McDonnell Douglas correlation, this means that both V^* and $\emptyset$ are greater than one.

(2) The relationship between Δp and $\overline{V}_e$ is no longer linear over the same average entering velocity range as studied in phase one of the experimental work (Section I-3).

(3) Pressure drop across the screen is a strong function of channel depth D. At the smallest depth of 2.2 cm, the pressure drop difference between the two extreme ends of the channel ($Z = 0.01$ and 0.98) is the greatest while at the largest depth of 3.5 cm, the difference between the two ends is the smallest. If the channel depth was increased to some finite value, the pressure drop difference between the ends of the channel would go to zero and then $\overline{V}_e$ and V_e would become identical.

2-5 Analysis of Experimental Data

2-5.1 McDonnell Douglas Correlation of V* versus Ø

The experimental data of Figure 2-8 were first plotted in the form of V* versus Ø in order to analyze the McDonnell Douglas theoretical model discussed in Section II-1. Results are presented in Figure 2-22; however, the parameters V* and Ø are modified in the following manner:

(1) V^* is based upon a fictitious velocity, not a local entering velocity; that is

$$V^*_{\text{at } Z} = \rho (V_e)_{\text{at } Z}\, LH/Q \tag{2-15}$$

where

$$(V_e)_{\text{at } Z} = \frac{\Delta p \text{ at } Z}{(K_o)_{avg}} \tag{2-16}$$

(2) Ø is based upon an average value of K_o; that is

$$\phi = \frac{2QH}{D^2 L (K_o)_{avg}} \tag{2-17}$$

$$\text{where } (K_o)_{avg} = \frac{(K_o)_{\text{at } Z=0} + (K_o)_{\text{at } Z=1}}{2} \tag{2-18}$$

Equation (2-18) is used in place of the original McDonnell Douglas definition,

$$K_o = \frac{p_o - \rho g X - p}{V} \tag{2-19}$$

Equation (2-19) implies a linear relationship between pressure and velocity; an inspection of Figure 2-8 shows that this is not the case. Therefore, equation (2-16) is used as the definition of K_o; that is, K_o is Δp at Z divided by V_e at Z and since Δp at Z varies as a function of Z, then K_o is a variable and a function of Δp at Z, V_e at Z, and Z.

V* and Ø in Figure 2-12 are calculated in the following manner.

(1) For a given volumetric flow rate, an average entering velocity is calculated.

(2) For the average entering velocity calculated in (1), Δp is read from Figure 2-8 at Z = 0.01 and Z = 0.98 and the value of K_o are calculated at Z = 0.01 and Z = 0.98. Than $(K_o)_{avg}$ is calculated by Equation (2-18).

(3) Once $(K_o)_{avg}$ is determined, V_e is calculated at Z = 0 and 1 (actually Z = 0.01 and 0.98) by equation (2-16). Then V* is calculated at Z = 0 and 1 by equation (2-15).

(4) $\emptyset$ is calculated by Equation (2-17) using $(K_o)_{avg}$ determined in step (2) above.

Thus, a given value of $\emptyset$ yield two values of V*, one at Z = 0 and Z = 1.

The results shown in Figure 2-22 follow the same trend as the McDonnell Douglas theoretical curve. However, the divergence of the curves for Z = 0 and Z = 1 at a given $\emptyset$ is not as great as predicted by theory. Finally, the plot in Figure 2-22 is based upon entering velocities not approach velocities; thus the curves converge to a value of approximately three instead of one. Since $V_e = V/\varepsilon$ and the void fraction for a 50 x 250 dutch twill screen is 0.325, Figure 2-22, if based upon approach velocity, would shift down to a value of approximately V* = 1.

Several points should be made about Figure 2-22, the calculation method used to determine V* and $\emptyset$, and the McDonnell Douglas theoretical model in general.

(1) The results of Figure 2-22 are encouraging in that the simple equation $\Delta p = K_oV$ may be used to predict the variation in pressure drop

as a function of Z. This is true because in the present measurement the local static pressure above the screen was almost uniform for a given volumetric flow rate and channel depth while the local static pressure below the screen varied in the Z-direction. This variation caused the pressure drop difference.

(2) The validity of the equations used is questioned. A linear relationship is used for Δp even when the actual relationship is quadratic. Also, a great deal of ambiguity exists in both the definition of K_o and the determination of its value. Finally, without recourse to an actual measured or calculated velocity profile, a fictitious velocity profile must be calculated.

(3) Realizing that the definitions employed for V* and $\emptyset$ are not those originally proposed by McDonnell Douglas we still feel that the data as presented in Figure 2-2 or Figure 2-22 are not a good way to predict the variations in pressure drop. Two reasons are proposed. First, the correlation is based upon the fact that the inertial contribution to the pressure drop is negligible. With this assumption, a linear relationship $\Delta p = K_o V + \rho g x$ (or $\Delta p = K_o$) is defined - this is perfectly valid since the viscous contribution is assumed to be the only contribution to the pressure drop. However, the present experimental data for the screens tested has shown that when a linear relationship exists between Δp and V, no discernible pressure difference can be measured. Thus the local velocity and average velocity are identical. As the pressure drop difference at Z = 0 and Z = 1 begins to differ significantly, the assumption that the inertial term is negligible

is no longer valid and the defining relationship for K_o should include a V^2 term. Second, even in the viscous range, when the defining relationship for K_o is valid, the question shall arise as to what value of K_o to use - a great deal of ambiguity exists for this term.

2-5.2 Determination of Velocity Profile

The equations of continuity and momentum are derived, in detail, for the present experimental apparatus in Appendix A. The equations are:

Continuity
$$Ve = \frac{D}{\varepsilon}\frac{du}{dx} \tag{2-21}$$

Momentum
$$\frac{dp}{dx} + \frac{f\rho u^2}{2D} + 3\,\rho u\frac{du}{dx} = 0 \tag{2-22}$$

Assuming that the second term of equation (2-22) can be neglected as noted in section 2.2, then equation (2-22) is written as

$$\frac{dp}{dx} + 3\,\rho u\frac{du}{dx} = 0 \tag{2-23}$$

Integrating equation(2-23) from zero to x

$$u(X) = \sqrt{\frac{2[\Delta p(x) - \Delta p(0)]}{3\rho}} \tag{2-24}$$

where at $x = H$, $u(H) = \dfrac{Q}{\rho LD}$ (2-25)

Now, using equation (2-24) and experiment data at $X = H$, $u(H)$ is calculated. The values of $u(H)$ calculated by equation (2-24) are compared with the values calculated by equation (2-25) which is exact. A correction is made to equation (2-24) so that the values calculated at $x = H$ agree closely with those calculated by equation (2-25). Thus equation (2-24) becomes

$$u(x) = 1.18\sqrt{\frac{\Delta p(x) - \Delta p(0)}{\rho}} \tag{2-26}$$

and is used for all subsequent calculations of the velocity u at location x.

The velocity, V_e, is now calculated from the continuity equation once du/dx has been determined from Figure 2-23.

Figures 2-23 and 2-24 show the velocity profiles u(x) and V_e versus Z for a 50 x 250 dutch twill screen in a channel of depth 2.2 cm.

By comparing V_e versus Z (Figure 2-24) and Δp versus Z (Figures 2-16 through 2-21) for D = 2.2 cm, Δp as a function of V_e is obtained. This is shown in Figure 2-25. The data, for low velocity, is nearly independent of the mass flow rate Q.

For practical calculations, a single line can be drawn through the data points as shown.

Based upon the single line of Figure 2-25, Euler number is plotted as a function of Reynolds Number in Figure 2-26. An empirical relationship between Eu and Re may be obtained from this figure.

2-5.3 . Determination of Average Properties from Local Data for 50 x 250 Dutch Twill Screen for Depths of 3.5 and 2.2 cm.

As most existing correlations are based upon the assumption of an average and uniform velocity, the present data were analyzed to determine the average pressure drop, $\overline{\Delta p}$, as a function of the average entering velocity, $\overline{V}_e$.

Figures 2-9 through 2-15 were integrated at each volumetric flow rate to determine $\overline{\Delta p}$. Each volumetric flow rate corresponded to an average entering velocity $\overline{V}_e$ ($\overline{V}_e = Q'/A\varepsilon$). Thus, Figures 2-27 and 2-28 present $\overline{\Delta p}$ versus $\overline{V}_e$ for depths of 3.5 cm and 2.2 cm, respectively.

Figure 2-29 presents the Euler number as a function of the Reynolds number based upon the average properties of Figures 2-27 and 2-28. At low Reynolds number, the Euler number is a function of the depth of the channel. As the Reynolds number increases, Eu becomes independent of channel depth.

Other dimensionless parameters, such as those shown in Figure 2-30, were investigated to see if the data for different channel depths, D, would conveniently clasp into one single curve. Figure 2-30 was found to be the best possible presentation which includes the depth, D, and channel length, H, as parameters.

2-6 Recommendations for Future Work

Based upon an analysis of the data of Section II , the following points are made and suggested for future study.

(1) Since only one available screen (50 x 250 dutch twill) and one liquid (water) were tested, it is obvious that other screens and liquids should be tested in the experimental apparatus discussed in Section II-3. Special attention should be paid to the viscous region where it appears that such parameters as Euler number are dependent upon channel depth.

(2) It is recommended that an approach to pressure drop prediction as discussed in Section II-1 be taken only as an approximation as any single correlation for all screens can not be accurate enough for detailed calculations. It is believed that the following equation is the most accurate way to represent the data for each single screen.

$$Eu = \frac{2L}{Da}\left[\frac{A1}{Re} + A_2\right] \qquad (2\text{-}27)$$

or in alternate form $\Delta p = A_c \rho \ V + \beta_c \ \mu \ V^2$ (2-28)

If further studies verify the fact that Eu is a function of channel depth in the viscous region, then equations (2-27) or (2-28) must either present value of A_c and B_c (or A_1 and A_2) as a function of depth or modify the definition of Reynolds number to include the effect. Based on the present work, it appears that equations (2-27) and (2-28) may be used in the inertial region without modification.

(3) If Equations (2-27) and (2-28) are to be used, an accurate determination of a velocity profile is needed. Accurate velocity profile should be measured for the screen tested (50 x 250) and others. The measured velocity profile for a 50 x 250 dutch twill screen should be compared with the calculated velocity profile (as described in II-5.2); if the two are in close agreement, then velocity profiles may be calculated from the following:

$$u(x) = \eta \frac{\Delta p(x) - \Delta p(0)}{\rho} \qquad (2\text{-}29)$$

where η is a constant

$$V_e = \frac{D}{\varepsilon} \frac{du}{dx} . \qquad (2\text{-}30)$$

REFERENCES

1. Hoerner, S. F., Fluid Dynamics Drag, (book published by author), 1958.

2. Armour, J. C., and J. N. Cannon, "Fluid Flow Through Woven Screens," AICHE Journal, Vol. 14, No. 3, May 1968.

3. Study and Design of a Cryogenic Propellant Acquisition System, Third Quarterly Report, MDC G2940, McDonnell Douglas Astronautics Co., April 15, 1972.

4. Blatt, M. H., K. R. Burton, and E. A. Evans, "Low Gravity Propellant Control Using Capillary Devices in Large Scale Cyrogenic Vehicles," Related IRAD Studies, GDC-DDB70-009, August 1970.

5. Blatt, et al.,"Low Gravity Propellant Control Using Capillary Devices in Large Scale Cyrogenic Vehicles," Second Quarterly Progress Report, report No. 584-4-269, Jan. 20, 1969.

6. Acquisition/Expulsion System for Earth Orbital Study System, Final Report, Contract NAS9-12182, Martin Marietta Corporation, June 1973.

7. "Low Gravity Propellant Control Using Capillary Devices in Large Scale Cyrogenic Vehicles," Related IRAD Studies, Contract NAS8-21465, General Dynamics/Convair, August 1970.

8. Schuartz, R., et al., Cyrogenic Acquisition and Transfer, Study 8, Contract NAS7-200, North American Rockwell/Space Division, December 21, 1971.

9. Study and Design of a Cyrogenic Propellant Acquisition System, First Quarterly Report, MDC G2562, McDonnell Douglas Astronautics Co., September 15, 1971.

LIST OF TABLES

TABLE I-1: SUMMARY OF RESULTS OF INVESTIGATORS

USING ARMOUR-CANNON TYPE CORRELATION

Investigators or Company	Equation Developed or Results	Screens Tested	Fluid Tested
Armour-Cannon (Ref. 2)	$f = \frac{8.61}{Re} + 0.52$	Too Numerous to List	GN_2, GHe
MDAC (Ref. 3)	No equation given; results below Armour-Cannon generally by a factor of two. Armour-Cannon correlation successful in aligning data points	250 x 1370 325 x 2300 200 x 1400	GN_2, GHe
GDCD (Ref. 4)	$f = \frac{2.49}{Re} + 0.3$	Six screens tested in 1969,	GH_2 GN_2
		Three screens tested in 1968,	Too numerous to list
Martin-Marietta (Ref. 6)	No equation given; results above Armour-Cannon correlation for $Re < 10^{-2}$ results between Armour-Cannon correlation and MDAC data for $10^{-2} < Re < 1$.	375 x 2300 325 x 2300 250 x 3700 200 x 1400	GN_2

Table I-2: Screen Geometry, Dutch Twill Screen

Screen Mesh	D_B Bubble Pt. Diameter (Microns)	D_A Avg. Capillary Dia. (Microns)	Thickness (in.)	Porosity (Meas.)	Dimensionless A_1	A_2	Wicking A_W	$A_c = \frac{A_1 L}{D_a^2 g_c}$	$B_c = \frac{A_2 L}{D_a g_c}$
200 × 1400	13.4	22.8*	0.0058	0.256	190	18		509687	3.61
165 × 1400	18.6	28.3*	0.0060	0.301	150	16	580	270185	2.68
200 × 600	19.05	36.7*	0.0055	0.347	52	3	368	51053	0.355
165 × 800	22.7	48.5**	0.0065	0.310	43	135		28568	14.3
150 × 700	22.7	60.8**	0.0070	0.171	500	133		227642	12.08
80 × 700	29.7	139.3**	0.0098	0.416	1000	34	6230	121427	1.89
50 × 250	33.9	129.5**	0.0127	0.325	115	191		20938	14.78
30 × 250	48.5	112.2**	0.0265	0.276	130	12	1120	65795	2.23
20 × 250	52.8	155.3**	0.0280	0.325	150	20		41869	2.84

*Microporosimeter
**Macroporosimeter

Table I-3: Screen Geometry, Square Weave Screens

Mesh	(Microns) D_B	Solidity S
400 × 400	38	0.64
325 × 325	44	0.70
200 × 200	74	0.66
150 × 150	104	0.63
100 × 100	140	0.698
80 × 80	180	0.686
50 × 50	280	0.700
40 × 40	440	0.640
20 × 20	860	0.538

TABLE I-4: GEOMETRIC PARAMETERS FOR WOVEN SCREENS

Screen	D_a, cm	B, cm	a, cm^{-1}	ε	T	S
200 x 200	-	-	-	-	-	0.66
325 x 325	-	-	-	-	-	0.70
50 x 250	12.95×10^{-3}	32.3×10^{-2}	151 cm^{-1}	0.325	1.3	-
200 x 600	3.67×10^{-3}	14×10^{-3}	-	0.347	1.3	-
325 x 2300	1.472×10^{-3}	8.9×10^{-3}	1102.3	0.245	1.3	-

The table below summarizes the changes in the experimental apparatus.

TABLE II-1: MODIFIED EXPERIMENTAL APPARATUS

Piece of Equipment	Modifications
Screen/Channel Assembly	(1) length H increased from 8.89 cm to 29.16 cm. (2) width L unchanged (8.89 cm) (3) depth D variable (3.5 cm, 2.85 cm, 2.2 cm) (4) number of pressure tap locations increased from four to fourteen (5) outlet increased in size
centrifugal pump filter inclined tube manometer control valves feed tank manifold system	none
screens	only 50 x 250 dutch twill screen used

LIST OF FIGURES

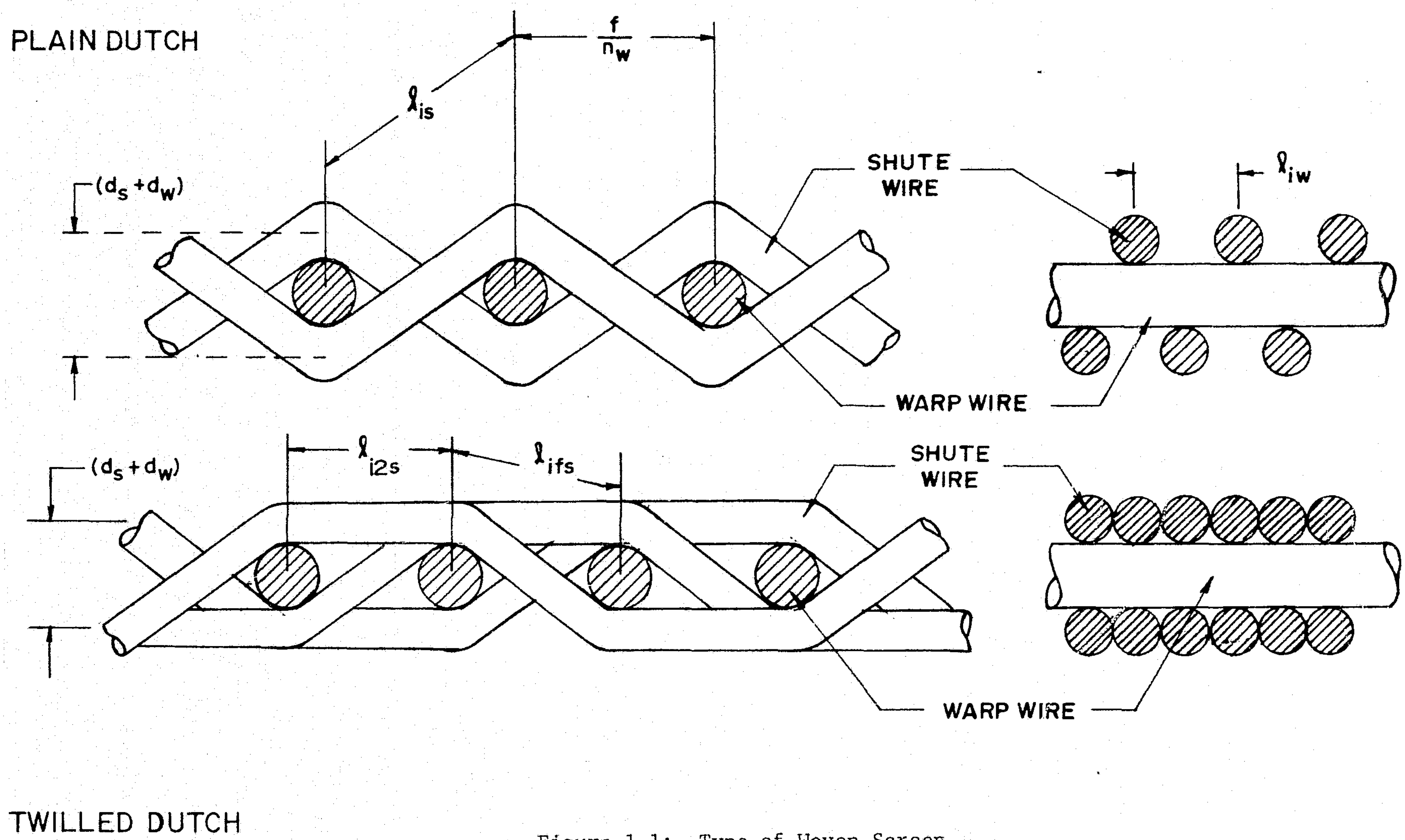

Figure 1-1: Type of Woven Screen

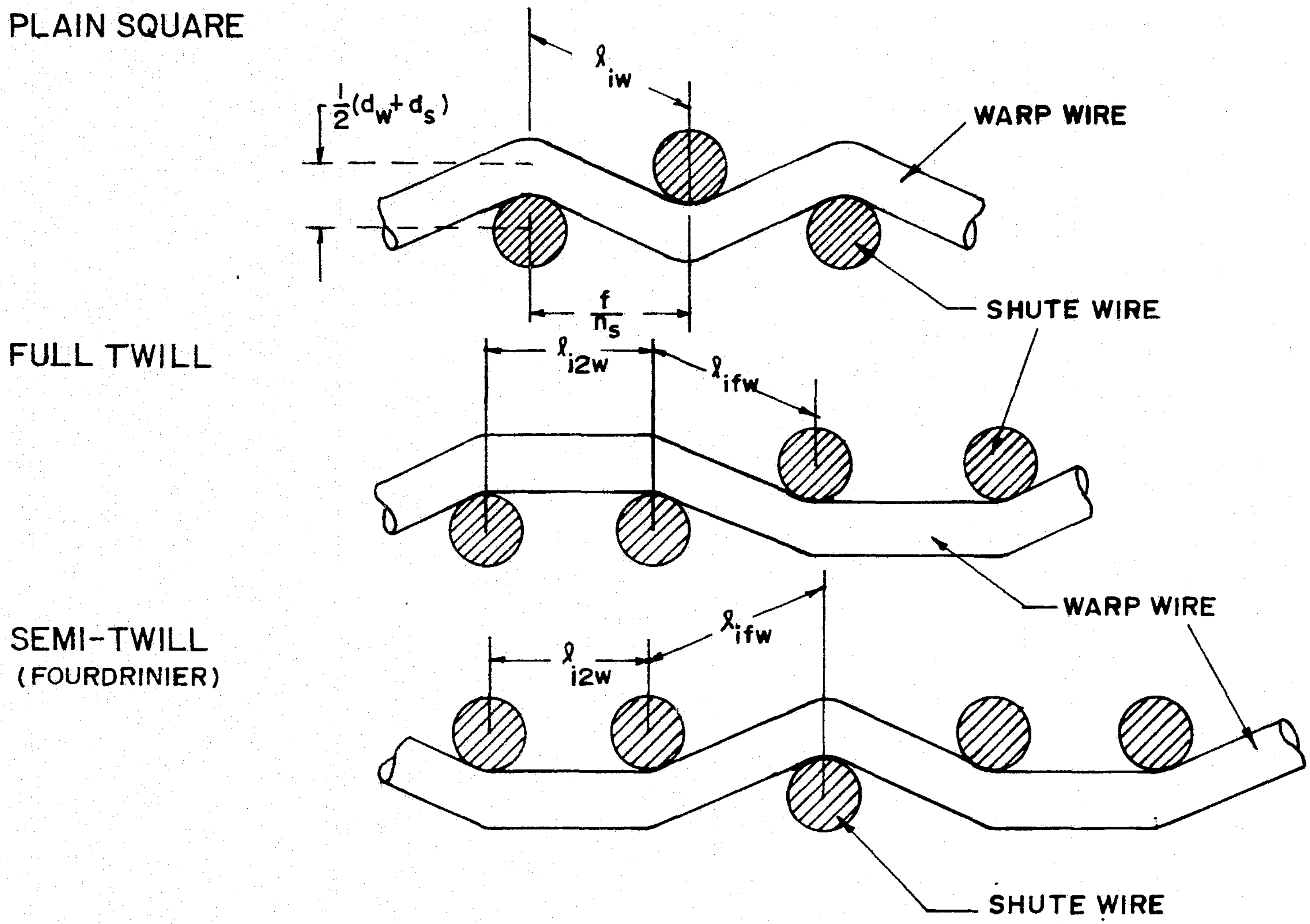

Figure 1-1: Type of Woven Screen

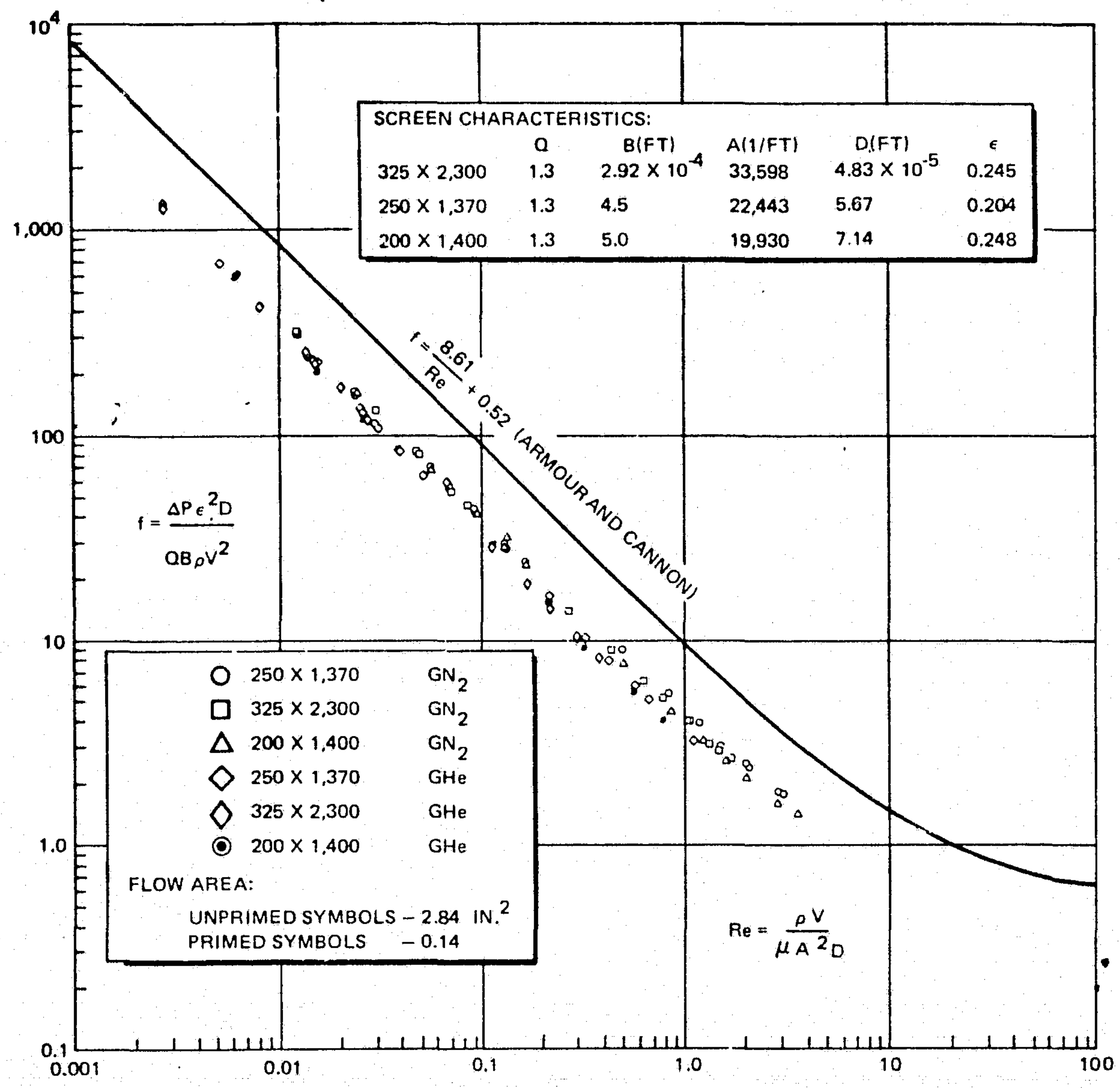

Figure 1-2 Comparison of MDAC Data with Armour-Cannon Correlation

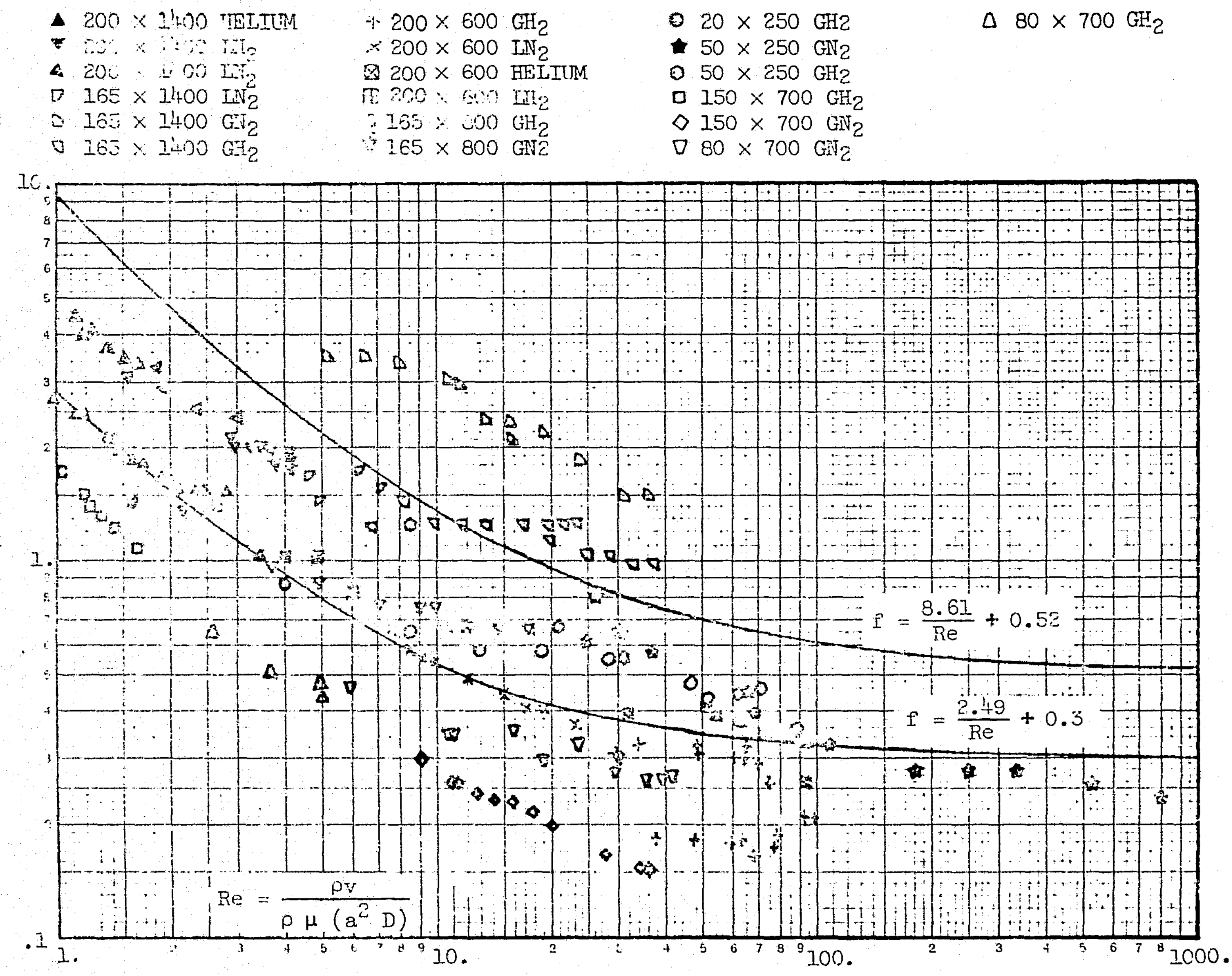

Figure 1-3 Comparison of GDCD Data with Armour-Cannon Correlation

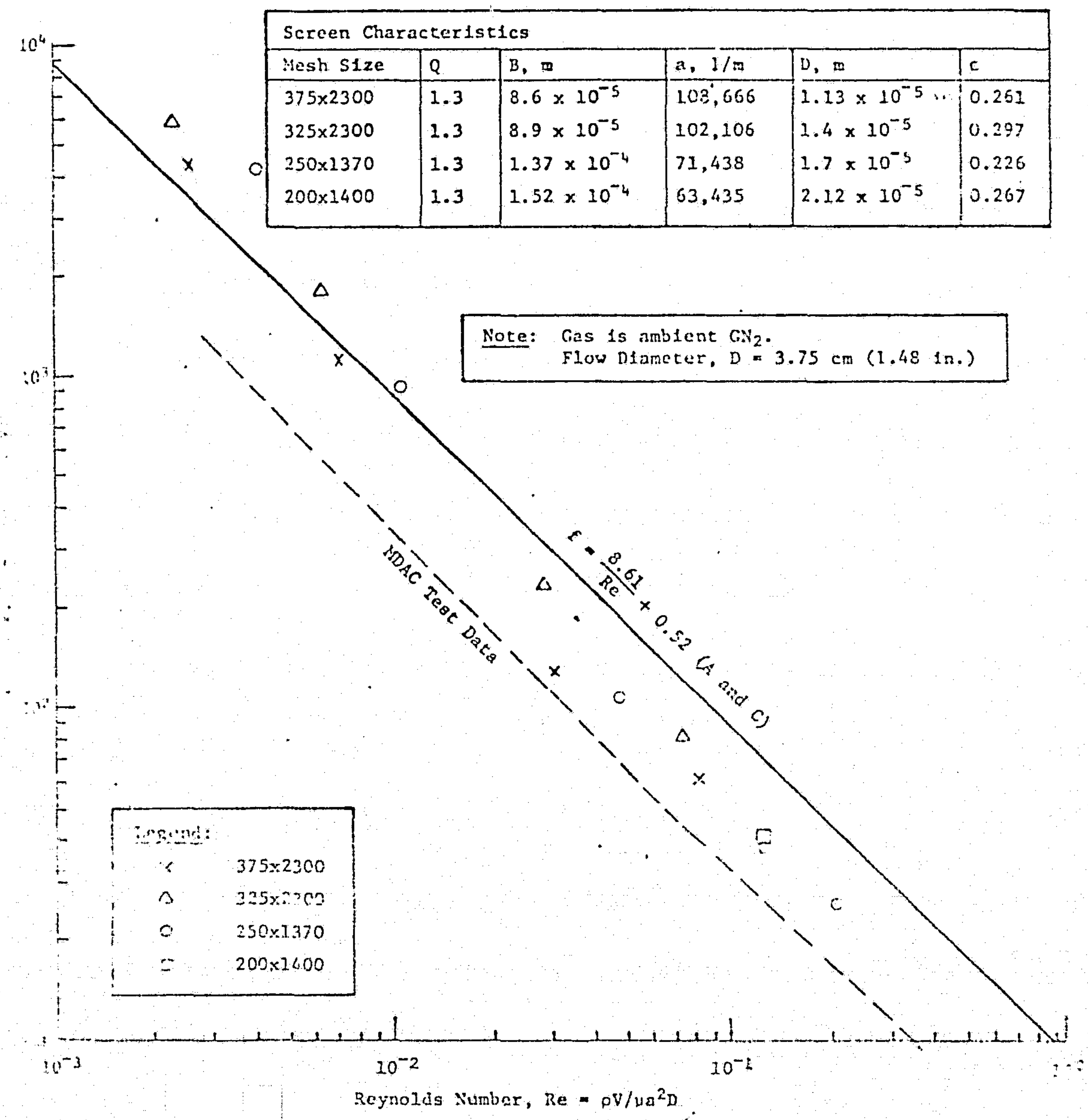

Screen Characteristics					
Mesh Size	Q	B, m	a, 1/m	D, m	c
375x2300	1.3	8.6×10^{-5}	108,666	1.13×10^{-5}	0.261
325x2300	1.3	8.9×10^{-5}	102,106	1.4×10^{-5}	0.297
250x1370	1.3	1.37×10^{-4}	71,438	1.7×10^{-5}	0.226
200x1400	1.3	1.52×10^{-4}	63,435	2.12×10^{-5}	0.267

Figure 1-4 Comparison of Martin Marietta Data with Armour-Cannon and MDAC Correlations

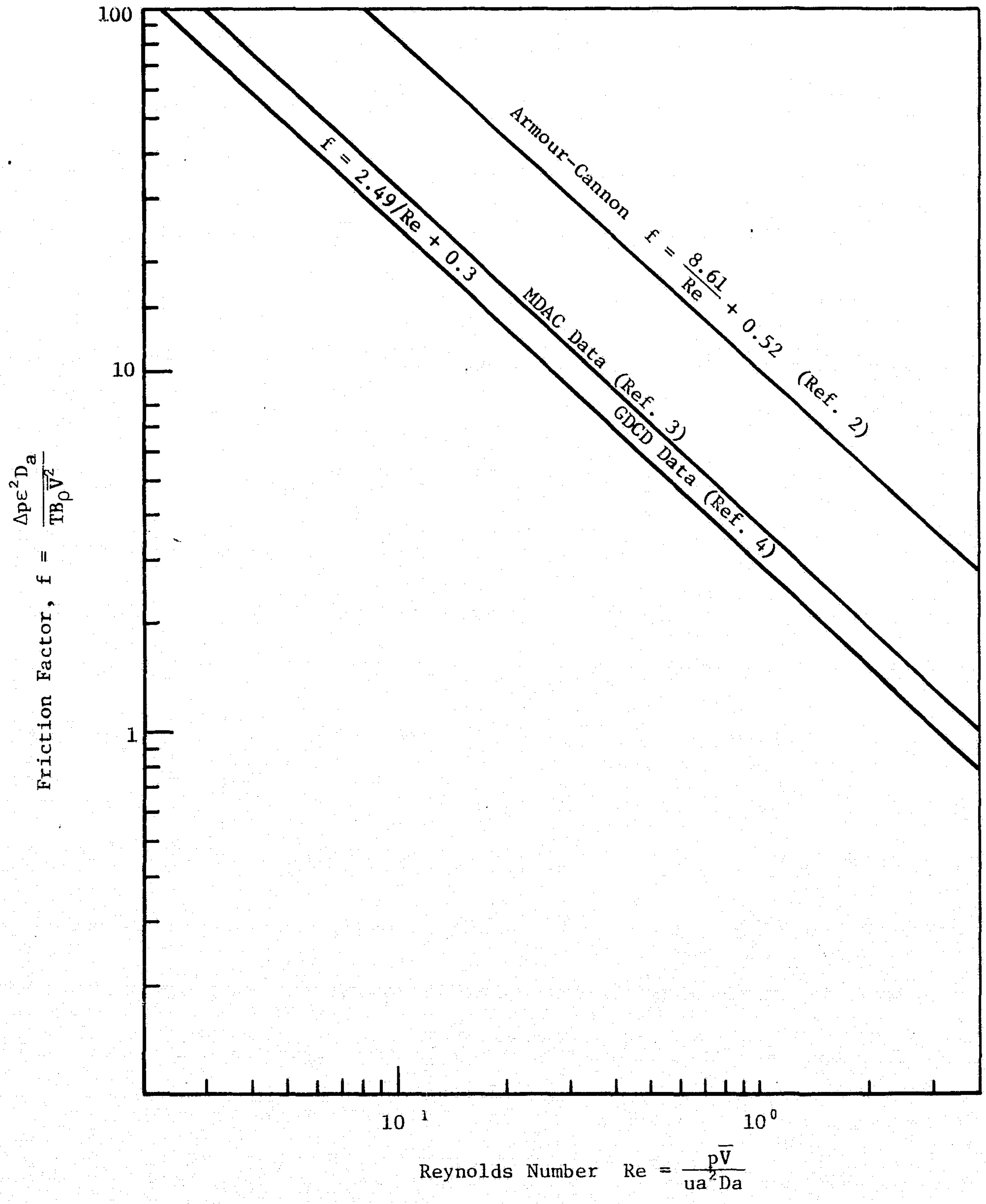

Figure 1-5 Summary of Previous Investigations Using Armour-Cannon Type Correlation

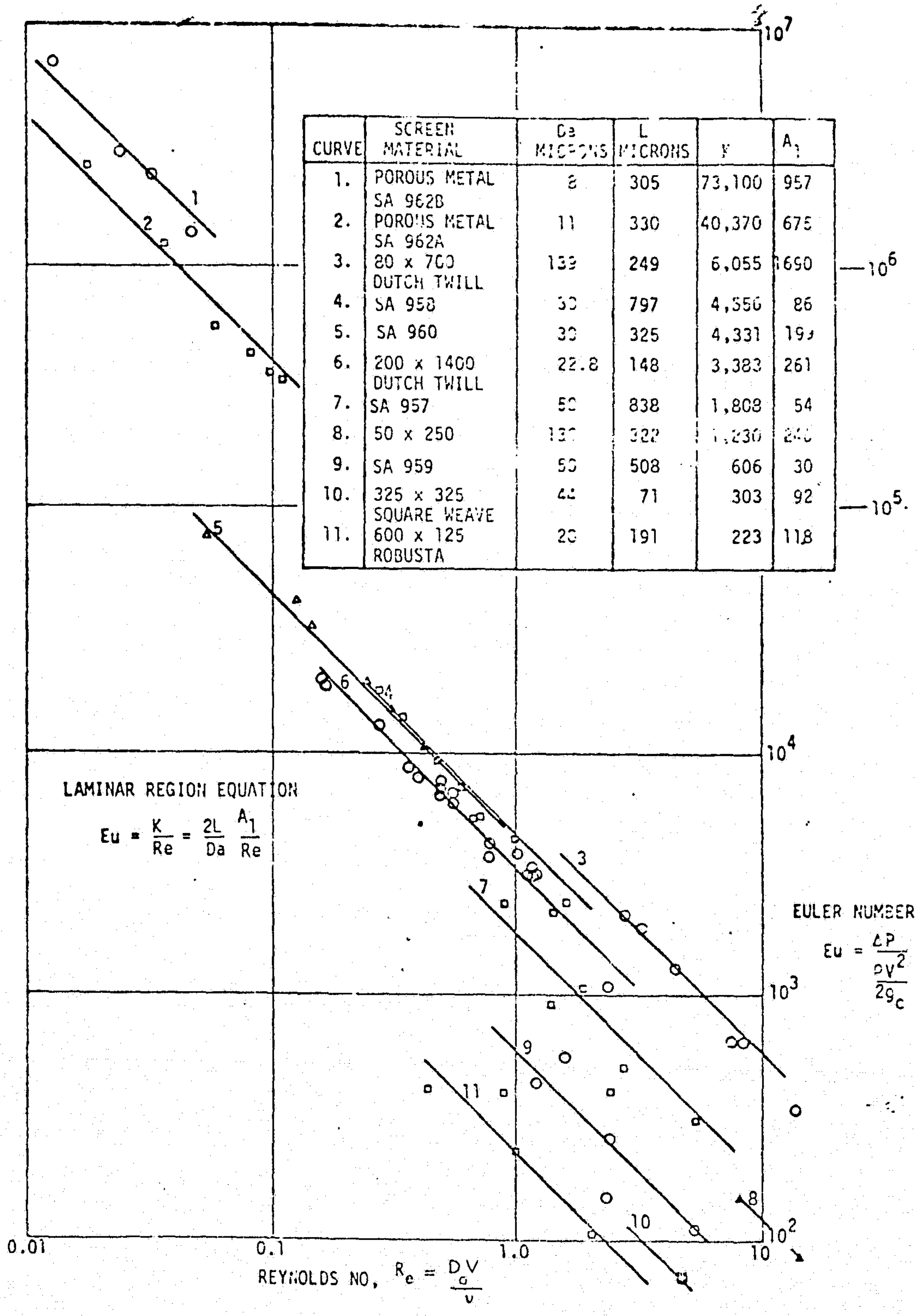

CURVE	SCREEN MATERIAL	Da MICRONS	L MICRONS	K	A_1
1.	POROUS METAL SA 962B	8	305	73,100	957
2.	POROUS METAL SA 962A	11	330	40,370	675
3.	80 x 700 DUTCH TWILL	139	249	6,055	1690
4.	SA 958	30	797	4,550	86
5.	SA 960	30	325	4,331	[illegible]
6.	200 x 1400 DUTCH TWILL	22.8	148	3,383	261
7.	SA 957	50	838	1,808	54
8.	50 x 250	[illegible]	[illegible]	[illegible]	[illegible]
9.	SA 959	50	508	606	30
10.	325 x 325 SQUARE WEAVE	44	71	303	92
11.	600 x 125 ROBUSTA	20	191	223	118

Figure 1-6 Euler Number Versus Reynolds Number, North American Rockwell Data

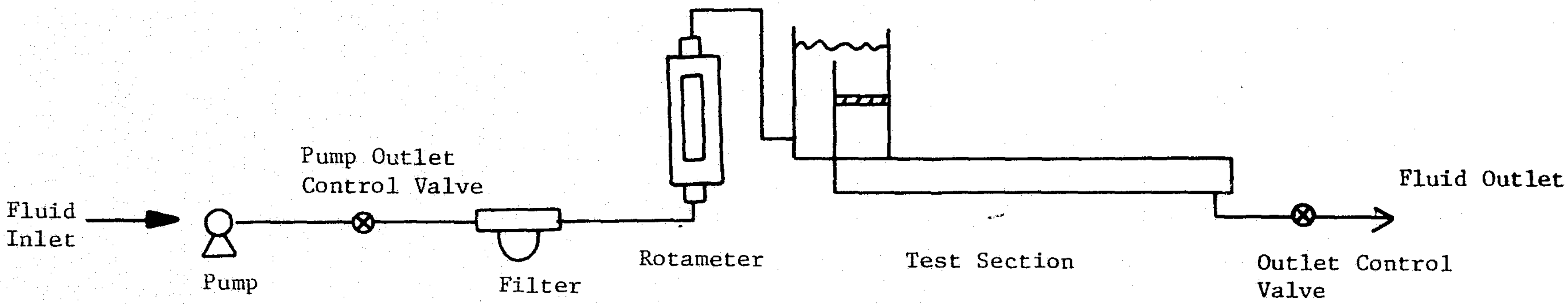

Figure 1-7. Schematic of Experimental Apparatus

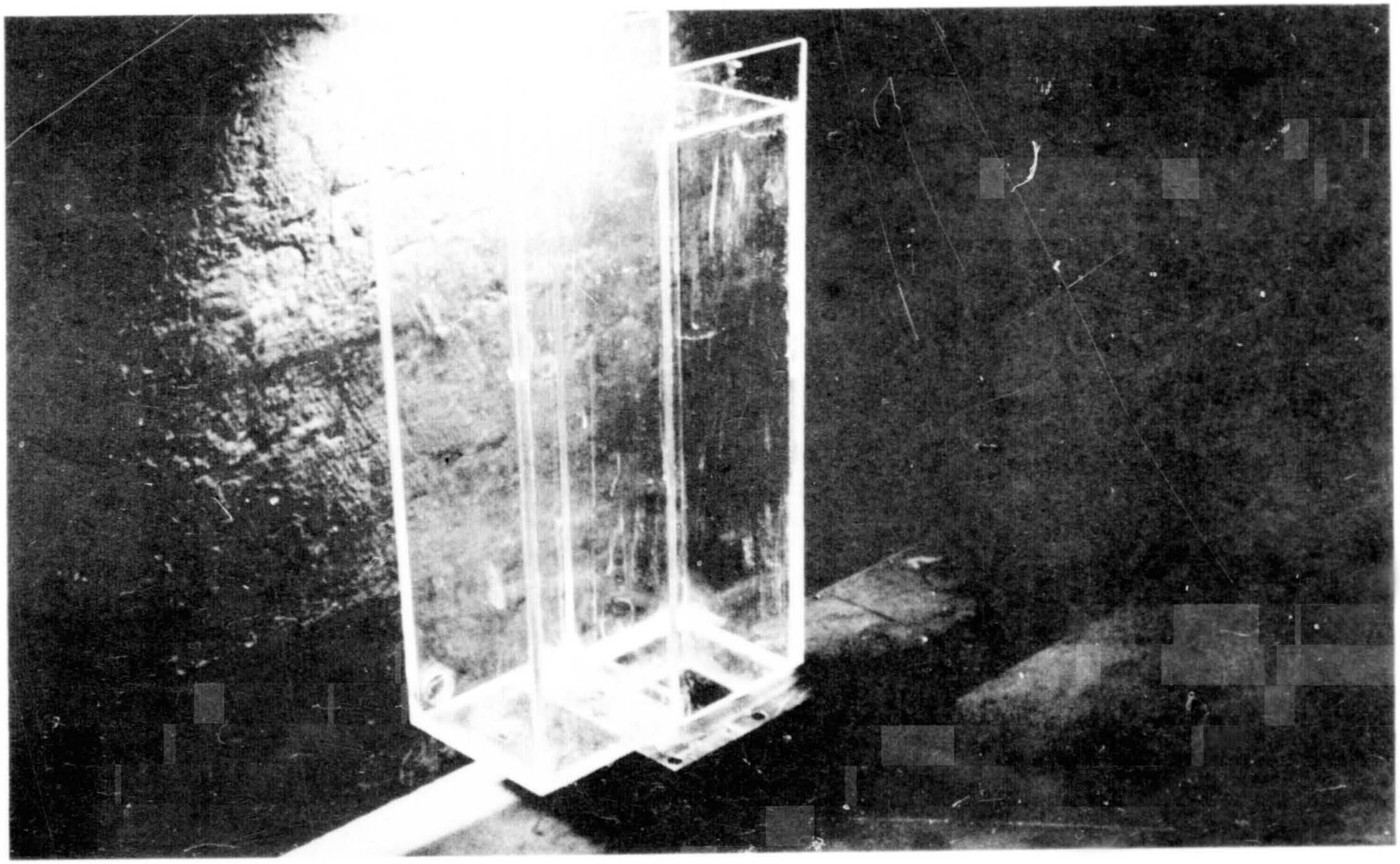

Figure 1-8. Experimental Equipment, Screen/Channel Assembly.

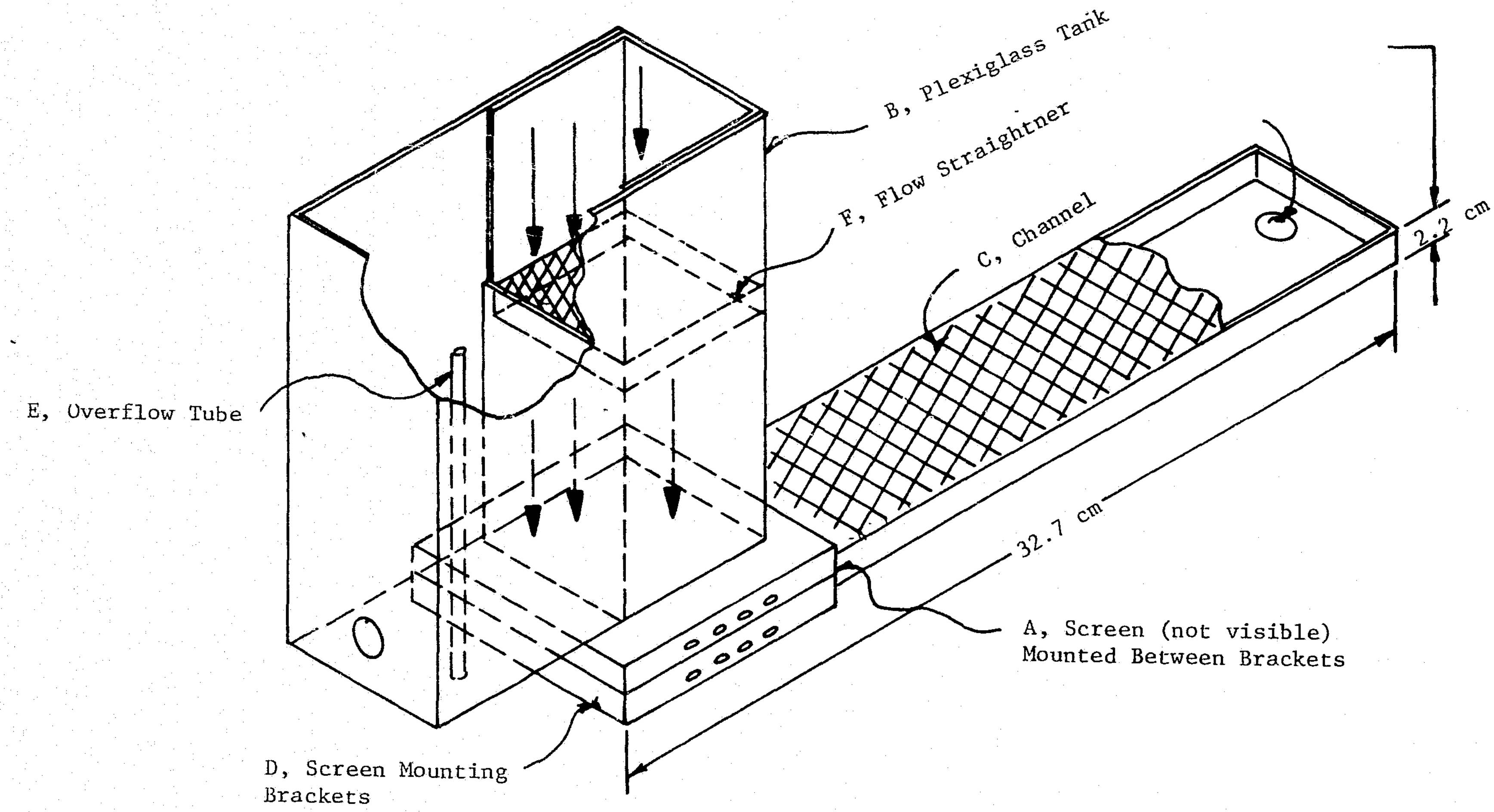

Figure 1-9 Screen/Channel Assembly

Figure 1-10 Upper and Lower Support Brackets (Top View)

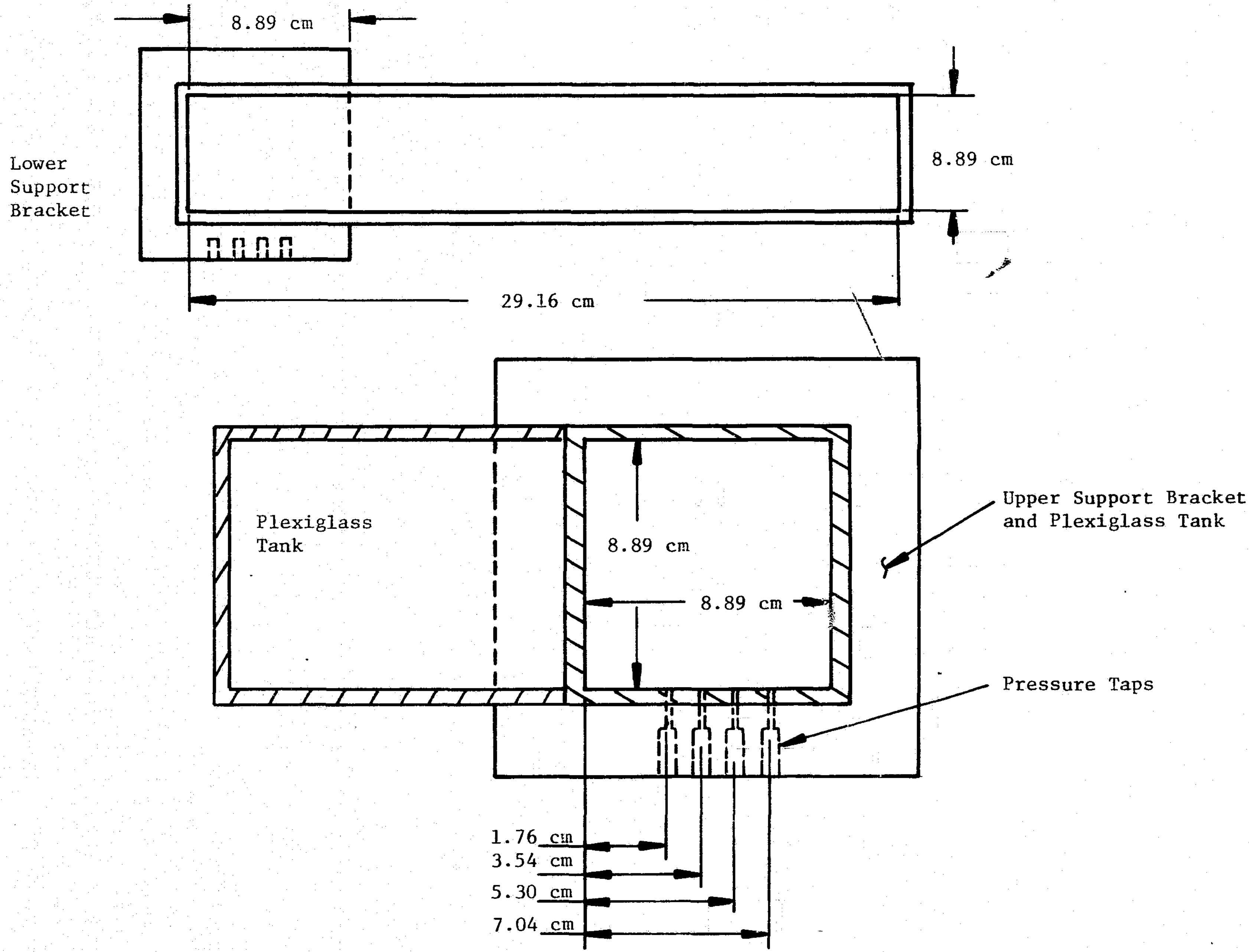

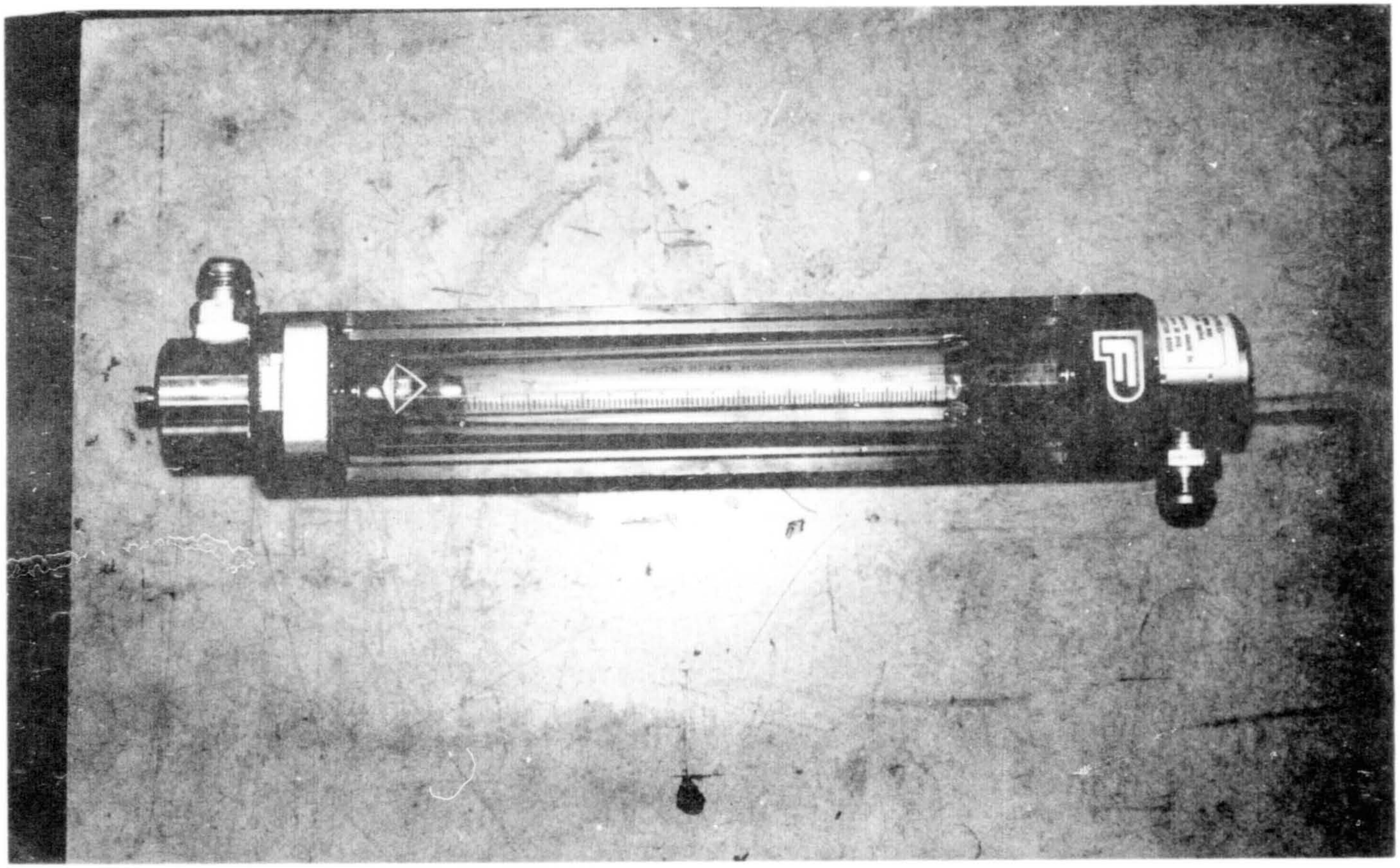

Figure 1-11.   Experimental Equipment, Rotameter

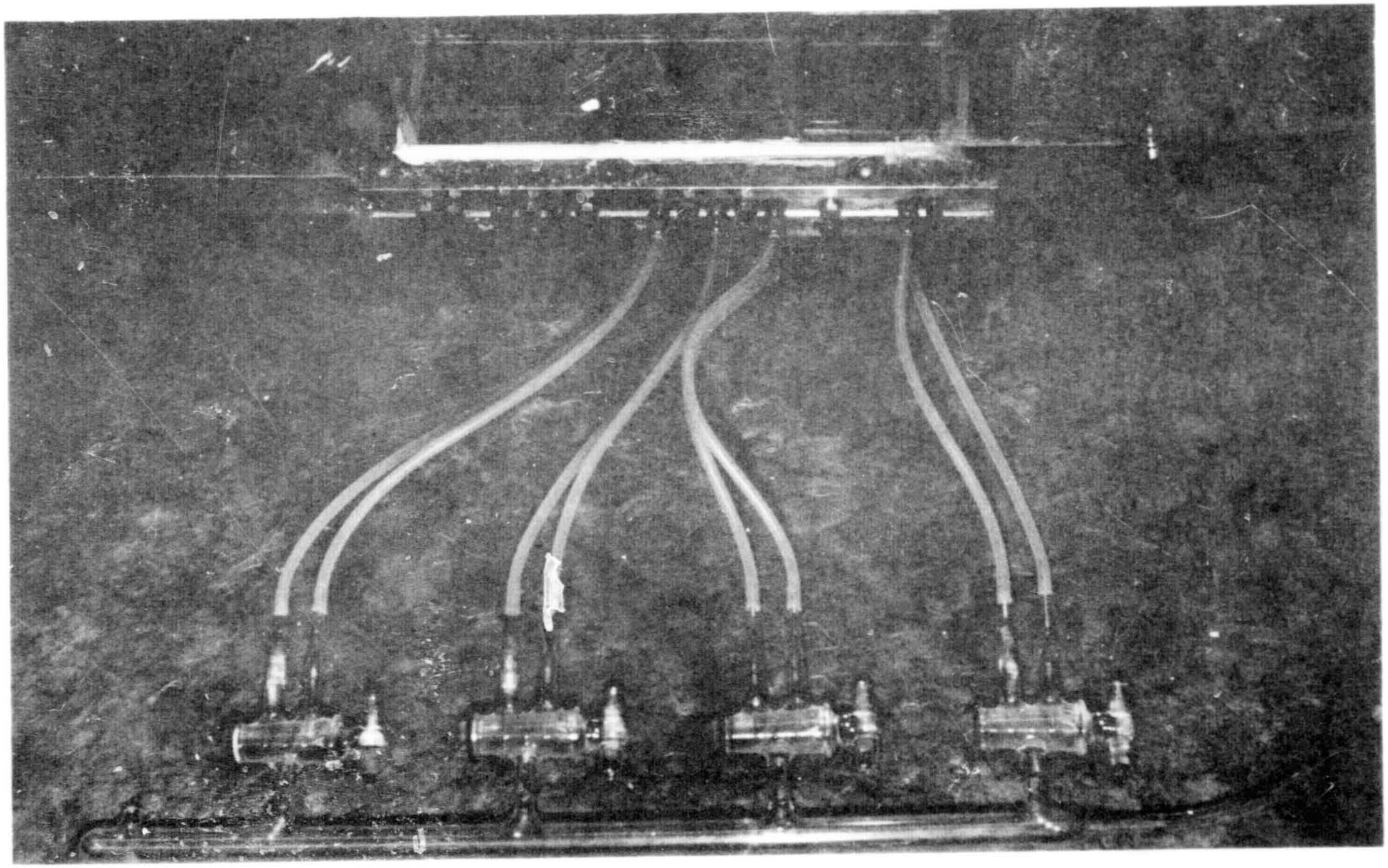

Figure 1-12. Experimental Equipment, Manifold System

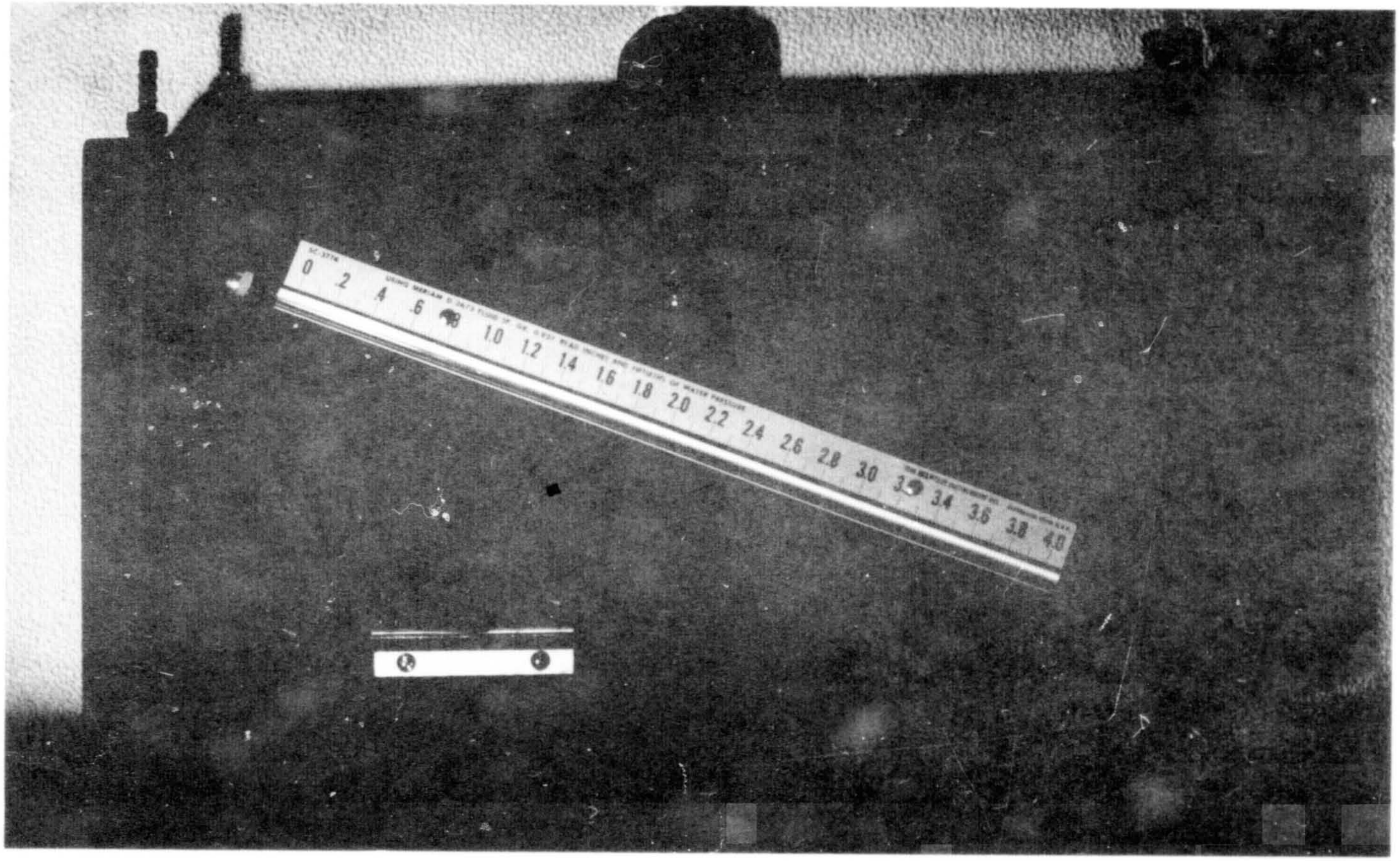

Figure 1-13. Experimental Equipment, Inclined Tube Manometer

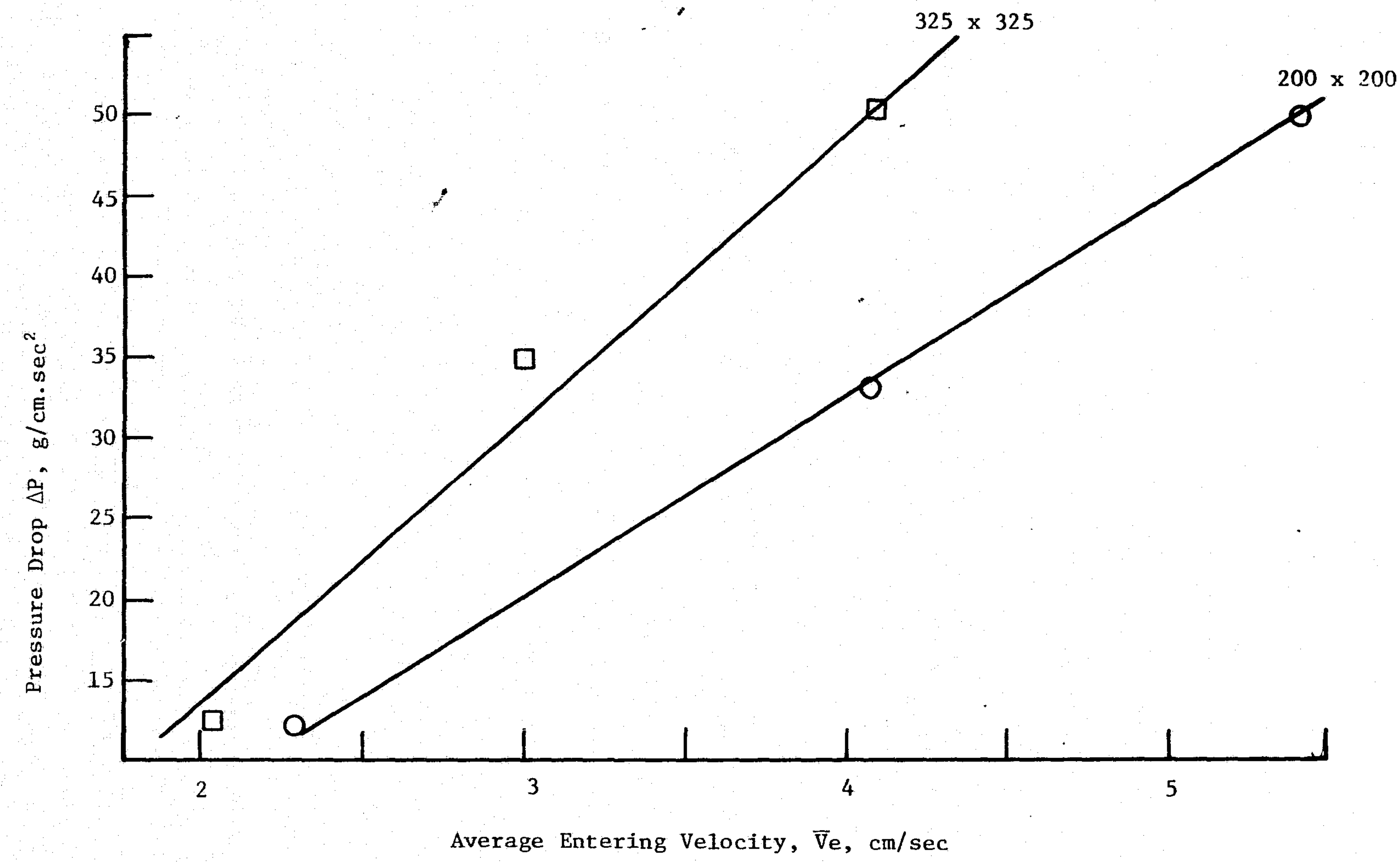

Figure 1-14 Pressure Drop as a Function of Average Entering Velocity, Square Weave Screens

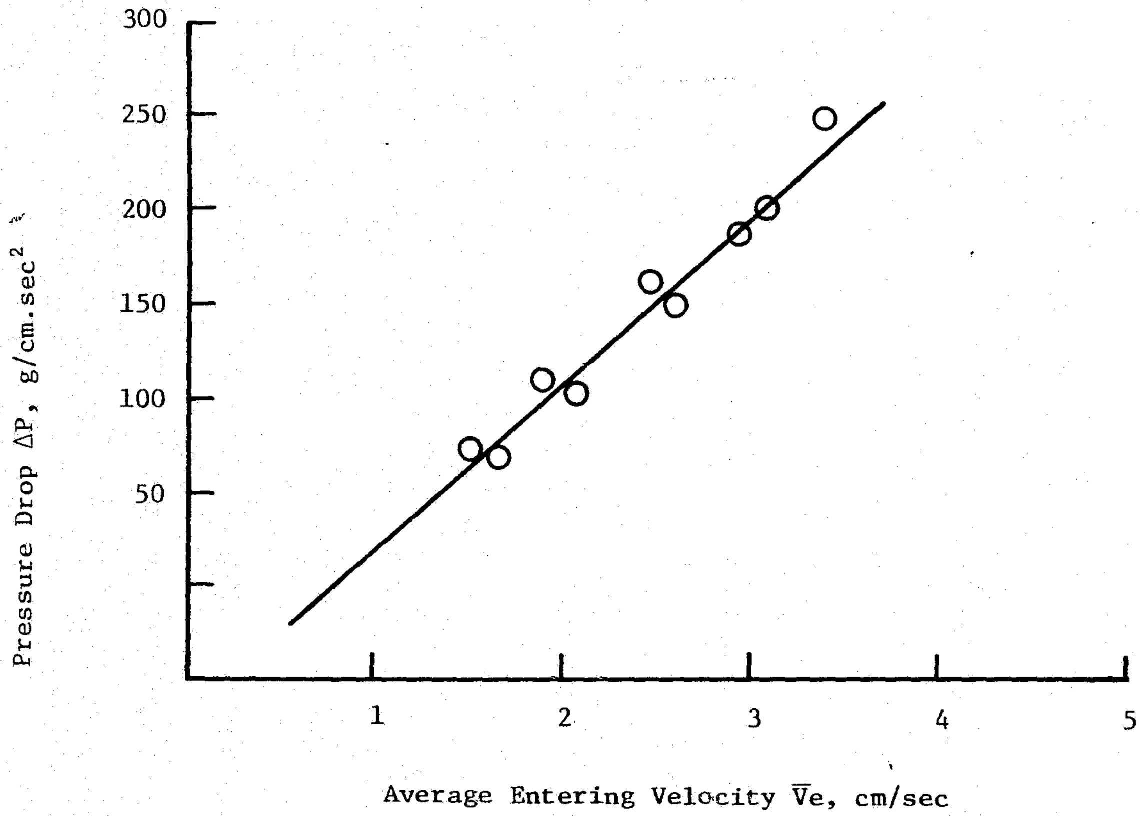

Figure 1-15 Pressure Drop as a Function of Average Entering Velocity, 200 x 600 Dutch Twill Screen

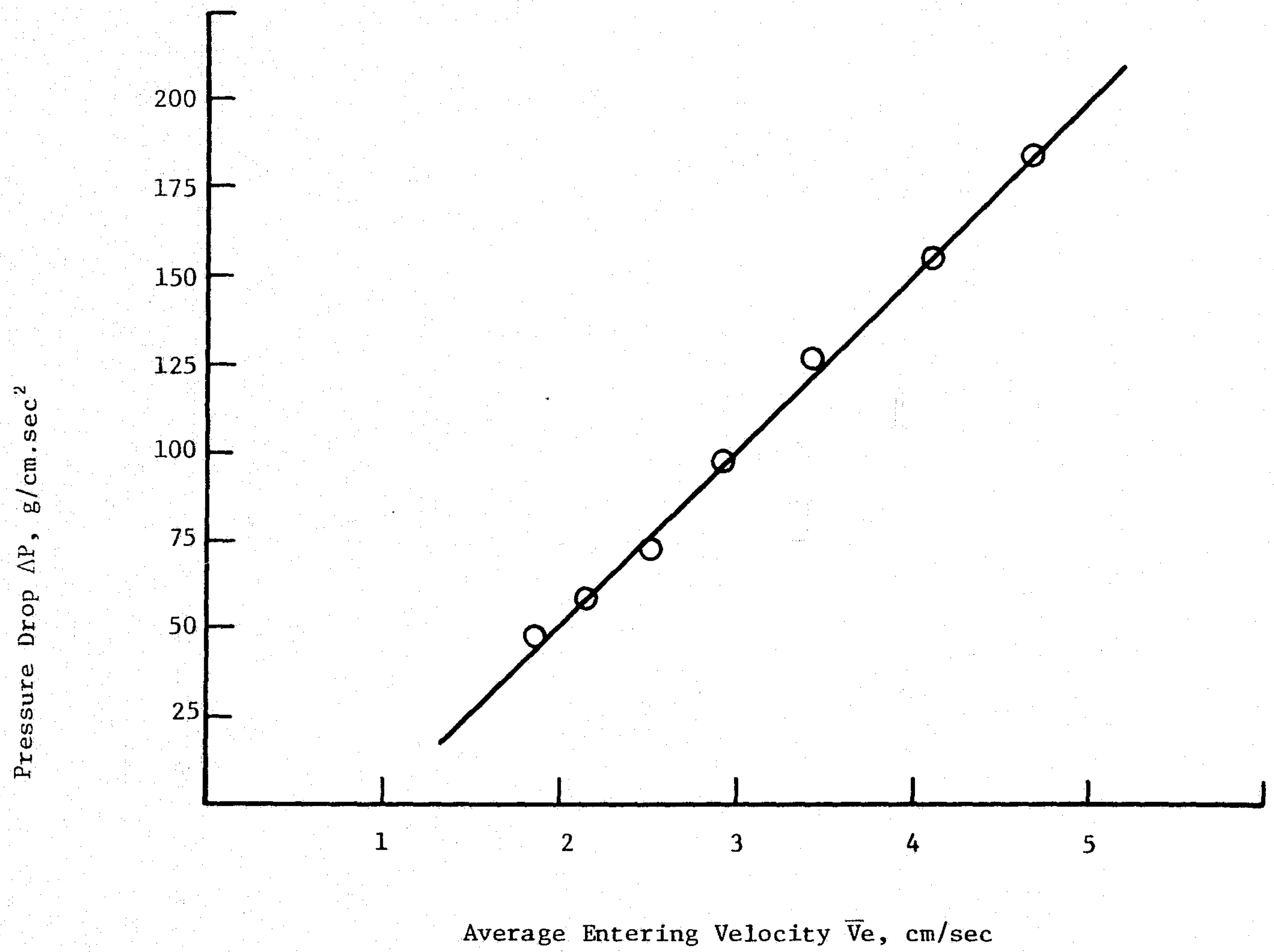

Figure 1-16 Pressure Drop as a Function of Average Entering Velocity, 50 x 250 Dutch Twill Screen

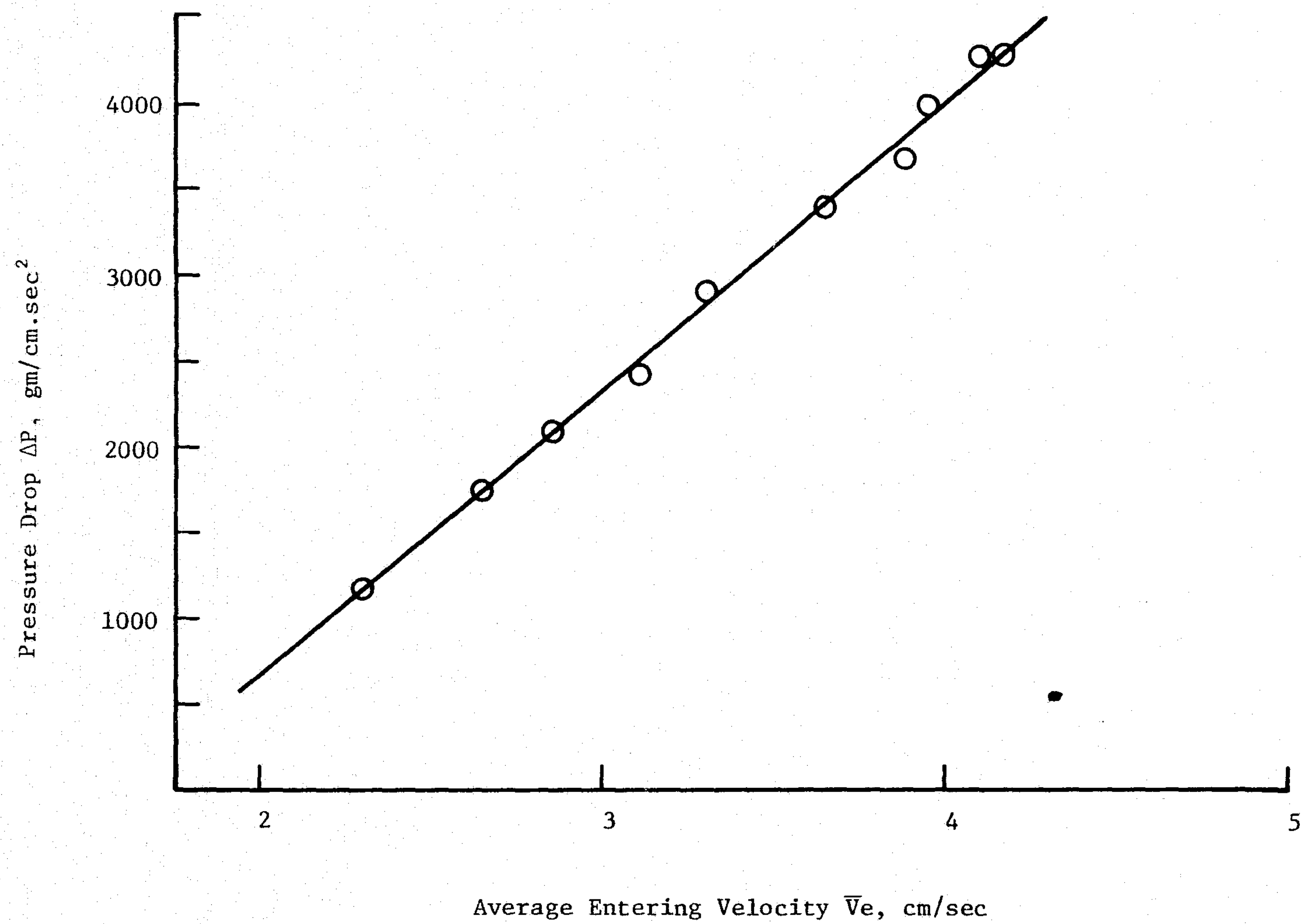

Figure 1-17 Pressure Drop as a Function of Average Entering Velocity, 325 x 2300 Dutch Twill Screen

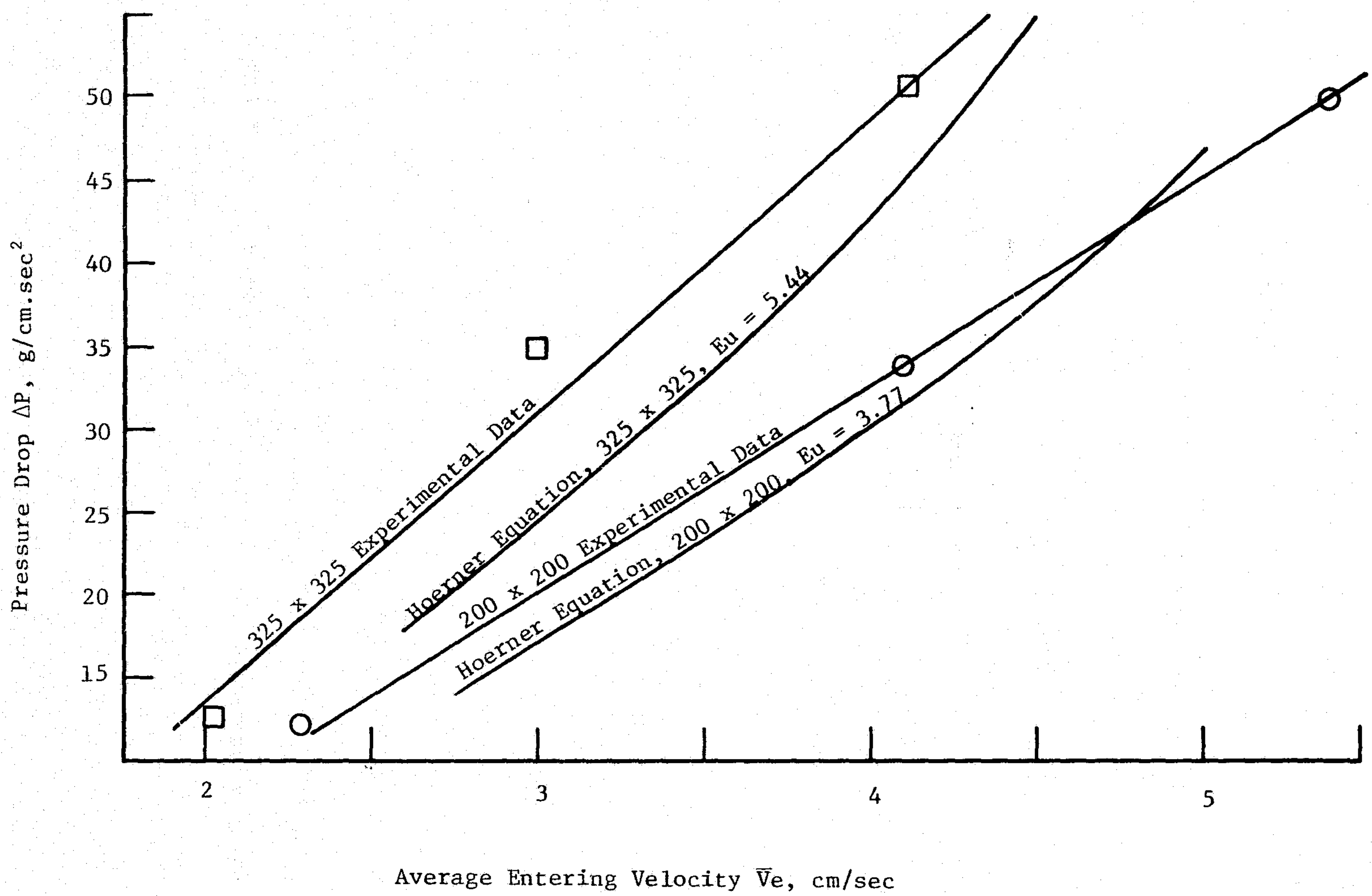

Figure 1-18 Comparison of Present Data for Square Weave Screens With Hoerner Equation $Eu = \left[\frac{S}{1-S}\right]^2$

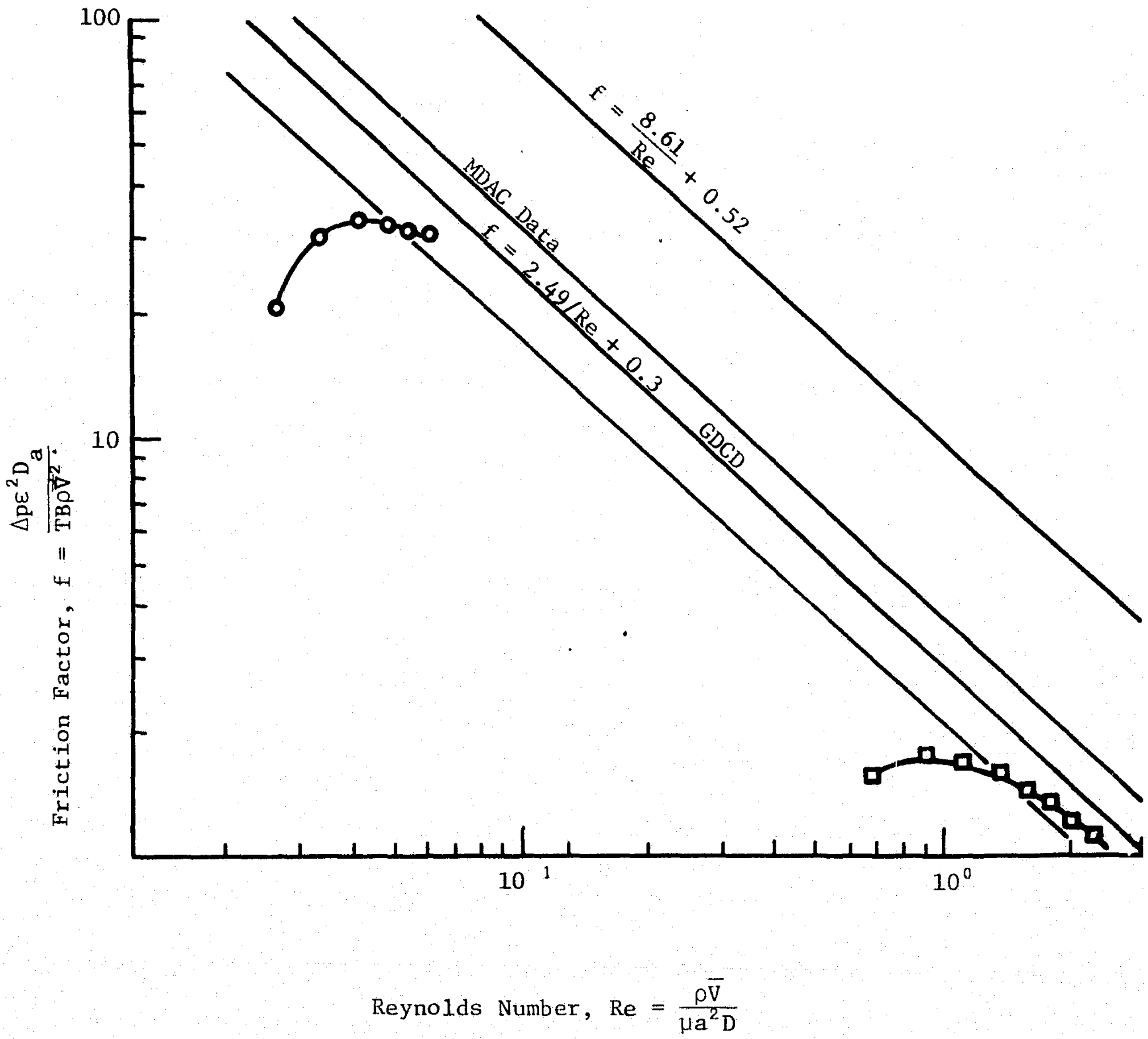

Figure 1-19 Comparison of Present Data For Dutch Twill Screens with Armour-Cannon Type Correlation

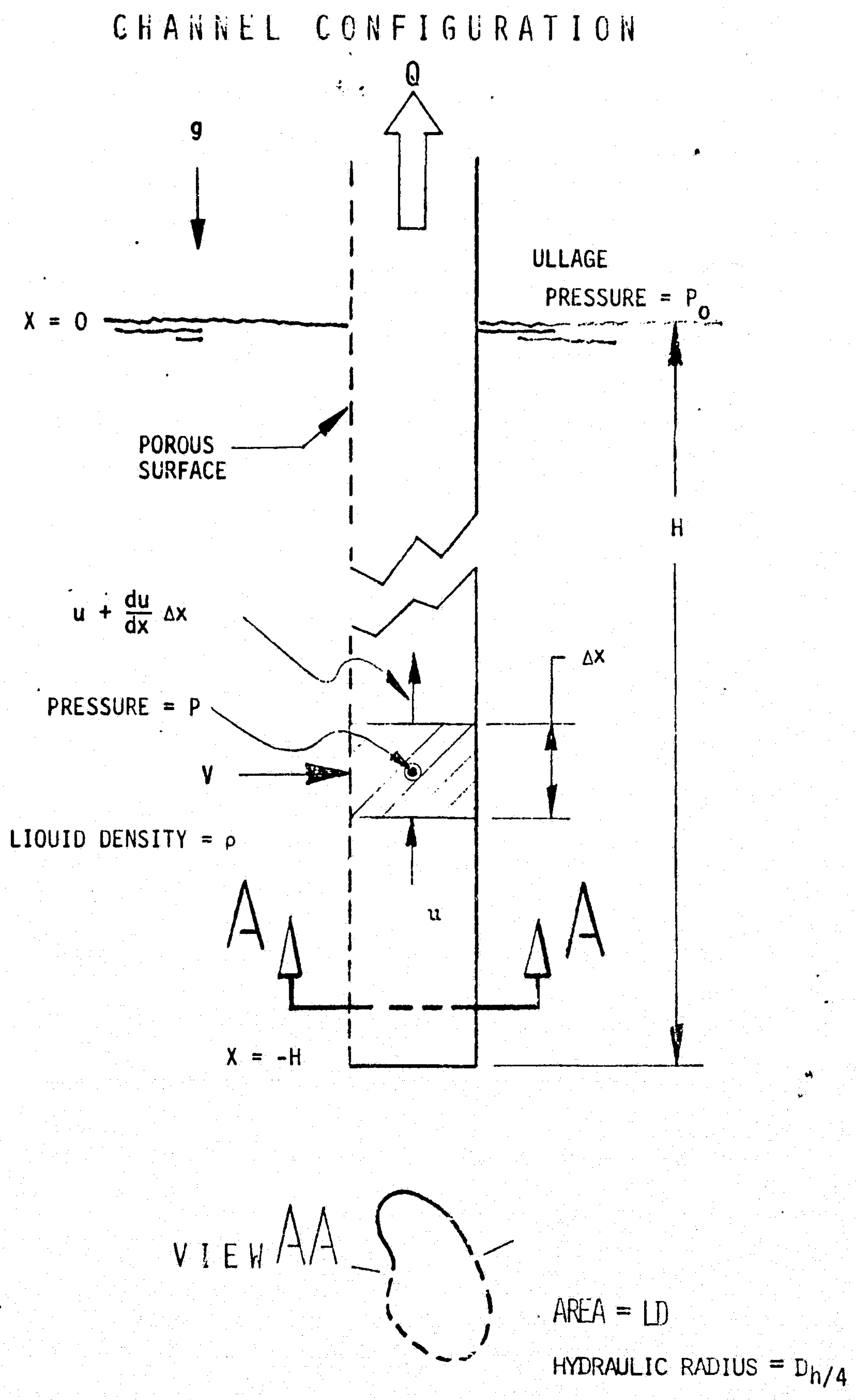

Fig. 2-1 Theoretical Model of McDonnell Douglas Channel Configuration.

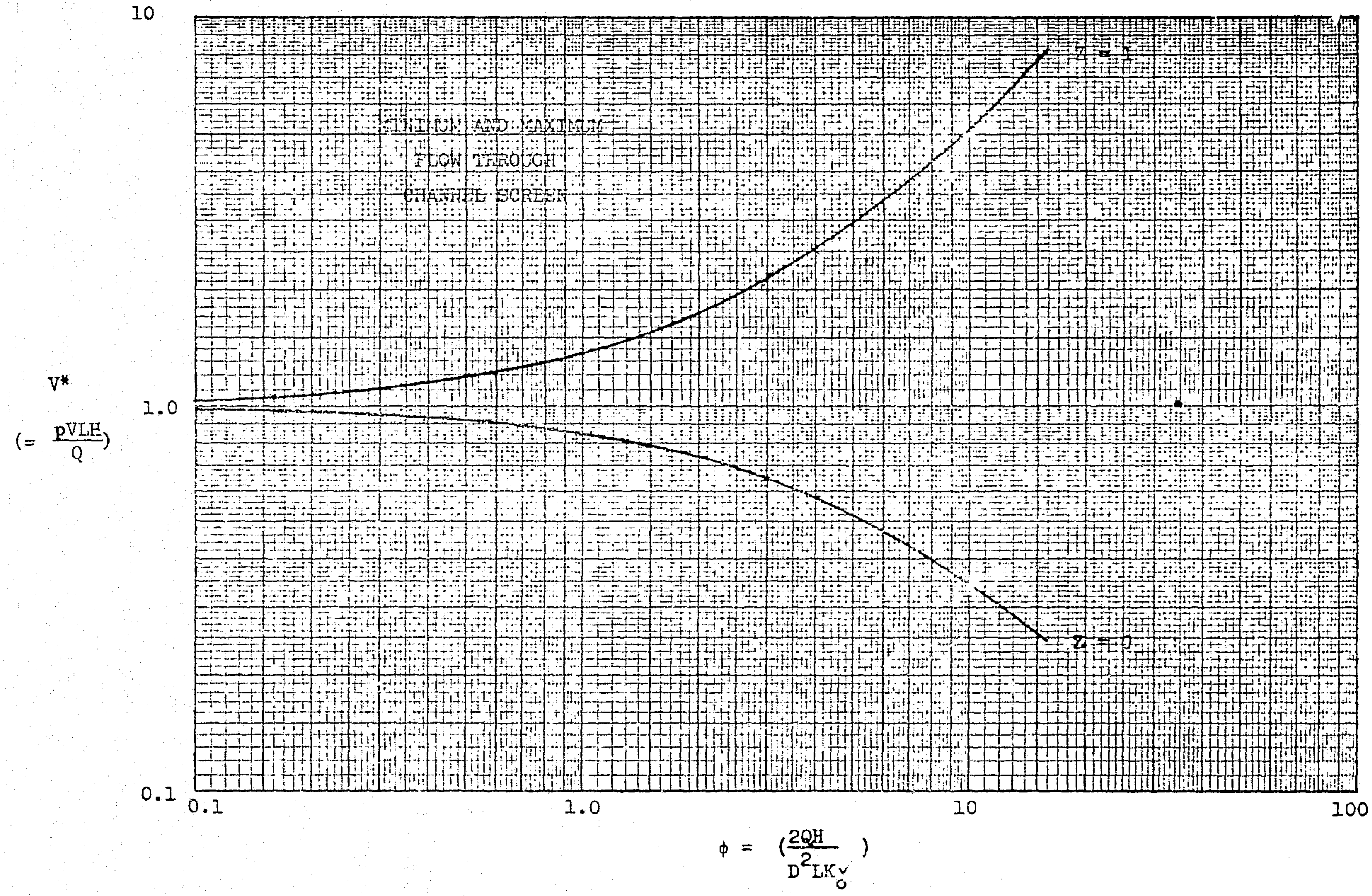

Figure 2-2 McDonnell Douglas Theoretical Results

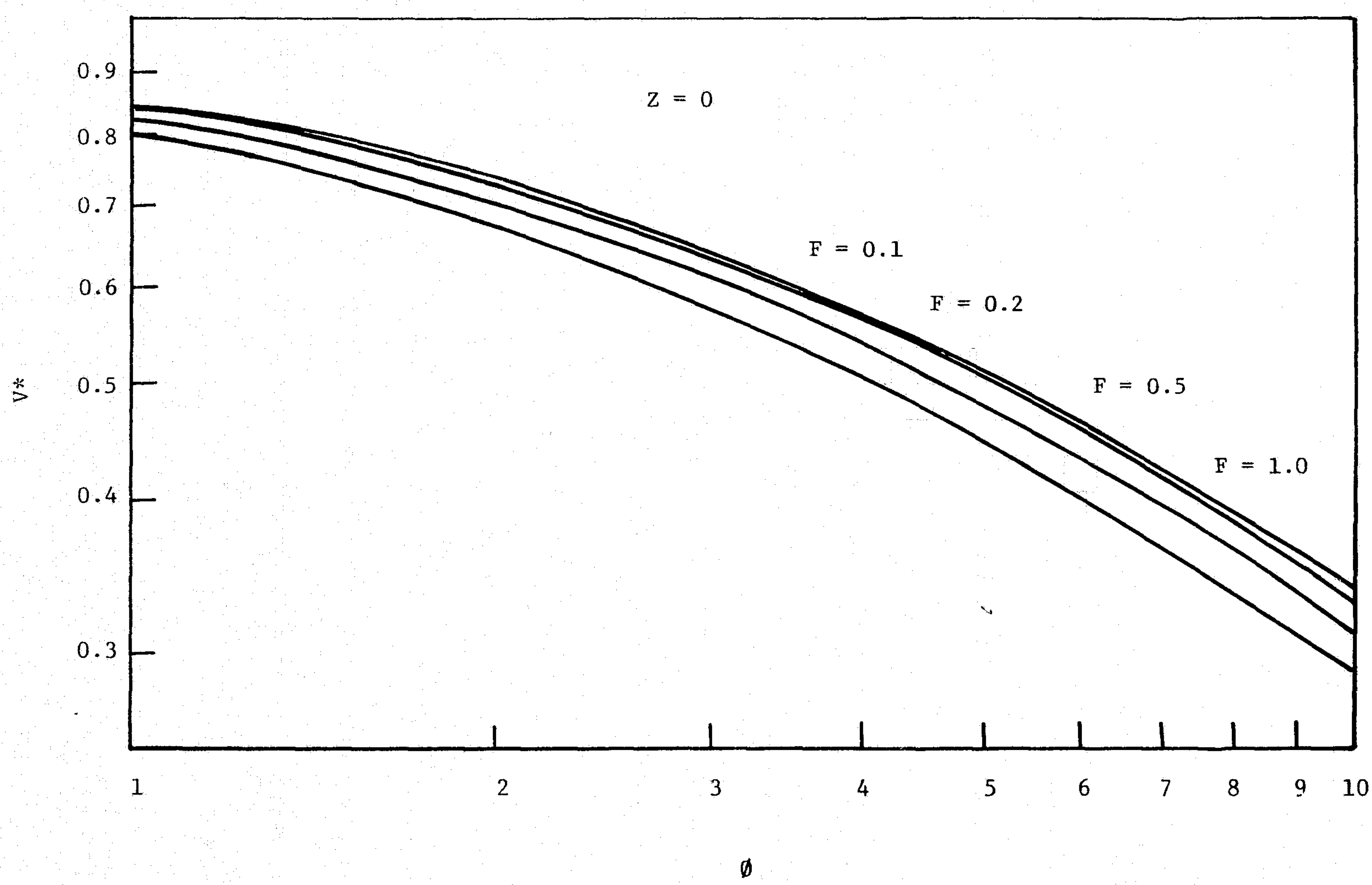

Figure 2-3

V* as a Function of ϕ at $Z = 0$ with F as an Independent Parameter, UAH Theoretical Result.

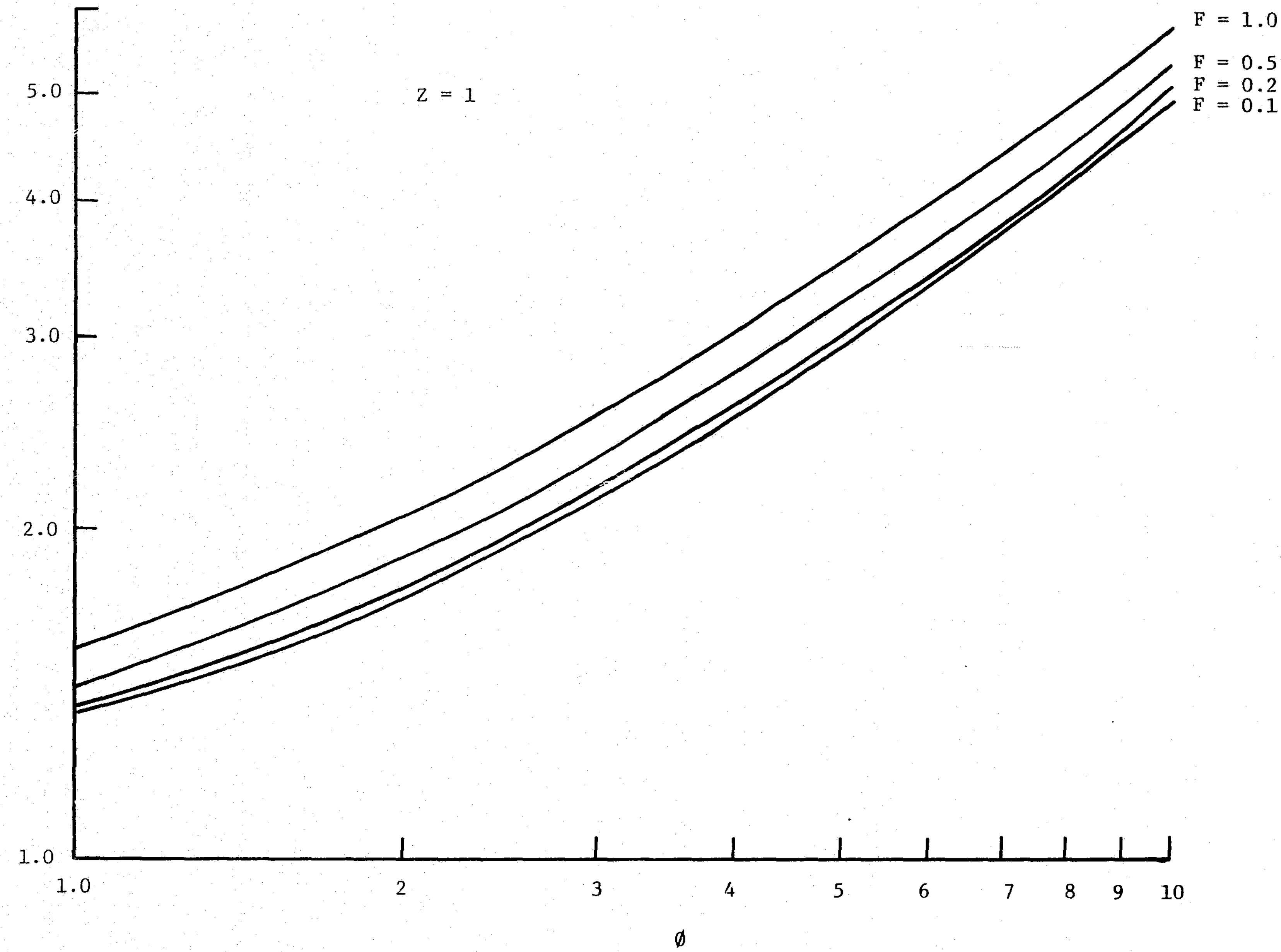

Figure 2
V* as a Function of ϕ at Z = 1 with F as an Independent Parameter, UAH Theoretical Result

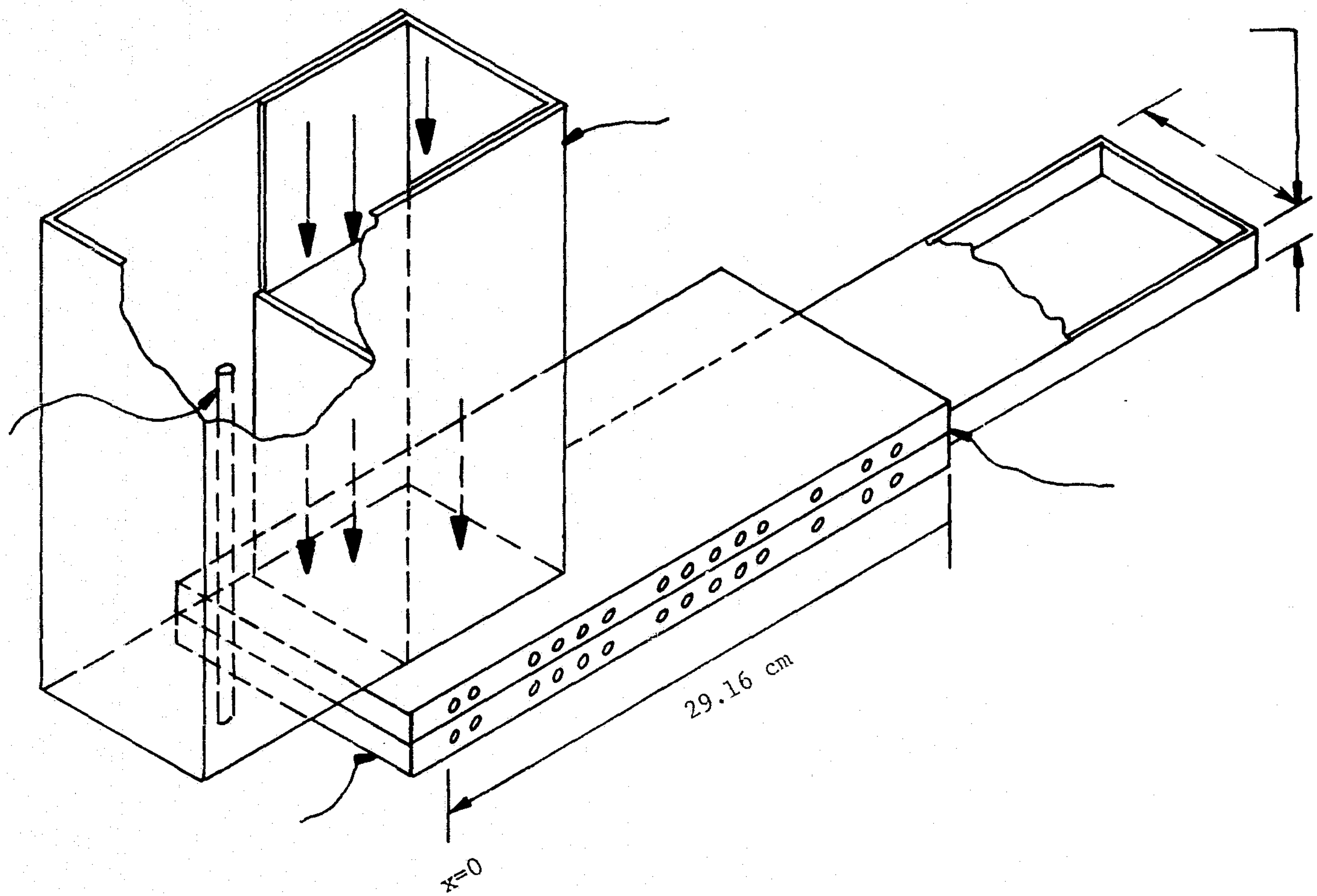

Figure 2-5   Modified Screen/Channel Assembly

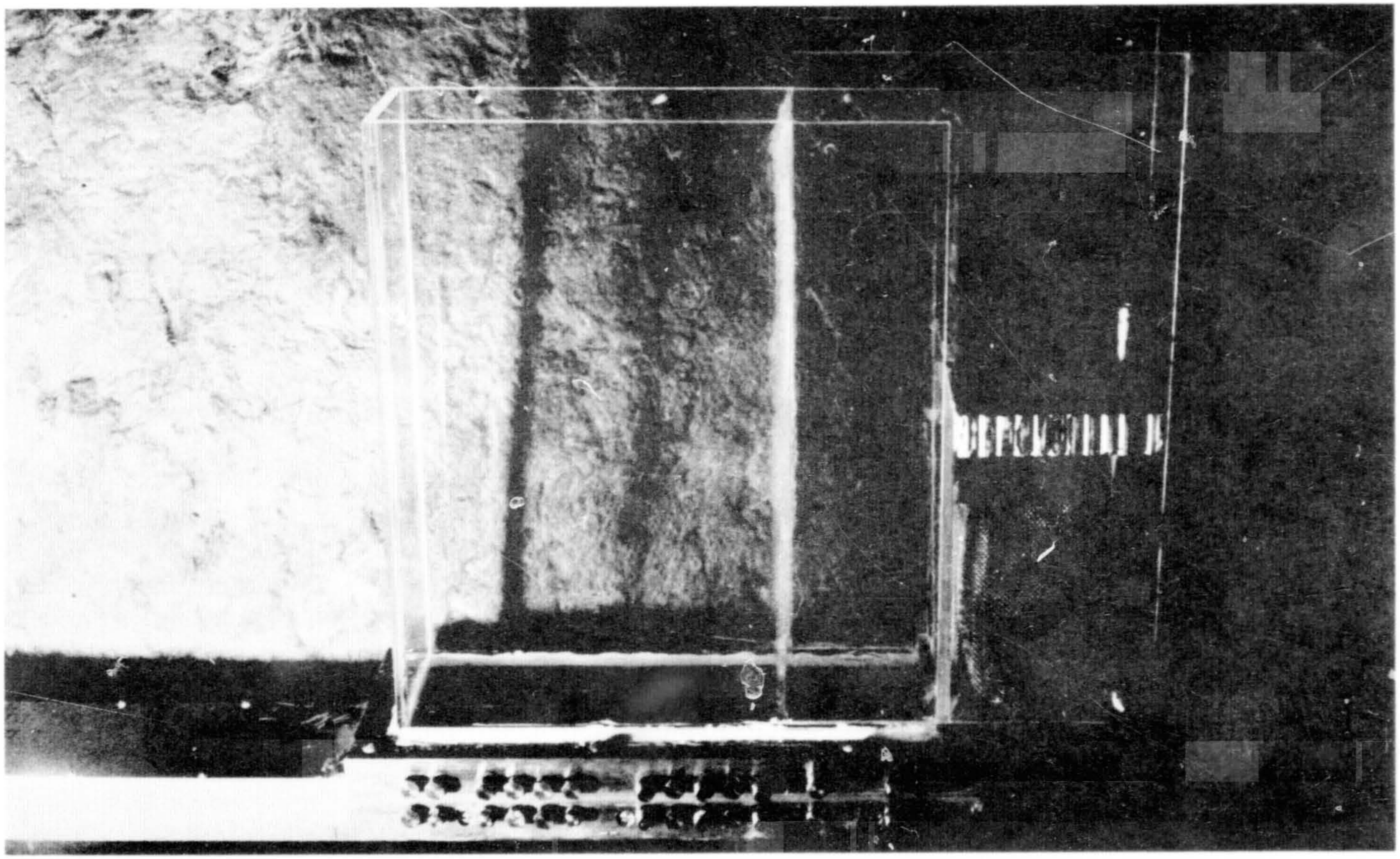

Figure 2-6. Modified Screen/Channel Assembly.

50 x 250 Dutch Twill Screen
H = 29.16 cm   L = 8.81 cm

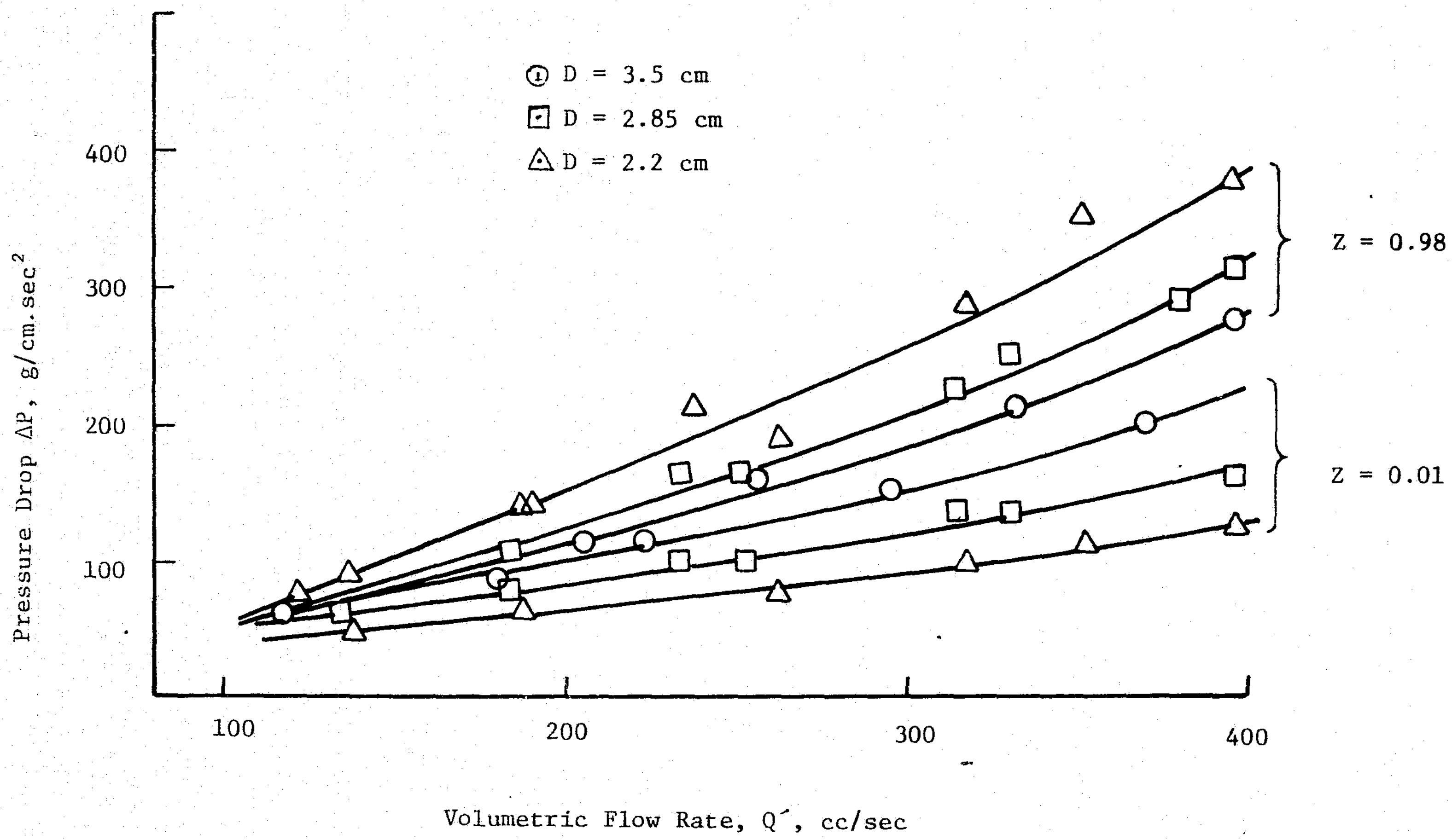

Figure 2-7

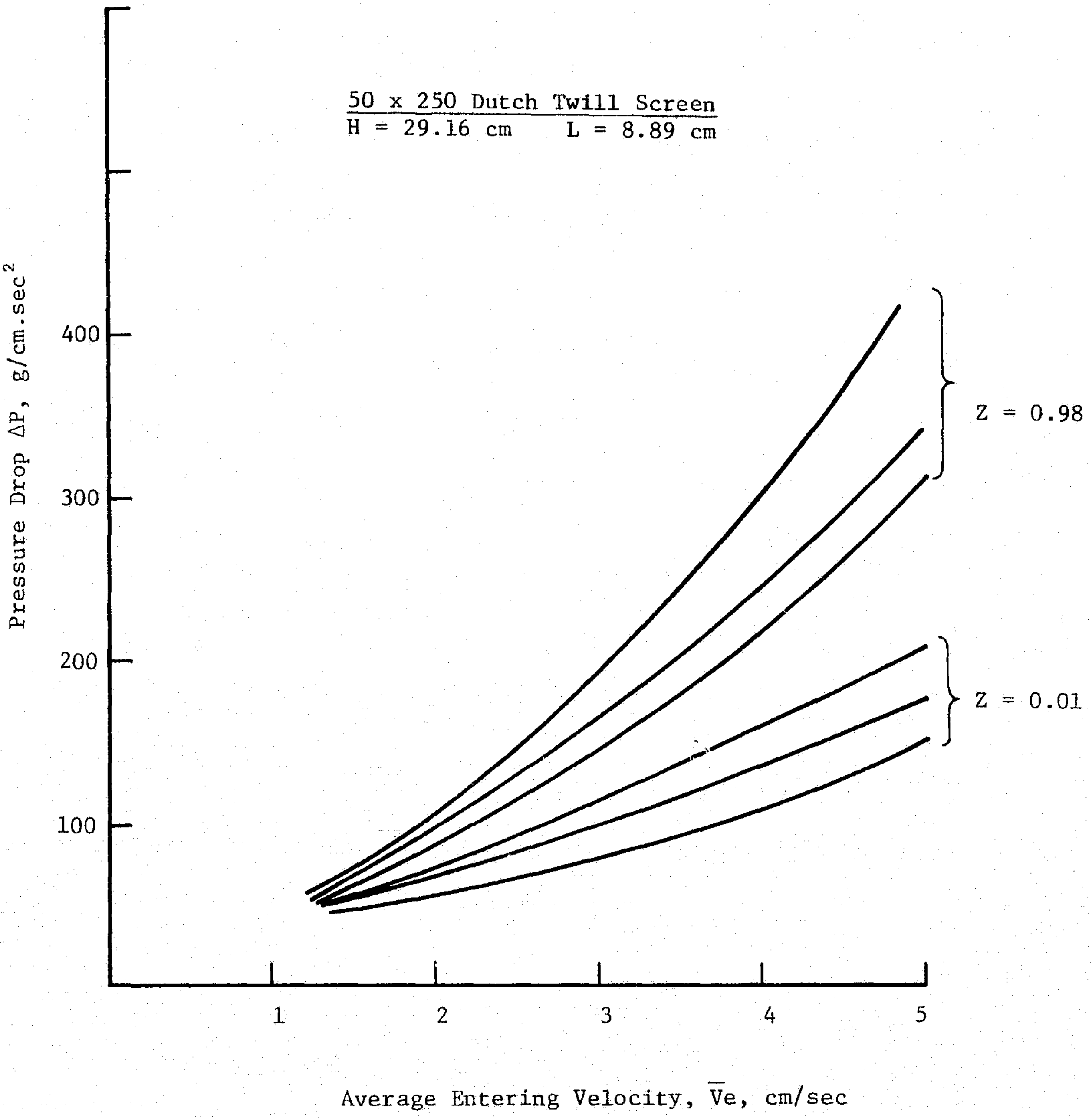
50 x 250 Dutch Twill Screen
H = 29.16 cm L = 8.89 cm
Pressure Drop ΔP, g/cm.sec²
400
300
200
100
Z = 0.98
Z = 0.01
1
2
3
4
5
Average Entering Velocity, $\overline{Ve}$, cm/sec

Figure 2-8

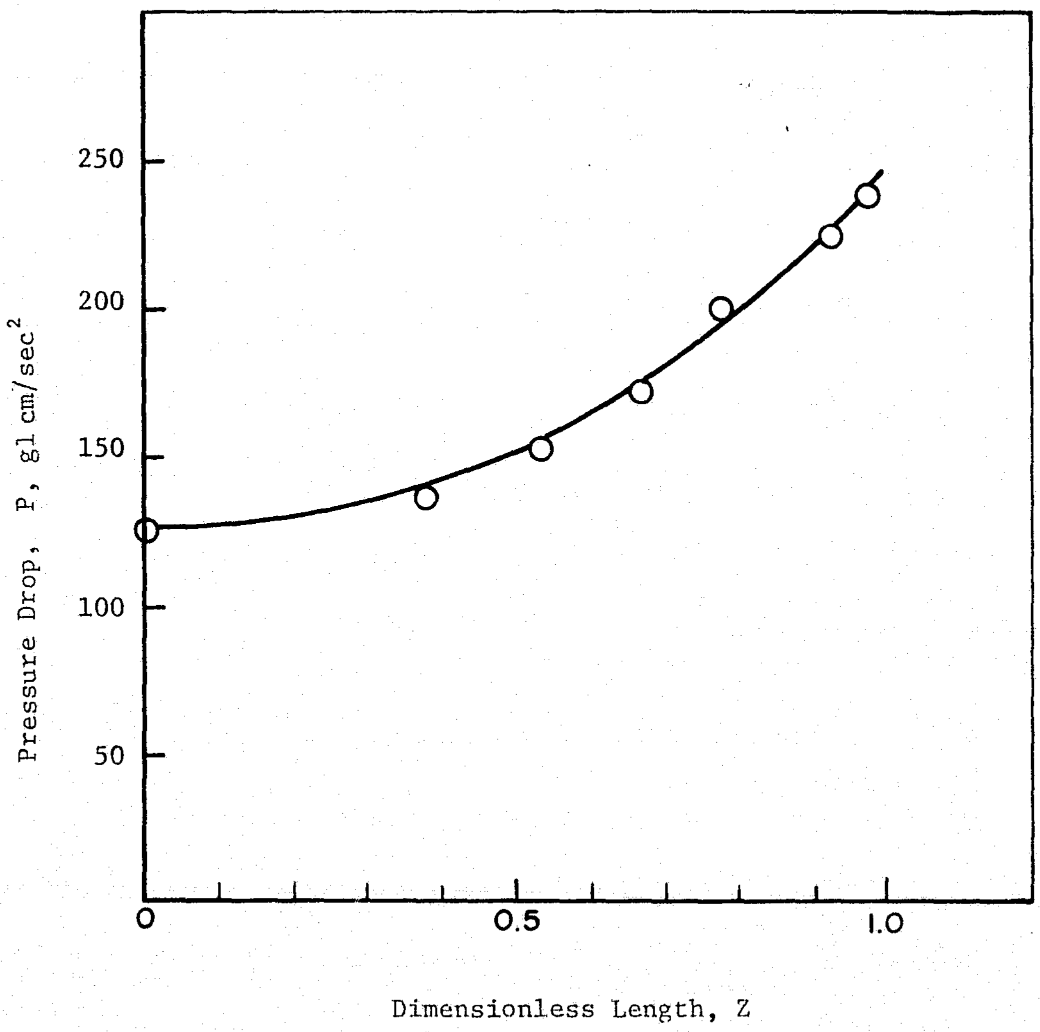

Figure 2-9
ΔP versus Z, Z = 400 cm^3/sec, D - 3.5 cm

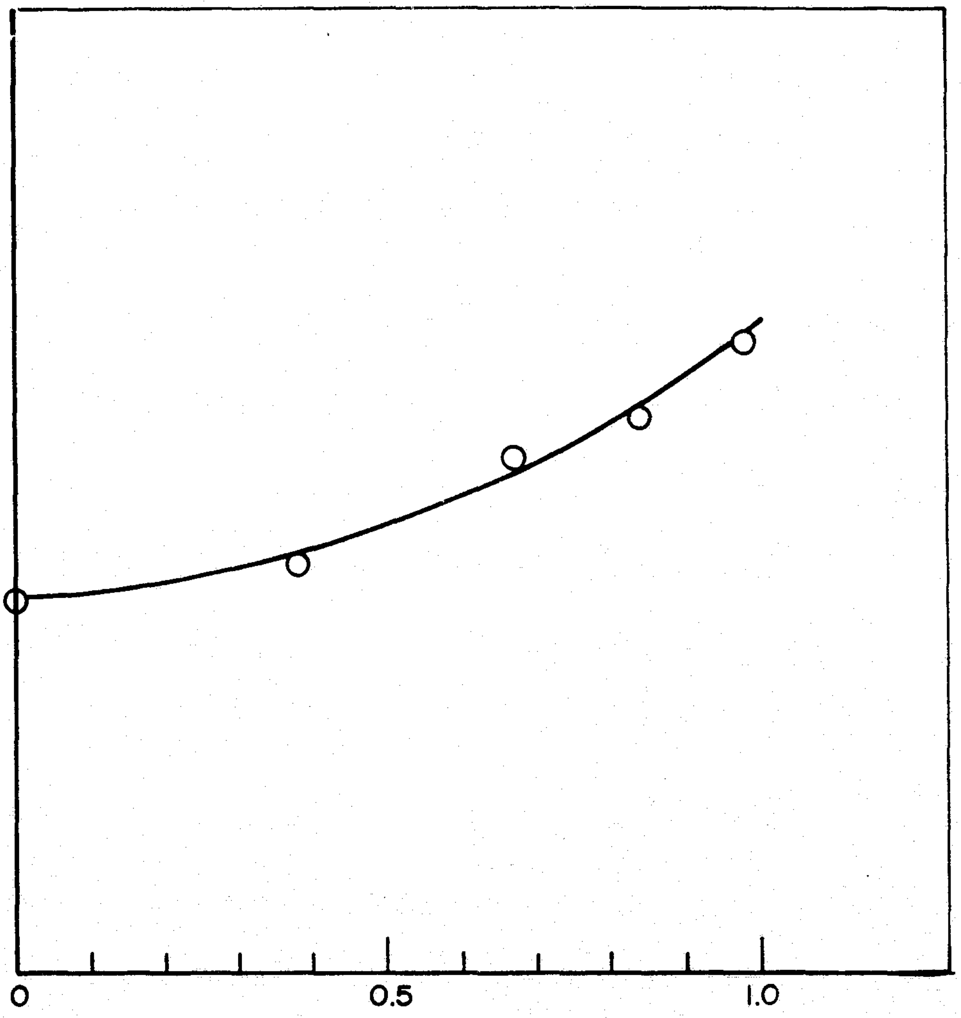

Dimensionless Length, Z

Figure 2-10

ΔP versus Z, Q = 350 cm^3/sec, D = 3.5 cm

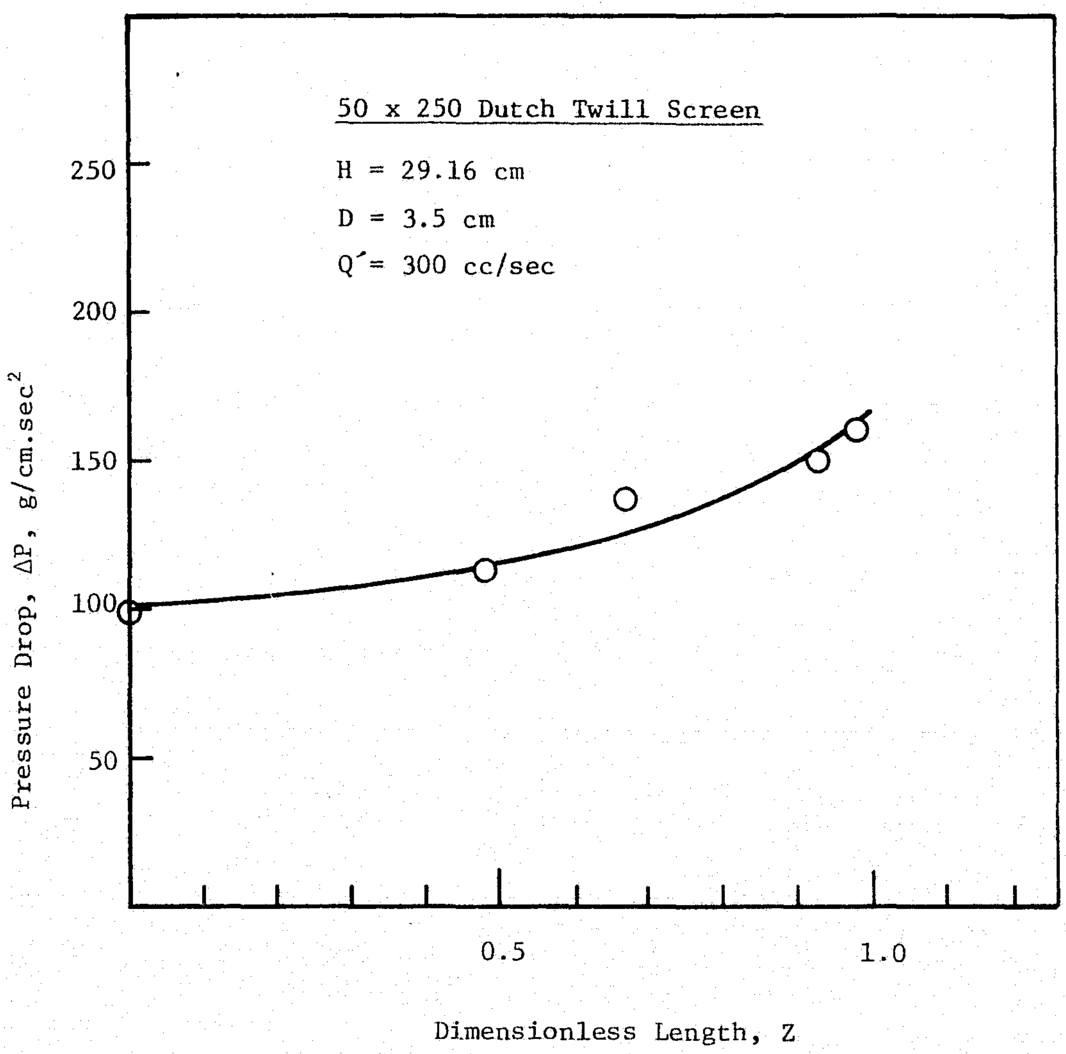

Figure 2-11

ΔP versus Z, Q - 300 cm³/sec, D - 3.5 cm

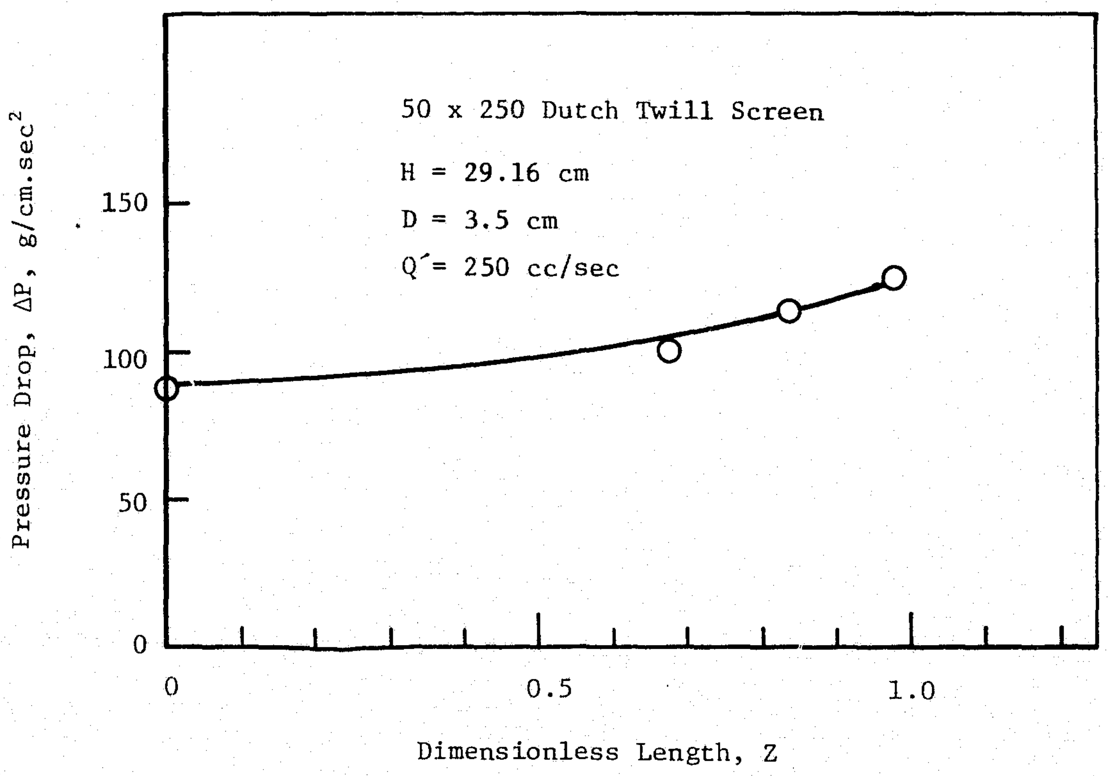

Figure 2-12

ΔP versus Z, Q = 250 cm^3/sec, D - 3.5 cm

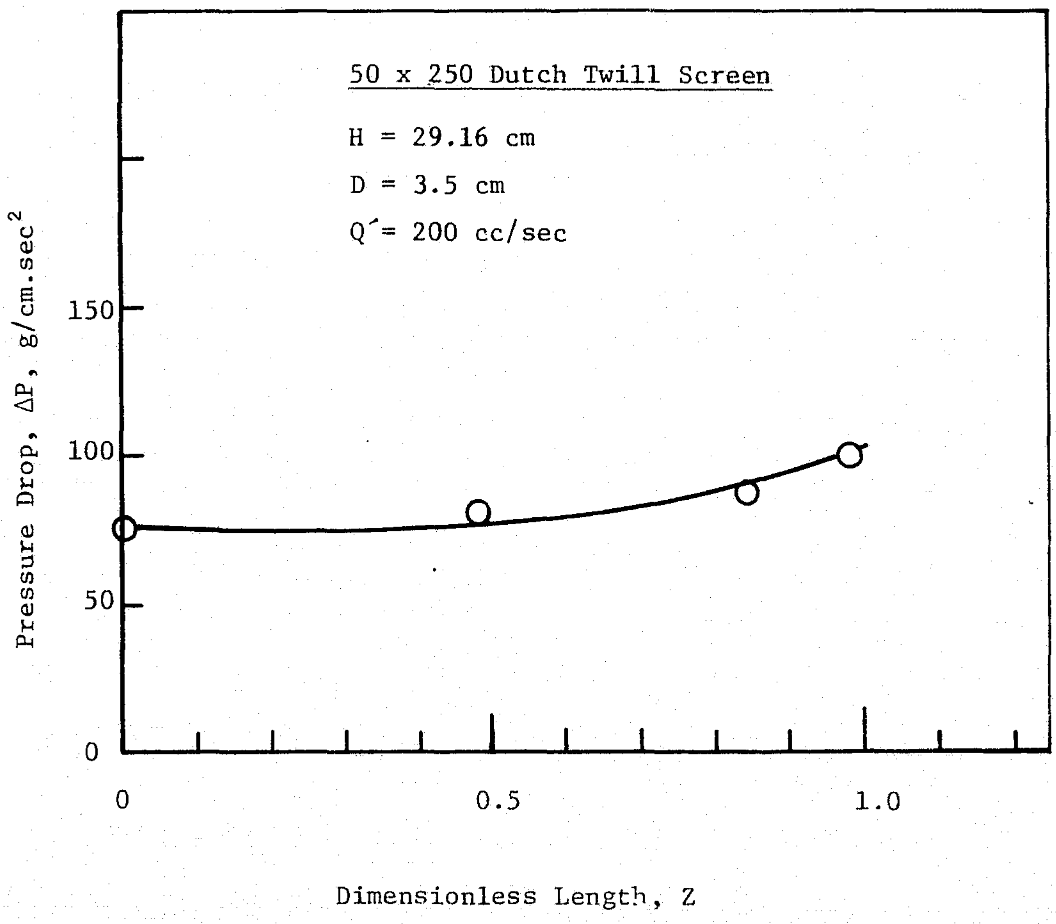

Figure 2-13

ΔP versus Z, Q - 200 cm^3/sec, D - 3.5 cm

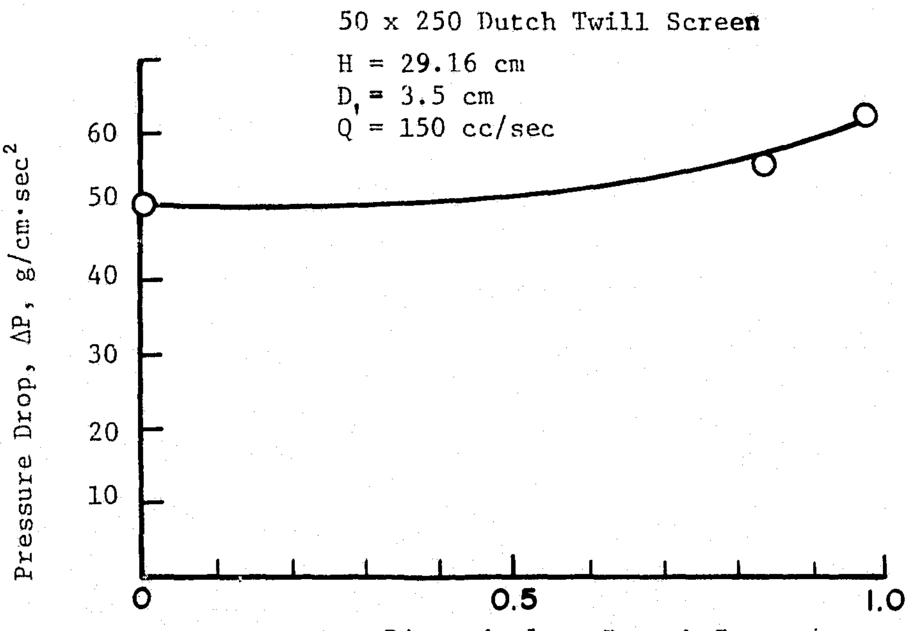

Figure 2-14 ΔP versus Z, Q - 150 cm³/sec, D - 3.5 cm.

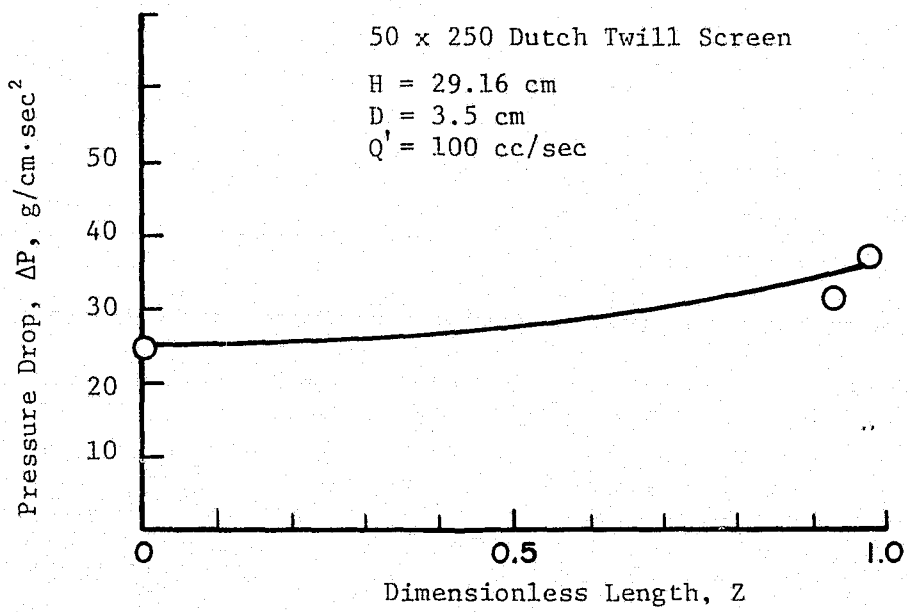

Figure 2-15 ΔP versus Z, Q = 100 cm³/sec, D - 3.5 cm

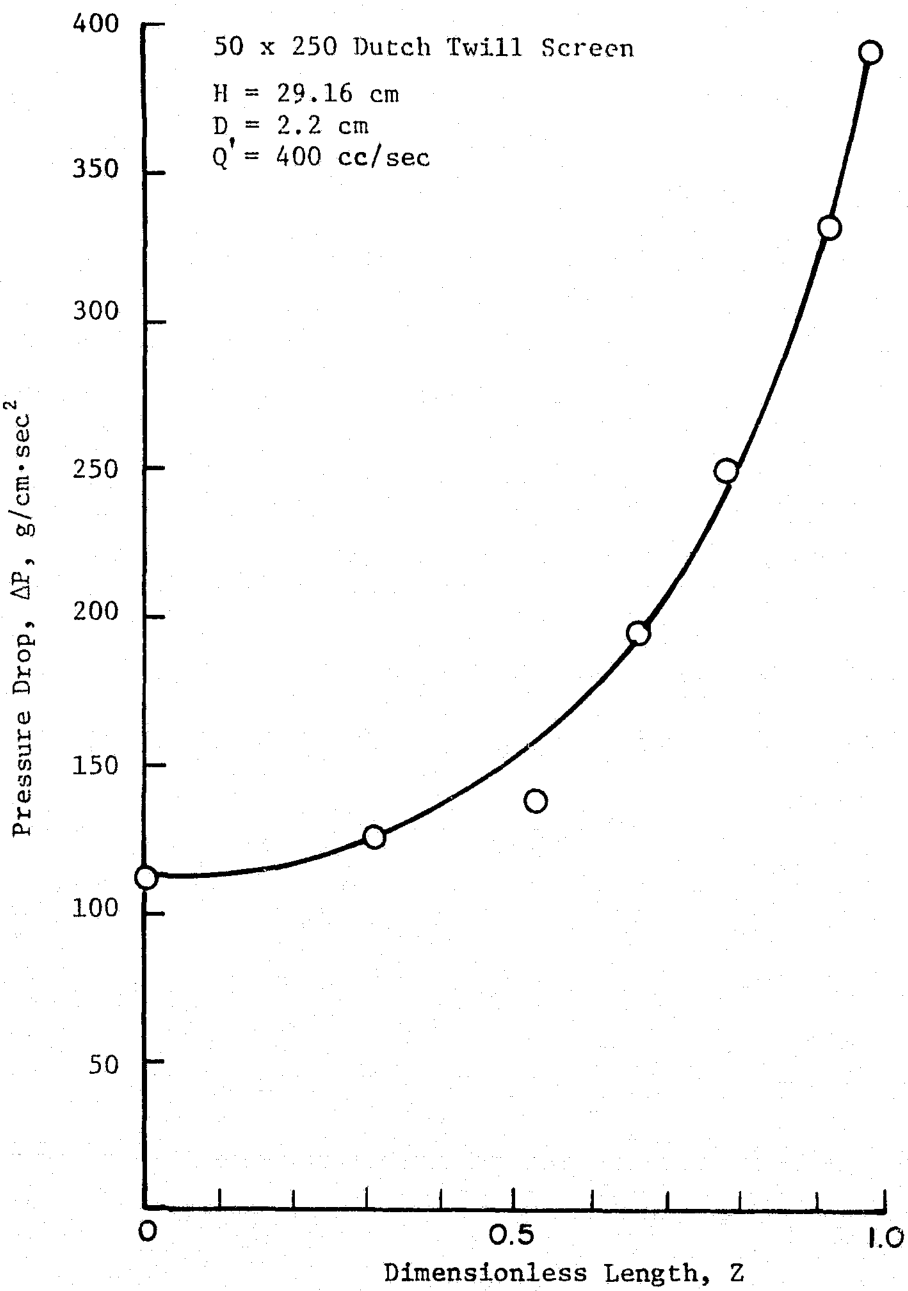

Figure 2-16 ΔP versus Z, Q = 400 cm³/sec, D - 2.2 cm

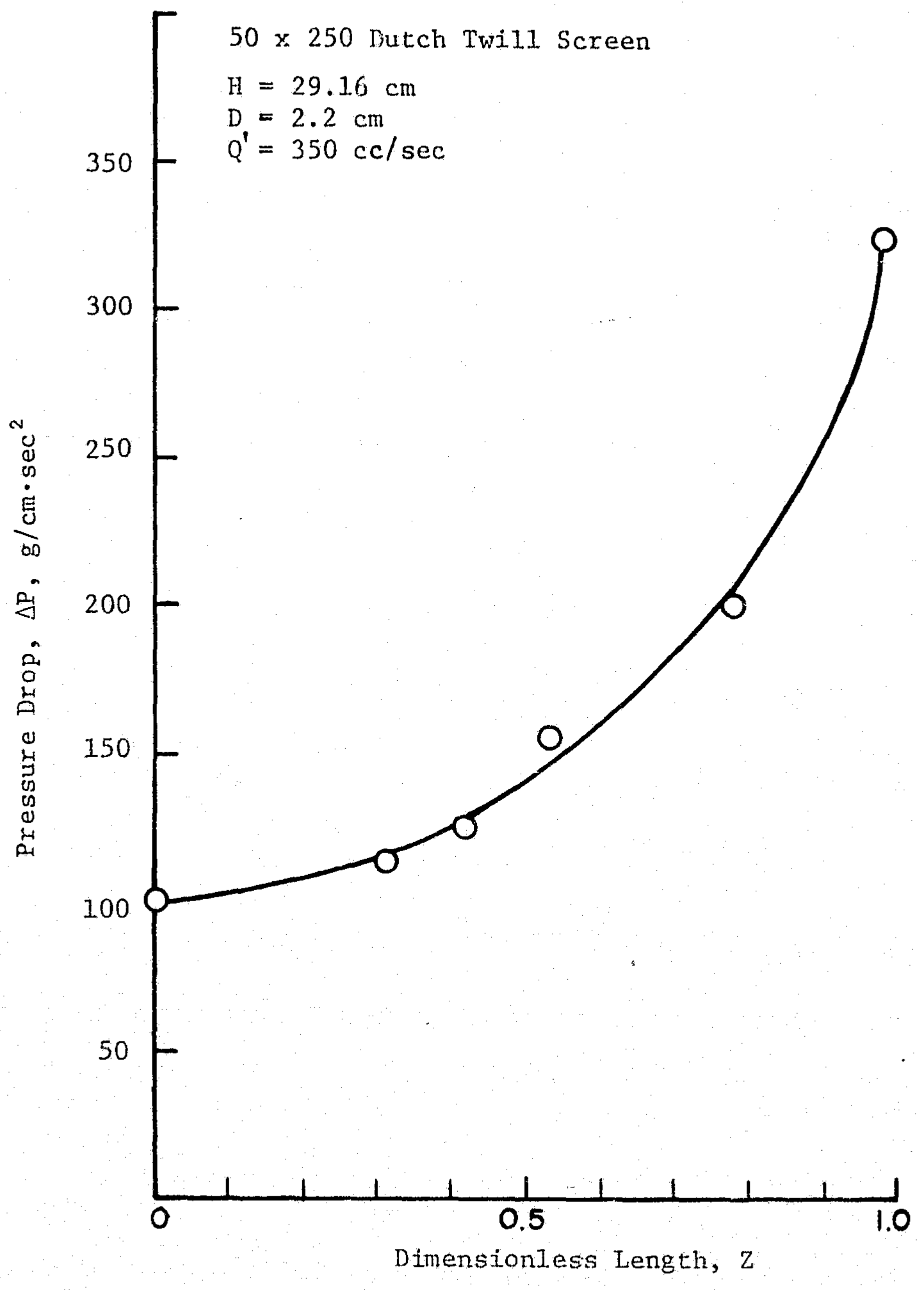

Figure 2-17 ΔP versus Z, Q = 350 cm³/sec, D - 2.2 cm

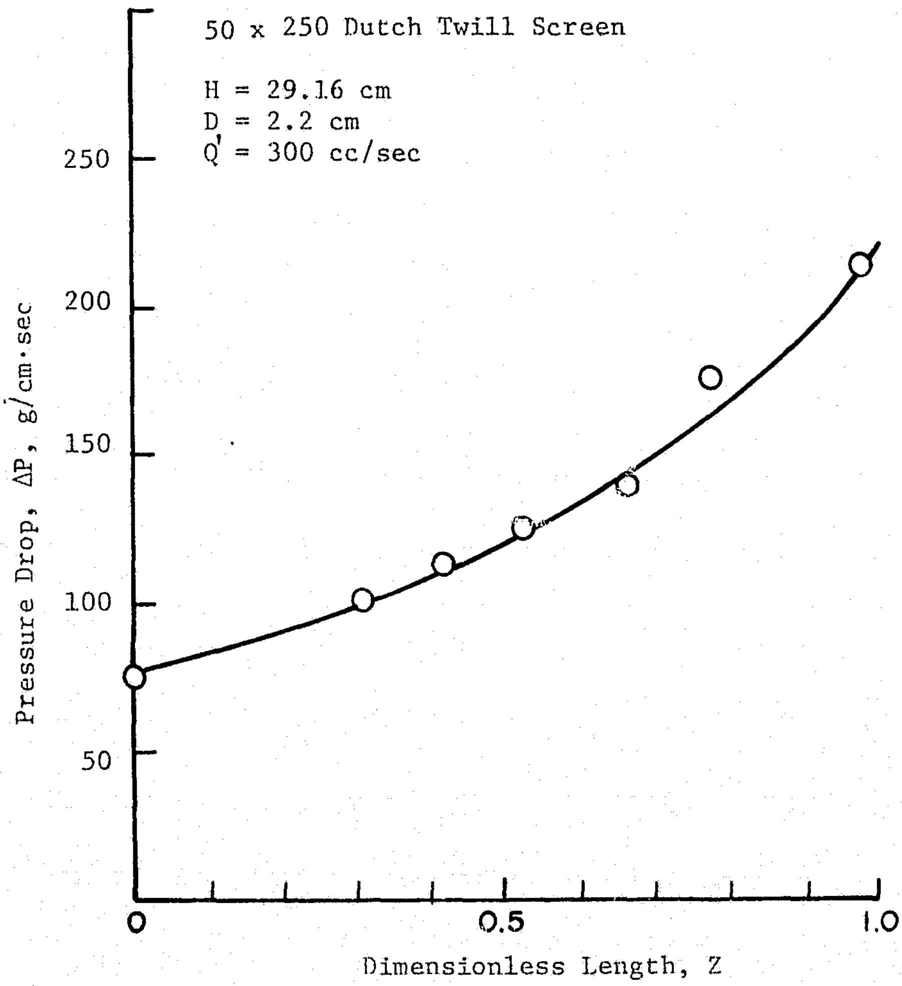

Figure 2-18 ΔP versus Z, Q - 300 cm^3/sec, D - 2.2 cm

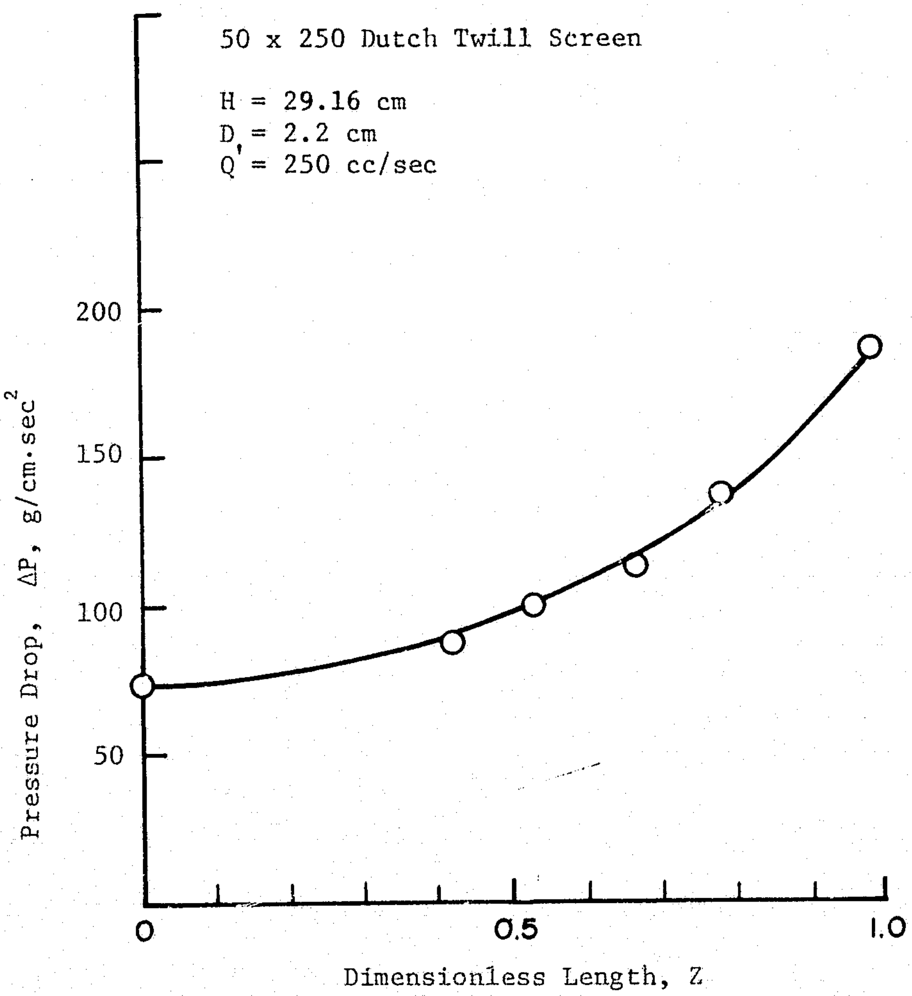

Figure 2-19 ΔP versus Z, Q - 250 cm³/sec, D - 2.2 cm

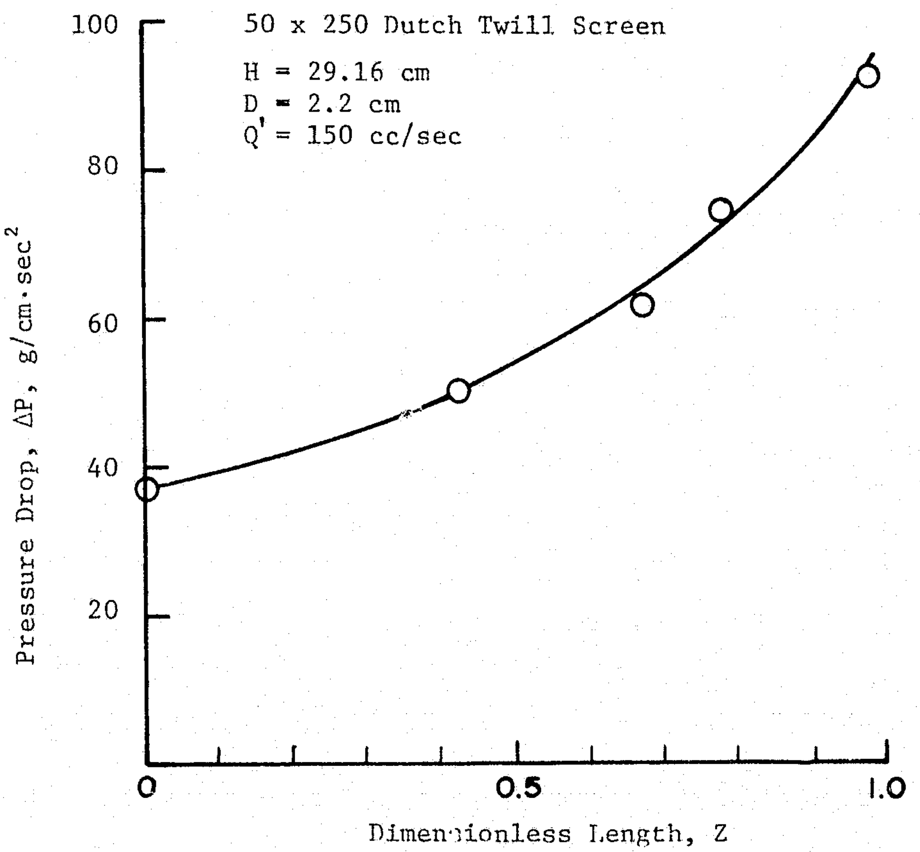

Figure 2-20 ΔP versu Q - 150 cm³/sec, D = 2.2 cm

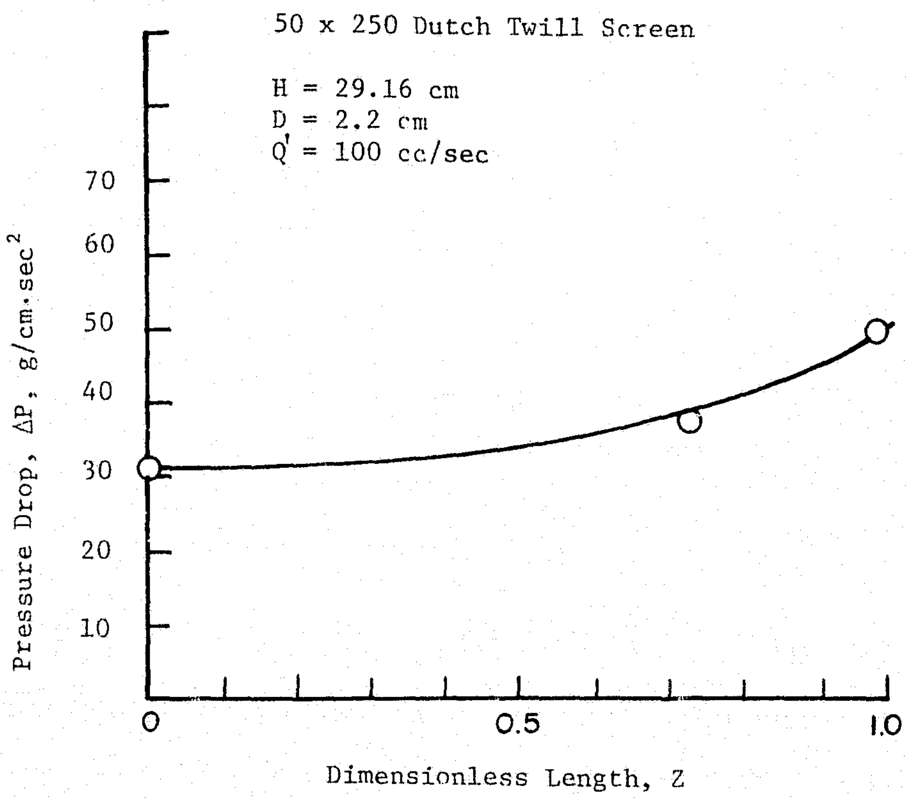

Figure 2-21 ΔP versus Z, Q = 100 cm³/sec, D = 2.2 cm

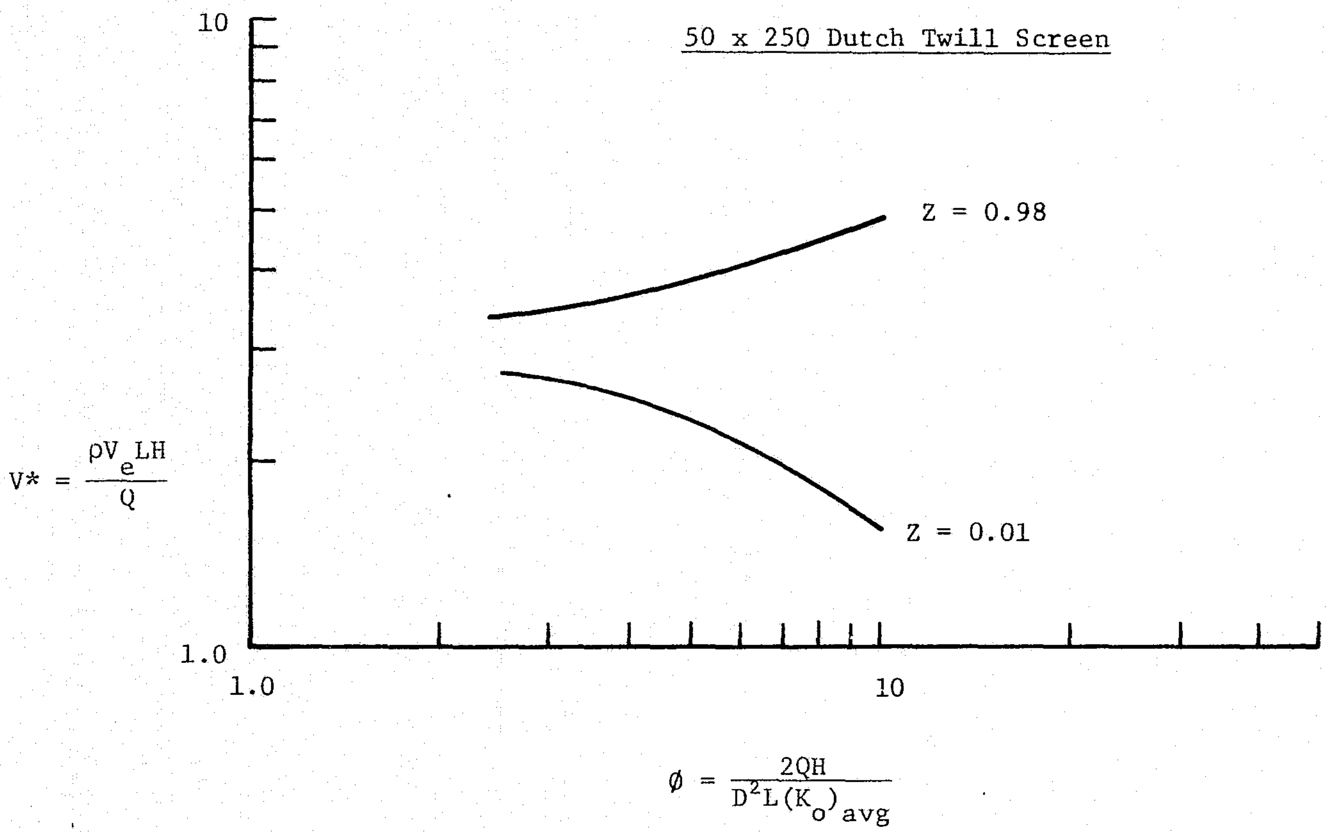

Figure 2-22
V* versus ϕ, UAH Experimental Results

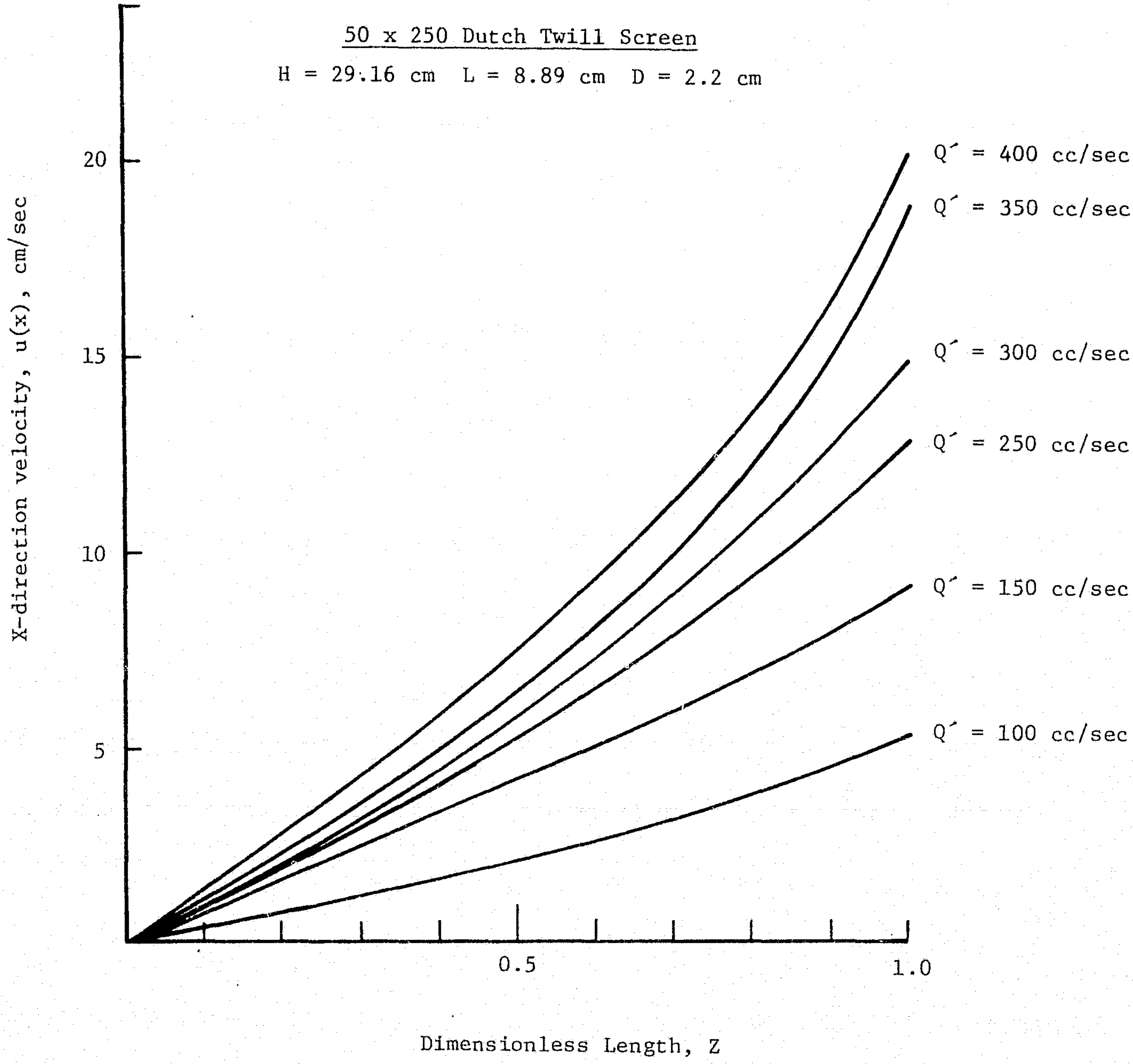

Figure 2-23
Horizontal Velocity as a Function of Z

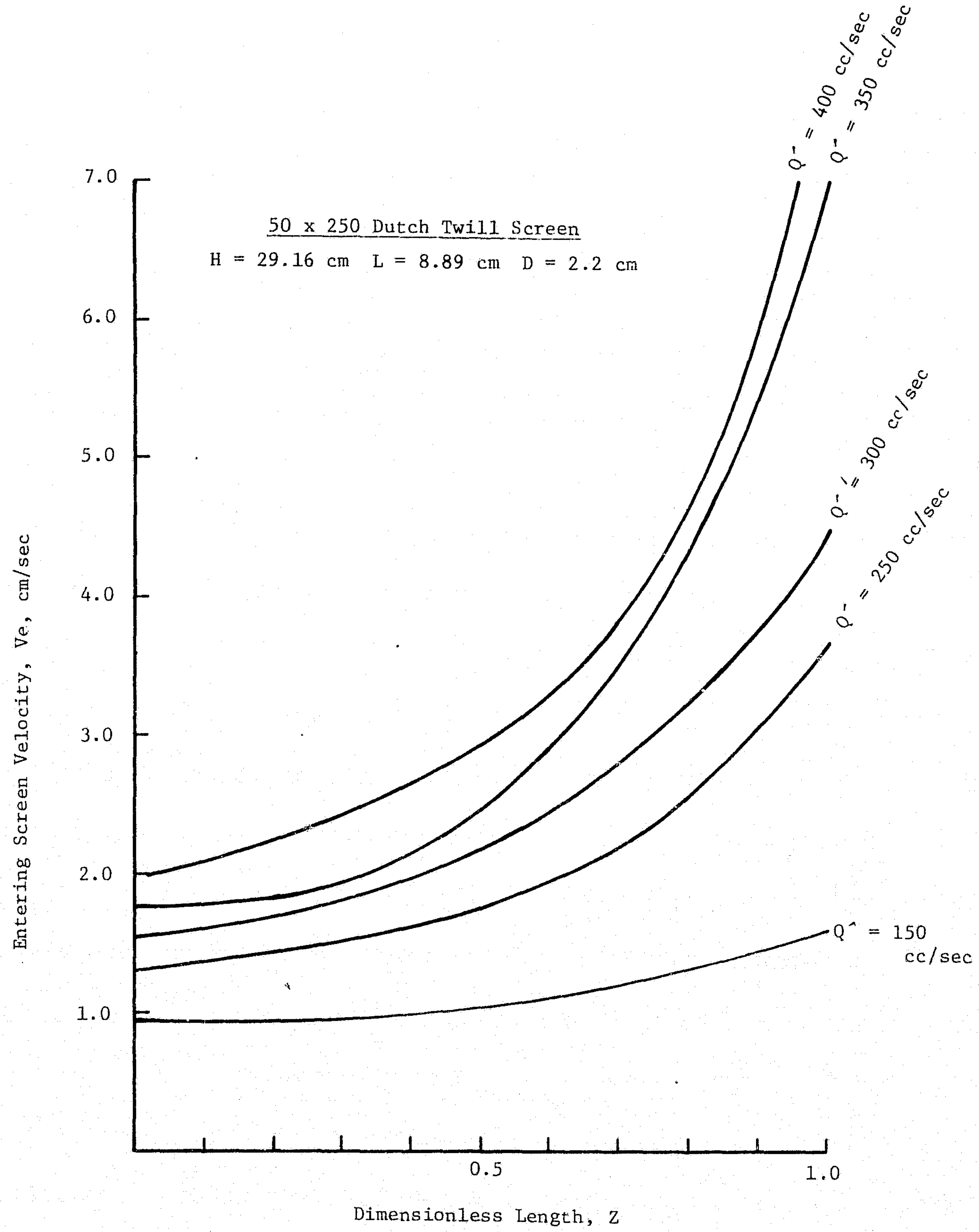

Figure 2-24

Vertical Entering Screen Velocity as a Function of Z

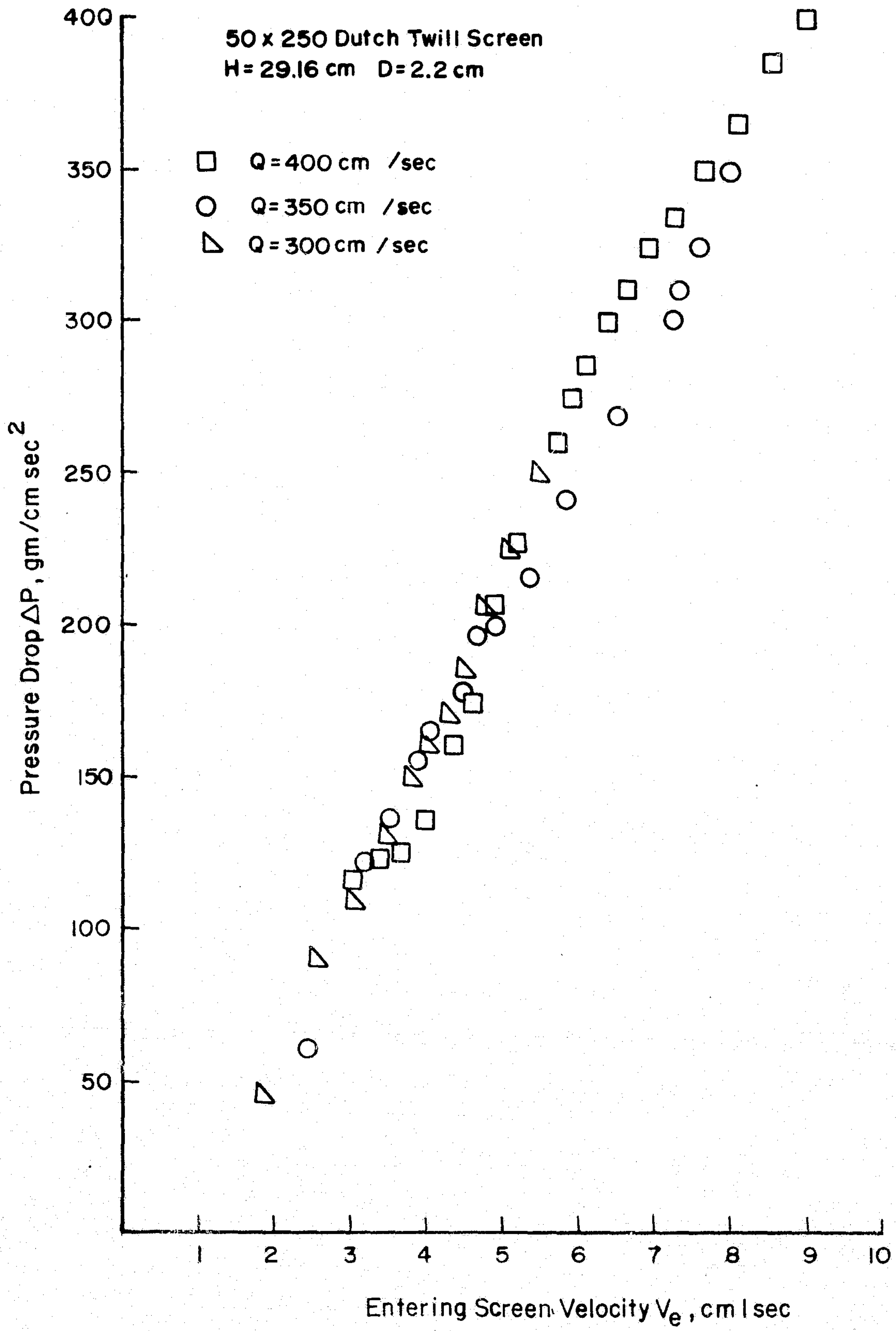

Figure 2-25 Pressure Drop as a Function of Entering Screen Velocity

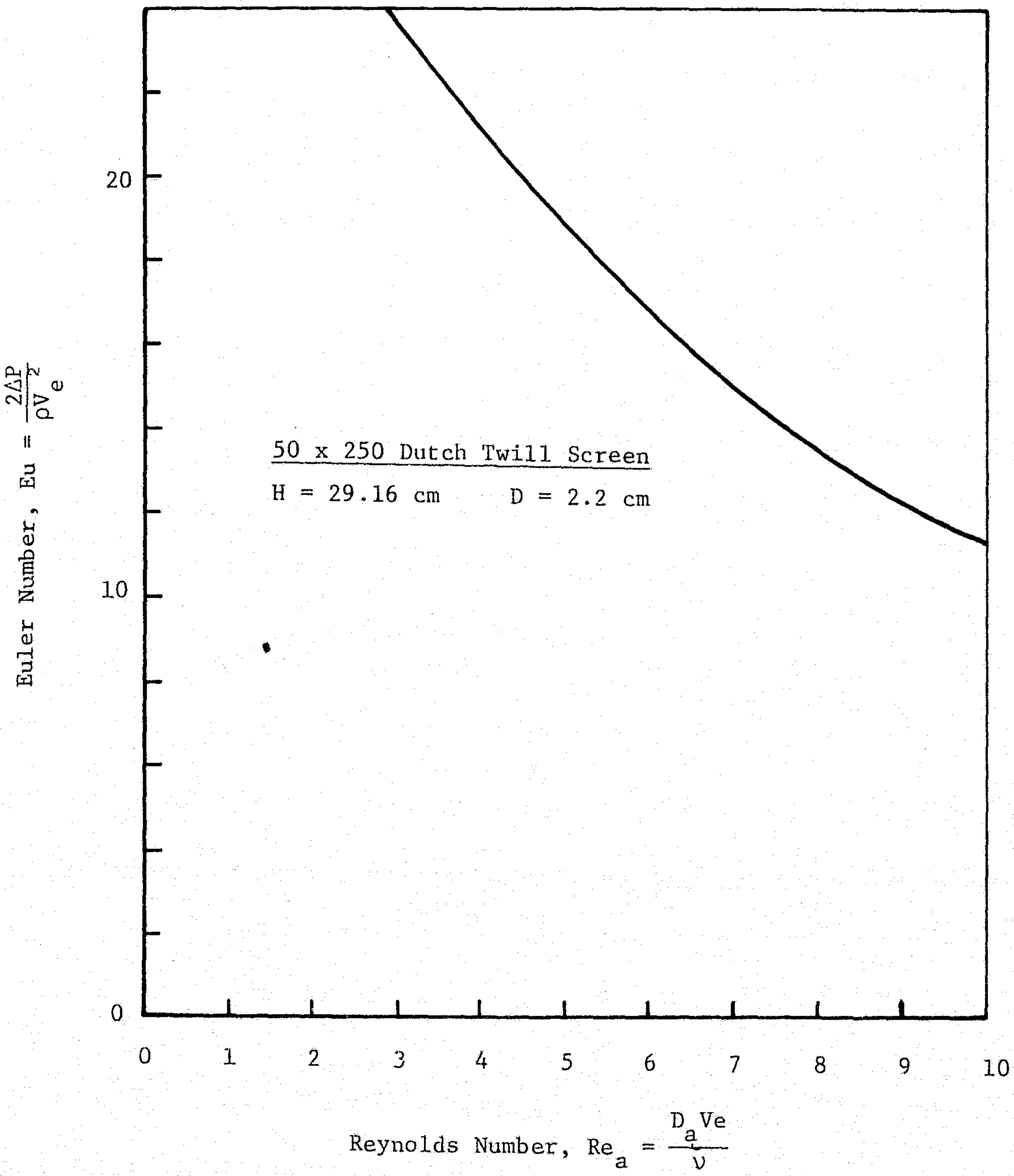

Figure 2-26 Euler Number versus Reynolds Number (Based on Figure 2-25)

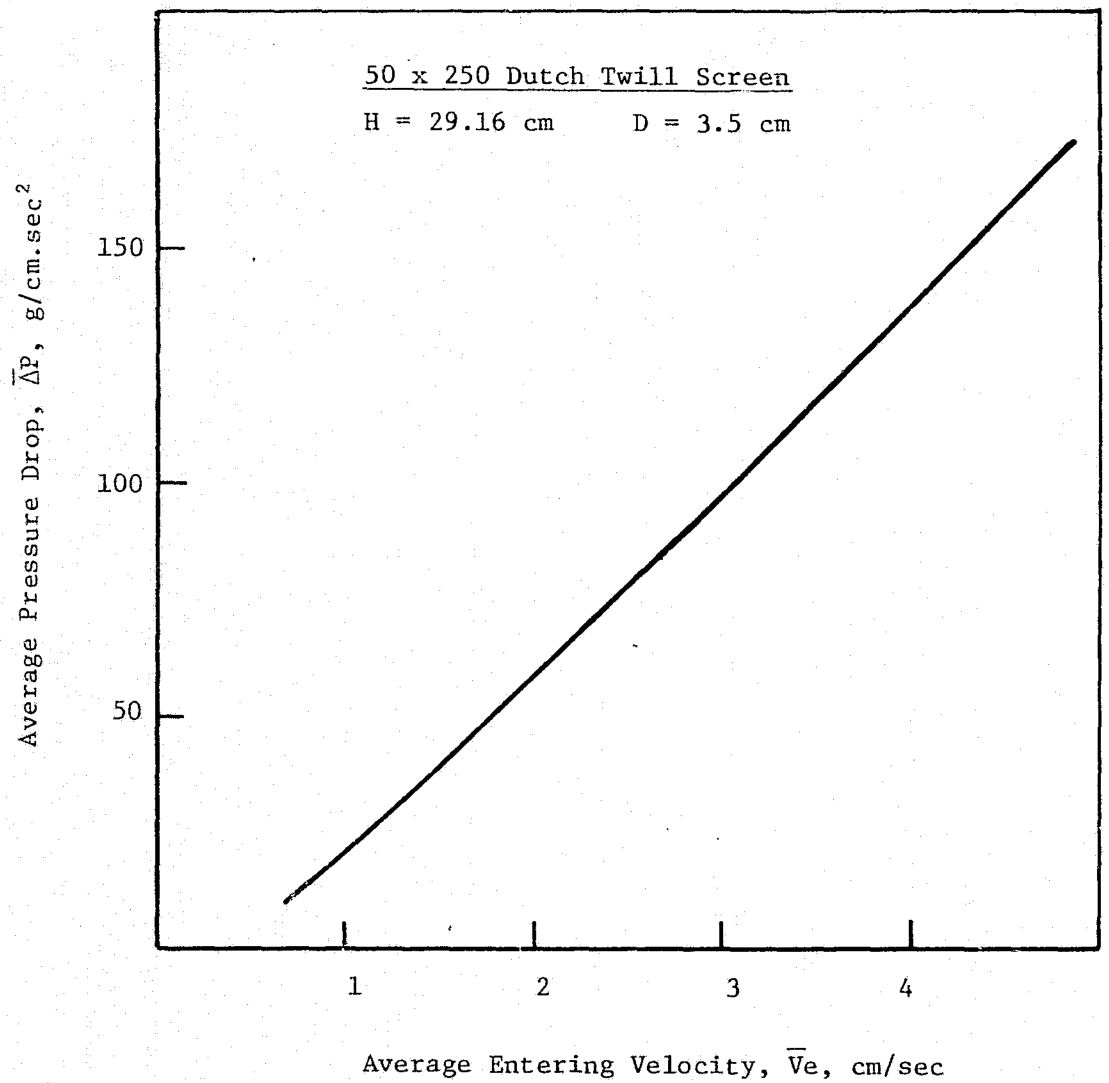

Figure 2-27
Average Pressure Drop Versus Average Entering Velocity, D - 2.2 cm

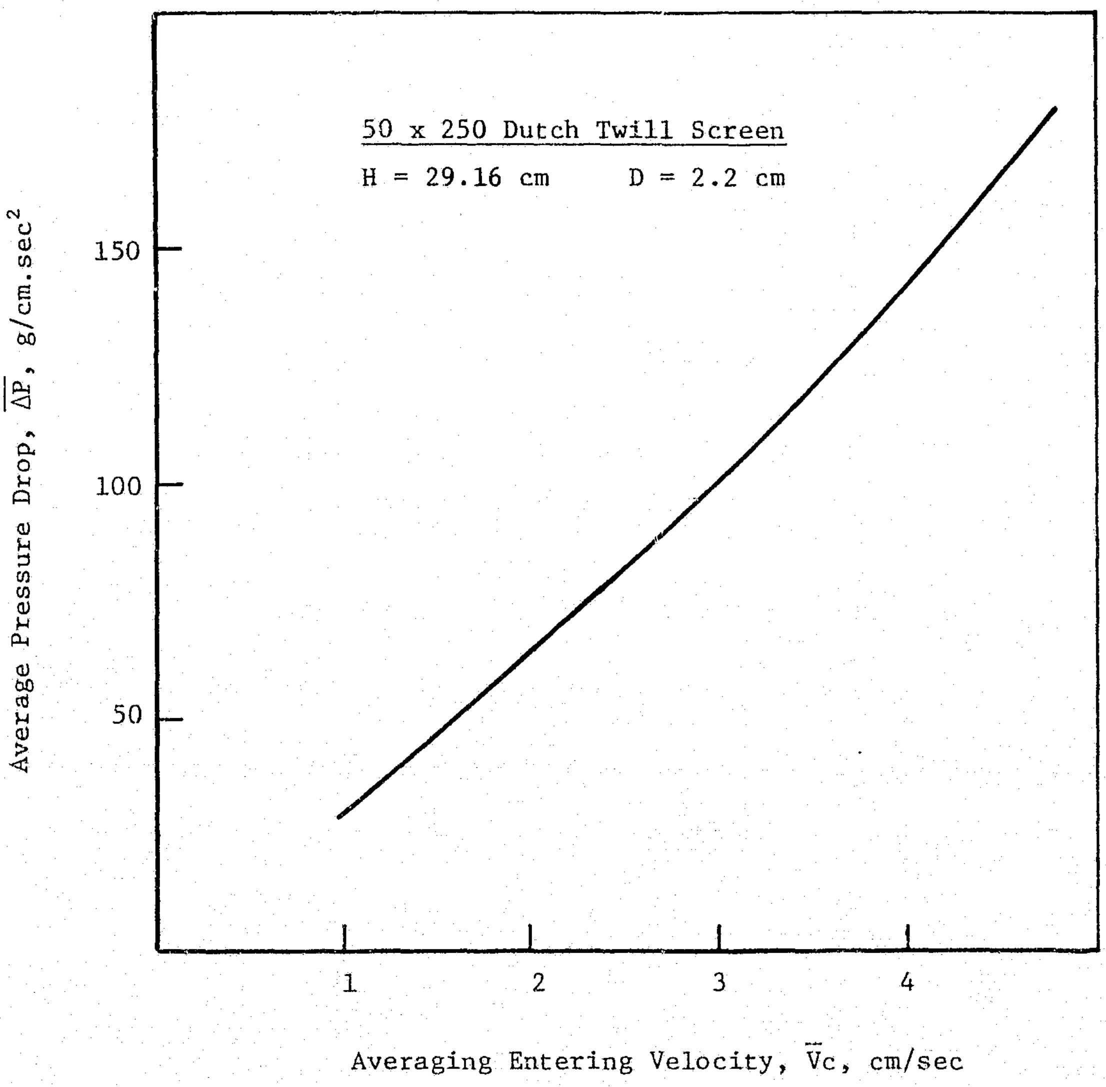

Figure 2-28

Average Pressure Drop Versus Average Entering Velocity, D = 2.2 cm.

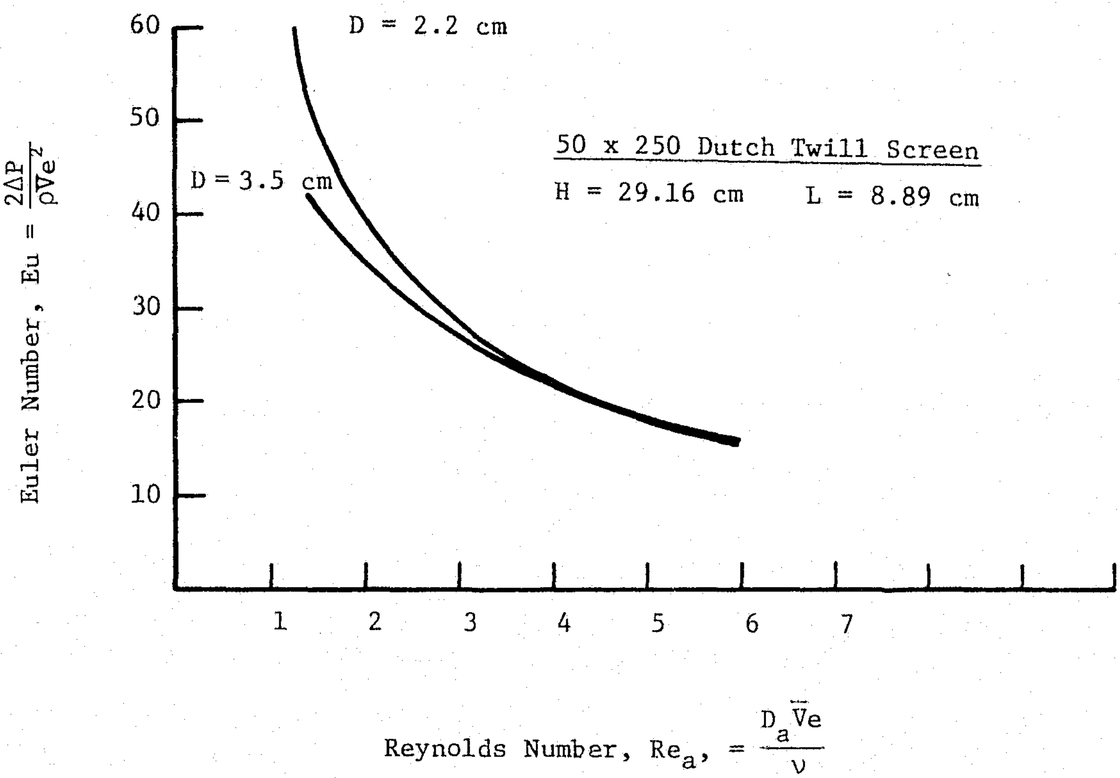

Figure 2-29

Euler Number Versus Reynolds Number (based on average pressure drop and average entering velocity).

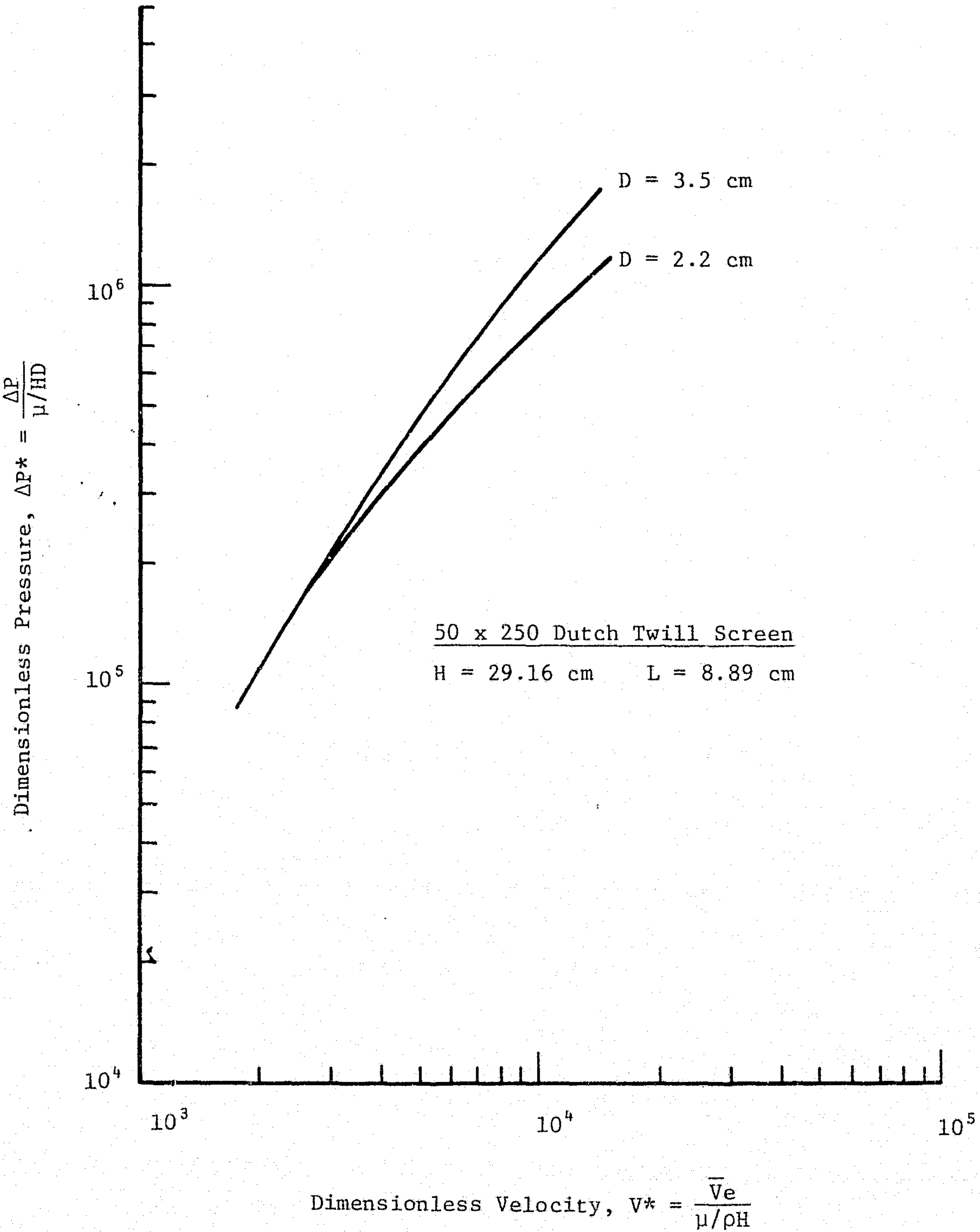

Figure 2-30 ΔP^* Versus V_e^*

APPENDIX A

This appendix contains the complete derivation of the continuity and momentum equations for the experimental model used at UAH.

The notation used in this appendix is the same as that used in Sections 1 and 2 of the report and listed in the definition of symbols.

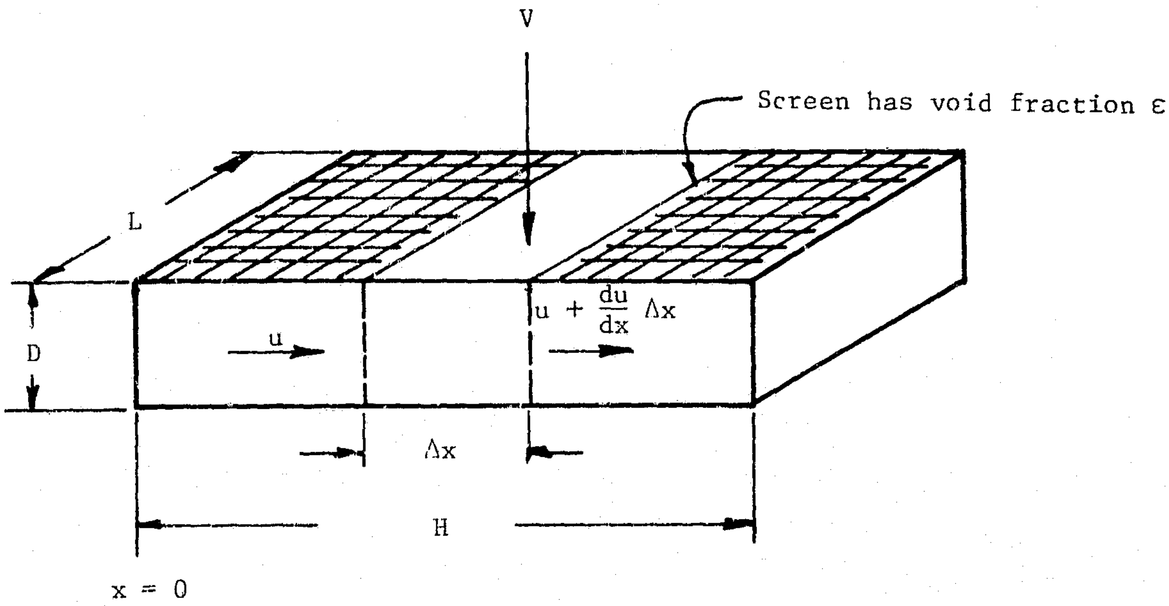

Continuity Equation

$$VL\Delta X\varepsilon = \left[u - \left(u + \frac{du}{dx}\Delta x\right)\right] LD \qquad (1)$$

dividing both sides by $L\Delta x$

$$V = \frac{D}{E}\ \frac{du}{dx} \qquad (2)$$

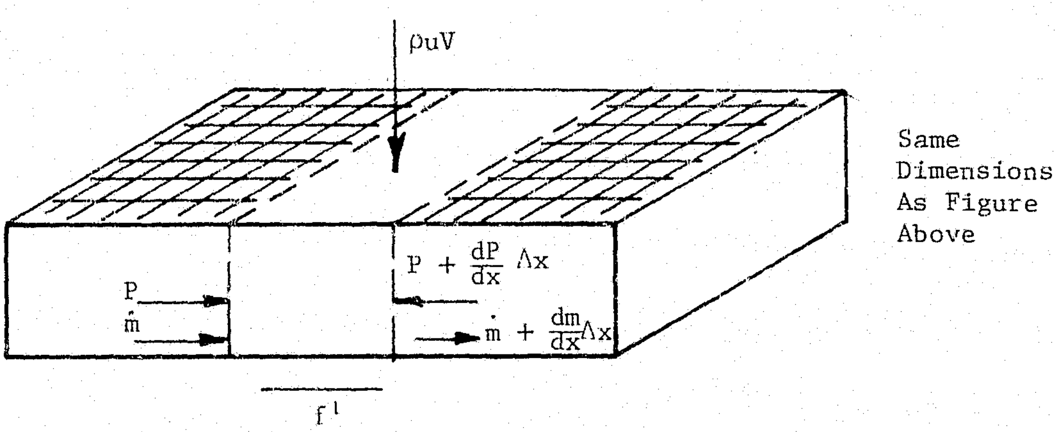

Momentum Equation

let $\dot{m} = \rho u^2$ (3)

$$m - (m+\frac{dm}{dx}\Delta x) \quad LD - \rho uVL\Delta x\varepsilon = \quad p + \frac{dp}{dx}\Delta x - p \quad LD + f'L\Delta x \tag{4}$$

simplifying (4)

$$- \frac{d}{dx} (\rho u^2)\Delta xLD - \rho uVL\Delta x\varepsilon = \frac{dp}{dx}\Delta x \; LD + f'L \; \Delta x \tag{5}$$

dividing both sides by ΔxLD

$$- \frac{d}{dx} (\rho u^2) - \frac{\rho uV\varepsilon}{D} = \frac{dp}{dx} + \frac{f'}{D} \tag{6}$$

rearranging

$$\frac{dp}{dx} + 2\rho u\frac{du}{dx} + \frac{uV}{D} + \frac{f'}{D} = 0 \tag{7}$$

from equation (2) $\frac{du}{dx} = \frac{V\varepsilon}{D}$

$$\frac{dp}{dx} + 3\rho u \frac{du}{dx} + \frac{f'}{D} = 0 \tag{8}$$

now, let $f' = f \cdot \frac{\rho u^2}{2}$, then

$$\frac{dp}{dx} + \frac{f\rho u^2}{2D} + 3 \rho u \frac{du}{dx} = 0 \tag{9}$$

C-2

Let us define

$$f' \equiv f \frac{\rho u^2}{2} \tag{7}$$

then Equation (6) is rewritten as

$$\frac{dP}{dx} + 3\rho u \frac{du}{dx} + f \frac{\rho u^2}{2D} = 0 \tag{8}$$

Nondimensionalizing Equation (8)

Equation (8) is written in a nondimensionalized form as

$$\frac{d^2u*}{dz^2} - F\phi\ u*^2 - \phi\, u* \frac{du*}{dz} = 0 \tag{13}$$

with the boundary condition

$$u* = 0 \qquad \text{at } Z = 0 \tag{14}$$

$$u* = 1 \qquad \text{at } Z = 1 \tag{15}$$

Let us omit the asterisk, *, from now on for convenience. Equation (13) will be numerically solved by utilizing the implicit finite difference technique of Crank-Nicolson as briefly introduced in the next section.

Numerical Solution

Defining the stations Z_{i-1}, Z_i, and Z_{i+1} as n-1, n, and n+1, respectively, as shown in the figure below:

we can write the first and second derivatives of velocity as

$$\frac{du}{dZ} = \frac{U_{n+1} - U_{n-1}}{2\Delta Z} \tag{16}$$

$$\frac{d\ U}{} = \frac{U_{n+1} - 2U_n + U_{n-1}}{\Delta Z^2} \tag{17}$$

Thus Equation (13) is expressed in a finite difference form as

$$\frac{U_{n+1} - 2U_n + U_{n-1}}{\Delta Z^2} - F\phi\ U_n U_n' - \phi U_n' \ \frac{U_{n+1} - U_{n-1}}{2\Delta Z} = 0 \tag{18}$$

where U_n' is an old value of U_n obtained by a previous iteration at station n.

We solve the equation below:

$$A_1\ U_{n-1} + A_2 U_n + A_3\ U_{n+1} = D_n \tag{19}$$

where

Coefficients of U_{n+1}:

$$A_3 = \frac{1}{\Delta Z^2} - \frac{\phi U_n'}{2\Delta Z} \tag{20}$$

Coefficients of U_n:

$$A_2 = \frac{2}{\Delta Z^2} - F\phi\ U_n' \tag{21}$$

Coefficients of U_{n-1}:

$$A_1 = \frac{1}{\Delta Z^2} + \frac{\phi U_n}{2\Delta Z} \tag{22}$$

$$D_n = 0 \tag{23}$$

The boundary condition at Z = 0 is $U_1 = 0$, thus Equation (19) gives

$$A(1,1)*U(1,JN)+A(1,2)*U(2,JN)$$
$$+A(1,3)*U(3,JN) = 0 \qquad (24)$$

$$U(1,JN) = 0 \qquad (25)$$

Therefore, we can set at Z = 0

$$\left.\begin{aligned} A(1,2) &= A(1,2) \\ A(1,3) &= A(1,3) \\ A(1,1) &= 0.0 \\ D(1) &= 0.0 \end{aligned}\right\} \qquad (26)$$

At A = 1, $U_{n_{max}} = 1$, then

$$A(NY2,1)*U(NY2, JN)+A(NY2,2)*U(NT1JN)$$
$$+A(NY2,3)*1.0 = 0 \qquad (27)$$

Therefore

$$\left.\begin{aligned} A(NY2,1) &= A(NY2,1) \\ A(NY2,2) &= A(NY2,2) \\ D(NY2) &= -A(NY2,3) \\ A(NY2,3) &= 0 \end{aligned}\right\} \qquad (29)$$

In the computer program the following symbols are defined:

$U(i,JN) = U_n$

$U(i,J\emptyset) = U_n'$

F $\doteq$ F

PHI $= \emptyset$

DZ $= \Delta Z$

VSTAR $= dU_n/dZ \ (\equiv dU^*/dZ)$

For a given combination of constants, F and ϕ the distribution of U_n along Z is calculated. Iterations are continued until a desired convergence is obtained. The definition of convergence is

$$\left| \frac{\frac{U_{n\ max}}{2} - \frac{U'_{n\ max}}{2}}{\frac{U_{n\ max}}{2}} \right| \leq \text{CONV.}$$

APPENDIX B

```
@FOR,IS MAIN,MAIN
C
      COMMON/BLUE/U(250,2),DZ,NY,NY1,NY2,Z(250),D(250),A(250,3)
      COMMON/PINK/PHI,F
      COMMON/WHIYE/ JO,JN
C
      NY=50
      NY1=NY-1
      NY2=NY-2
      DPHI=0.10
      JN=1
      JO=2
      DZ=1.0/FLOAT(NY1)
C
    1 F=0.10
    2 PHI=0.10
    5 CONTINUE
      DO 10 I=2,NY
   10 Z(I)=DZ*FLOAT(I-1)
      Z(1)=0.0
C
C     U-PROFILE TO INITIATE CALCULATION
C
      DO 20 I=1,NY
   20 U(I,JO)=Z(I)
C
      CALL GREEN
      CALL PRINT
      IF(PHI.LT.1.0) PHI=PHI+DPHI
      IF(PHI.GE.1.0) PHI=PHI+1.0
      IF(PHI.LE.15.0) GO TO 5
      F=F+0.10
      IF(F.GT.1.0) STOP
      GO TO 2
      END
@FOR,IS GREEN,GREEN
      SUBROUTINE GREEN
C
      COMMON/BLUE/U(250,2),DZ,NY,NY1,NY2,Z(250),D(250),A(250,3)
      COMMON/PINK/  PHI,F
      COMMON/WHIYE/ JO,JN
      M=NY/2
      NMAX = 250
      ITMAX=100
      IT = 0
      Z1=1.0/(DZ*DZ)
      Z2=0.50/DZ
  100 CONTINUE
      I=2
   10 A(I-1,1) = Z1 + Z2*PHI*U(I,JO)
      A(I-1,2)=-2.0*Z1-PHI*U(I,JO)*F*2.0/3.0
      A(I-1,3)=-A(I-1,1)+2.0*Z1
      D(I-1)=0.0
      I=I+1
```

```
      IF (I.LE.NY1) GO TO 10
C     MODIFY FIRST AND LAST EQUATIONS BY B.C.
      A(1,1)=0.0
      D(1)=0.0
      D(NY2)= -A(NY2,3)
      A(NY2,3)=0.0
C
C     SOLVE EQUATIONS FOR U(I,JN),I=2,3...NY1
C
      CALL TRIM (A,U(2,JN),D,NY2,NMAX)
C
C     APPLYB.C. FOR U(1,JN) AND U(NY,JN)
C
      U(1,JN)=0.0
      U(NY,JN)=1.0
C
      TEST=(U(M,JN)-U(M,JO))/U(M,JN)
      IF(ABS(TEST).LE.0.010.OR.IT.GT.ITMAX) GO TO 40
      IT=IT+1
      DO 20 K=1,NY
   20 U(K,JO)=U(K,JN)
      GO TO 100
   40 WRITE(6,30) IT
   30 FORMAT (10X,20HNUMBER OF ITERATION=,I5/)
      RETURN
      END
@FOR,IS TRIM,TRIM
      SUBROUTINE   TRIM (A,X,D,N,NN)
C
      DIMENSION   A(NN,3),AA(250),D(NN),DD(250),X(NN)
C
C     ***FORWARD TO ELIMINATION ****
C
      AA(1)=A(1,3)/A(1,2)
      DD(1)=D(1)/A(1,2)
      DO 1 I=2,N
      AAA=A(I,2)-AA(I-1)*A(I,1)
      AA(I)=A(I,3)/AAA
C
    1 DD(I)=(D(I)-DD(I-1)*A(I,1))/AAA
C
C     *** BACK SUBSTITUTION ***
C
      X(N)=DD(N)
      DO 2 I=2,N
      J=N-I+1
    2 X(J)=DD(J)-X(J+1)*AA(J)
      RETURN
      END
@FOR,IS PRINT,PRINT
      SUBROUTINE PRINT
C
      COMMON/BLUE/U(250,2),DZ,NY,NY1,NY2,Z(250),D(250),A(250,3)
      COMMON/PINK/PHI,F
      COMMON/WHIYE/ JO,JN
C
      WRITE(6,10) F,PHI
```

```
   10 FORMAT(1H1,10X,4HF   =,0PE11.5,10X6HPHI   =,0PE11.5/)
      WRITE(6,20)
   20 FORMAT(4H NO.,10X4H Z   ,10X9H VELOCITY,10X8H OLDVEL.,10X5HVSTAR)
      I=1
   30 CONTINUE
      IF(I.GT.1.AND.I.LT.NY)  VSTAR=0.50*(U(I+1,JN)-U(I-1,JN))/DZ
      IF(I.EQ.1) VSTAR=0.50*(-U(3,JN)+4.*U(2,JN)-3.*U(1,JN))/DZ
      IF(I.EQ.NY) VSTAR=(U(NY,JN)-U(NY1,JN))/DZ
      WRITE(6,100) I,Z(I),U(I,JN),U(I,JO),VSTAR
  100 FORMAT(I5,0P4F16.7)
      I=I+1
      IF(I.GT.NY) RETURN
      GO TO 30
      END
@XQT
```

F = .10000 PHI = .10000+00

Z	VELOCITY	OLDVEL.	VSTAR
.0000000	.0000000	.0000000	.9827410
.0204082	.0200564	.0200520	.9827813
.0408163	.0401135	.0401048	.9828419
.0612245	.0601723	.0601594	.9829430
.0816327	.0802336	.0802164	.9830849
.1020408	.1002983	.1002768	.9832676
.1224490	.1203670	.1203414	.9834915
.1428571	.1404408	.1404111	.9837567
.1632653	.1605204	.1604868	.9840634
.1836735	.1806066	.1805692	.9844118
.2040816	.2007004	.2006593	.9848022
.2244898	.2208026	.2207580	.9852348
.2448980	.2409141	.2408660	.9857100
.2653061	.2610357	.2609844	.9862279
.2857143	.2811683	.2811139	.9867885
.3061224	.3013128	.3012556	.9873925
.3265306	.3214700	.3214102	.9880398
.3469388	.3416409	.3415786	.9887307
.3673469	.3618264	.3617619	.9894656
.3877551	.3820273	.3819608	.9902449
.4081633	.4022445	.4021763	.9910689
.4285714	.4224791	.4224094	.9919380
.4489796	.4427318	.4426609	.9928523
.4693877	.4630037	.4629318	.9938117
.4897959	.4832955	.4832231	.9948176
.5102041	.5036085	.5035356	.9958696
.5306122	.5239433	.5238704	.9969677
.5510204	.5443010	.5442283	.9981133
.5714286	.5646826	.5646104	.9993062
.5918367	.5850890	.5850176	1.0005466
.6122449	.6055212	.6054509	1.0018351
.6326531	.6259803	.6259113	1.0031722
.6530612	.6464670	.6463998	1.0045577
.6734694	.6669826	.6669174	1.0059928
.6938775	.6875280	.6874650	1.0074780
.7142857	.7081042	.7080438	1.0090131
.7346939	.7287122	.7286547	1.0105990
.7551020	.7493531	.7492988	1.0122357
.7755102	.7700279	.7699770	1.0139238
.7959184	.7907377	.7906905	1.0156643
.8163265	.8114836	.8114403	1.0174574
.8367347	.8322666	.8322275	1.0193031
.8571428	.8530878	.8530531	1.0212020
.8775510	.8739483	.8739181	1.0231557
.8979592	.8948493	.8948238	1.0251646
.9183673	.9157918	.9157712	1.0272280
.9387755	.9367770	.9367614	1.0293469
.9591837	.9578059	.9577955	1.0315222
.9795918	.9788799	.9788747	1.0337547
1.0000000	1.0000000	1.0000000	1.0348850

NUMBER OF ITERATION= 1

F = .10000 PHI = .10000+01

Z	VELOCITY	OLDVEL.	VSTAR
.0000000	.0000000	.0000000	.8474300
.0204082	.0172976	.0173427	.8477306
.0408163	.0346012	.0346914	.8481824
.0612245	.0519172	.0520521	.8489375
.0816327	.0692518	.0694310	.8499982
.1020408	.0866110	.0868341	.8513674
.1224490	.1040014	.1042677	.8530482
.1428571	.1214293	.1217380	.8550441
.1632653	.1389012	.1392514	.8573595
.1836735	.1564236	.1568142	.8599986
.2040816	.1740032	.1744331	.8629666
.2244898	.1916467	.1921147	.8662692
.2448980	.2093611	.2098656	.8699126
.2653061	.2271534	.2276929	.8739036
.2857143	.2450306	.2456036	.8782492
.3061224	.2630003	.2636047	.8829572
.3265306	.2810697	.2817038	.8880364
.3469388	.2992467	.2999083	.8934958
.3673469	.3175389	.3182260	.8993453
.3877551	.3359546	.3366649	.9055953
.4081633	.3545020	.3552330	.9122569
.4285714	.3731896	.3739388	.9193424
.4489796	.3920262	.3927910	.9268645
.4693877	.4110208	.4117985	.9348370
.4897959	.4301828	.4309706	.9432753
.5102041	.4495218	.4503168	.9521947
.5306122	.4690479	.4698470	.9616116
.5510204	.4887713	.4895715	.9715444
.5714286	.5087028	.5095008	.9820119
.5918367	.5288534	.5296462	.9930344
.6122449	.5492348	.5500189	1.0046338
.6326531	.5698589	.5706310	1.0168331
.6530612	.5907382	.5914949	1.0296569
.6734694	.6118857	.6126236	1.0431312
.6938775	.6333150	.6340307	1.0572840
.7142857	.6550401	.6557301	1.0721458
.7346939	.6770760	.6777368	1.0877487
.7551020	.6994380	.7000663	1.1041259
.7755102	.7221424	.7227347	1.1213144
.7959184	.7452060	.7457589	1.1393536
.8163265	.7686466	.7691569	1.1582851
.8367347	.7924829	.7929474	1.1781534
.8571428	.8167345	.8171500	1.1990058
.8775510	.8414219	.8417855	1.2208937
.8979592	.8665669	.8668758	1.2438729
.9183673	.8921922	.8924437	1.2680020
.9387755	.9183221	.9185137	1.2933443
.9591837	.9449818	.9451115	1.3199678
.9795918	.9721983	.9722640	1.3479459
1.0000000	1.0000000	1.0000000	1.3622829

NUMBER OF ITERATION= 3

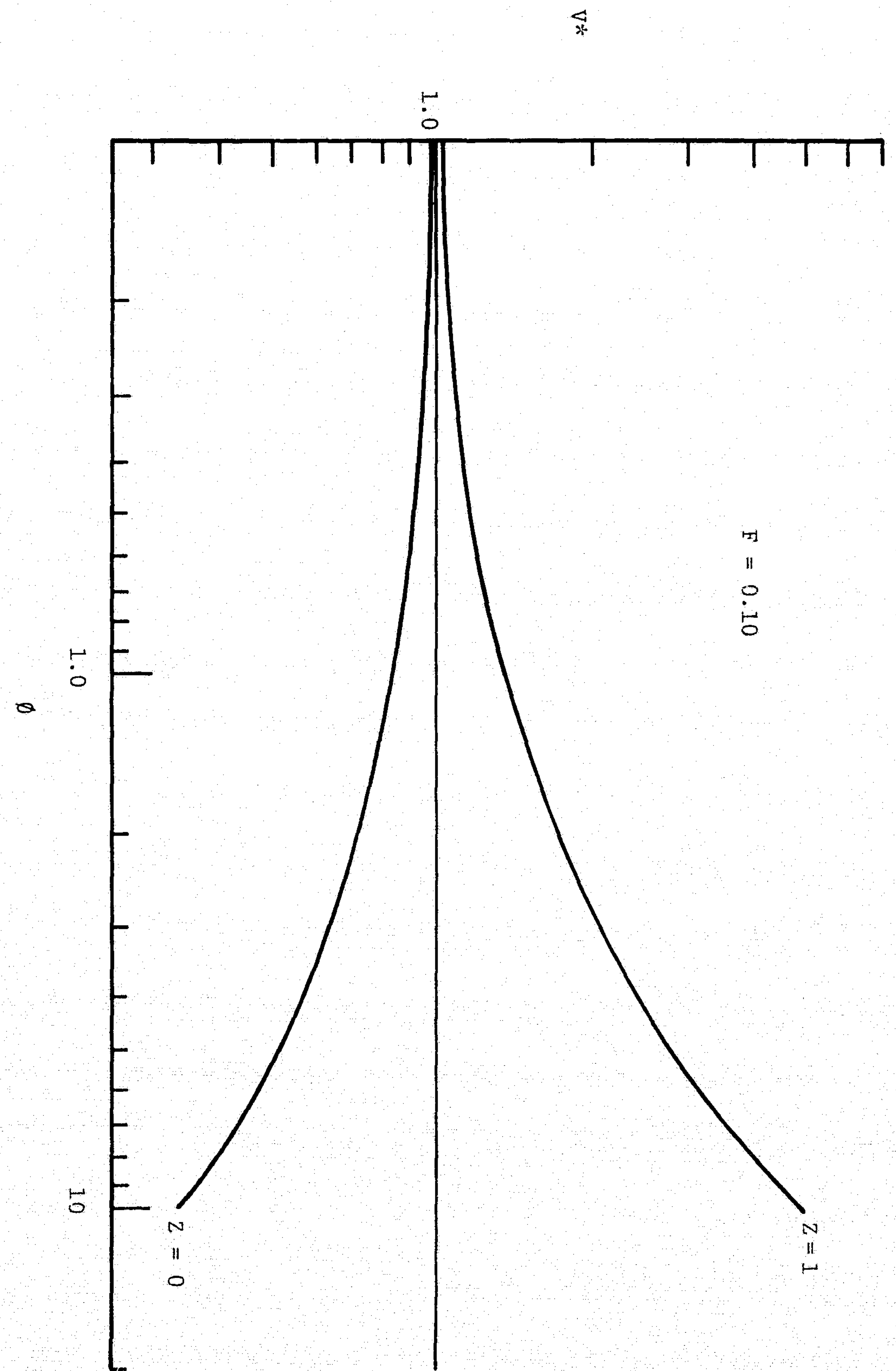

Figure B-1

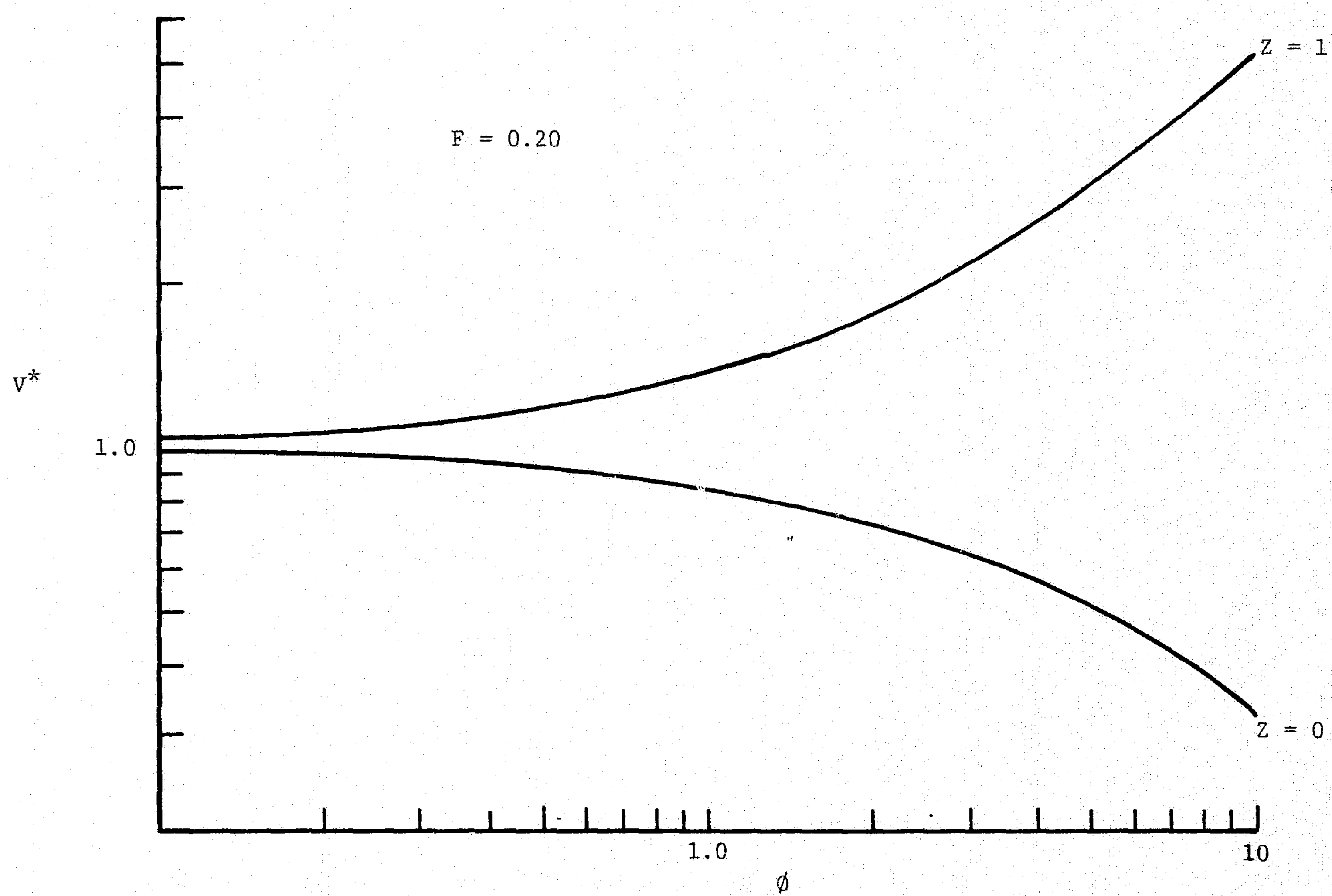

Figure B-2

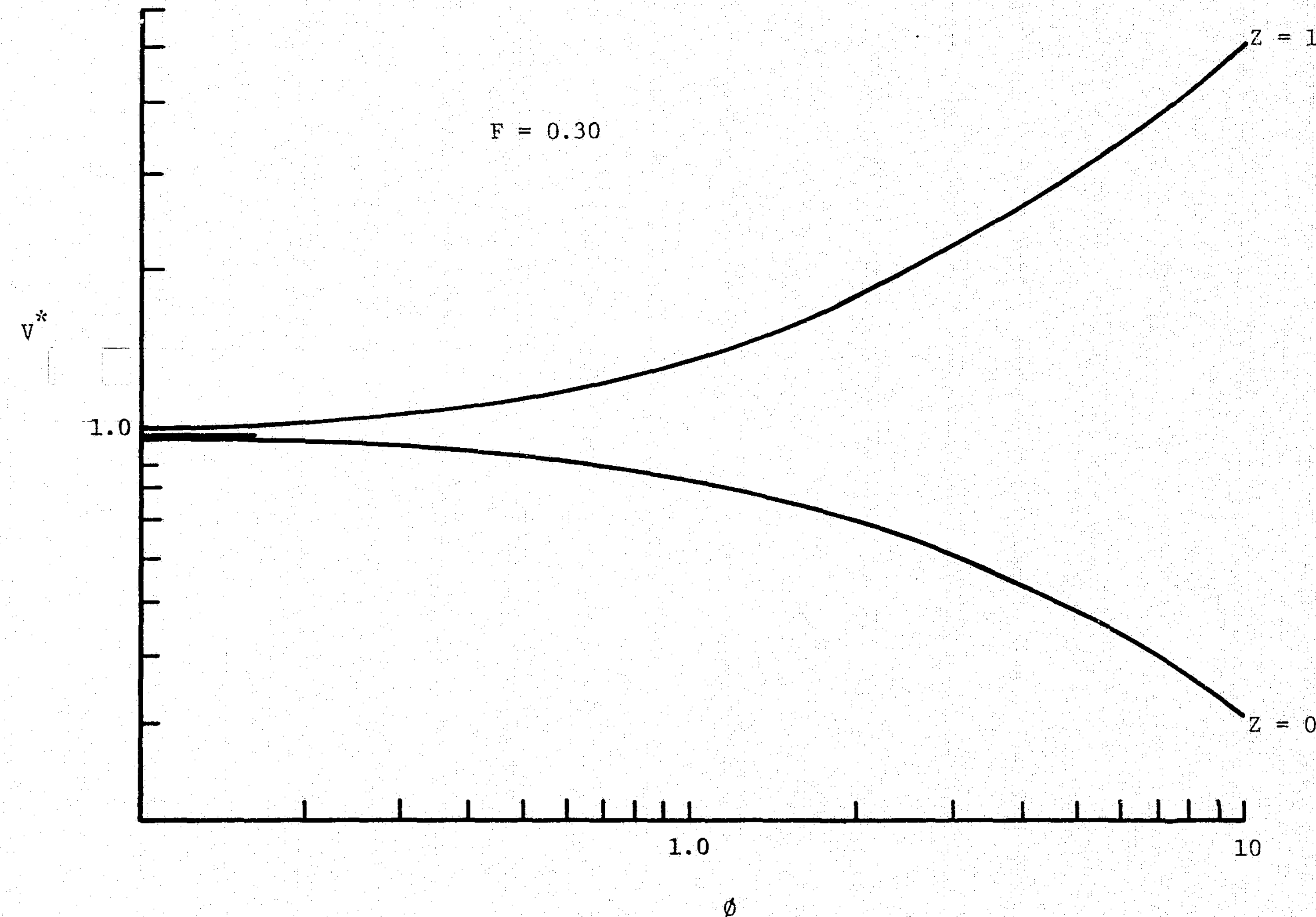

Figure B-3

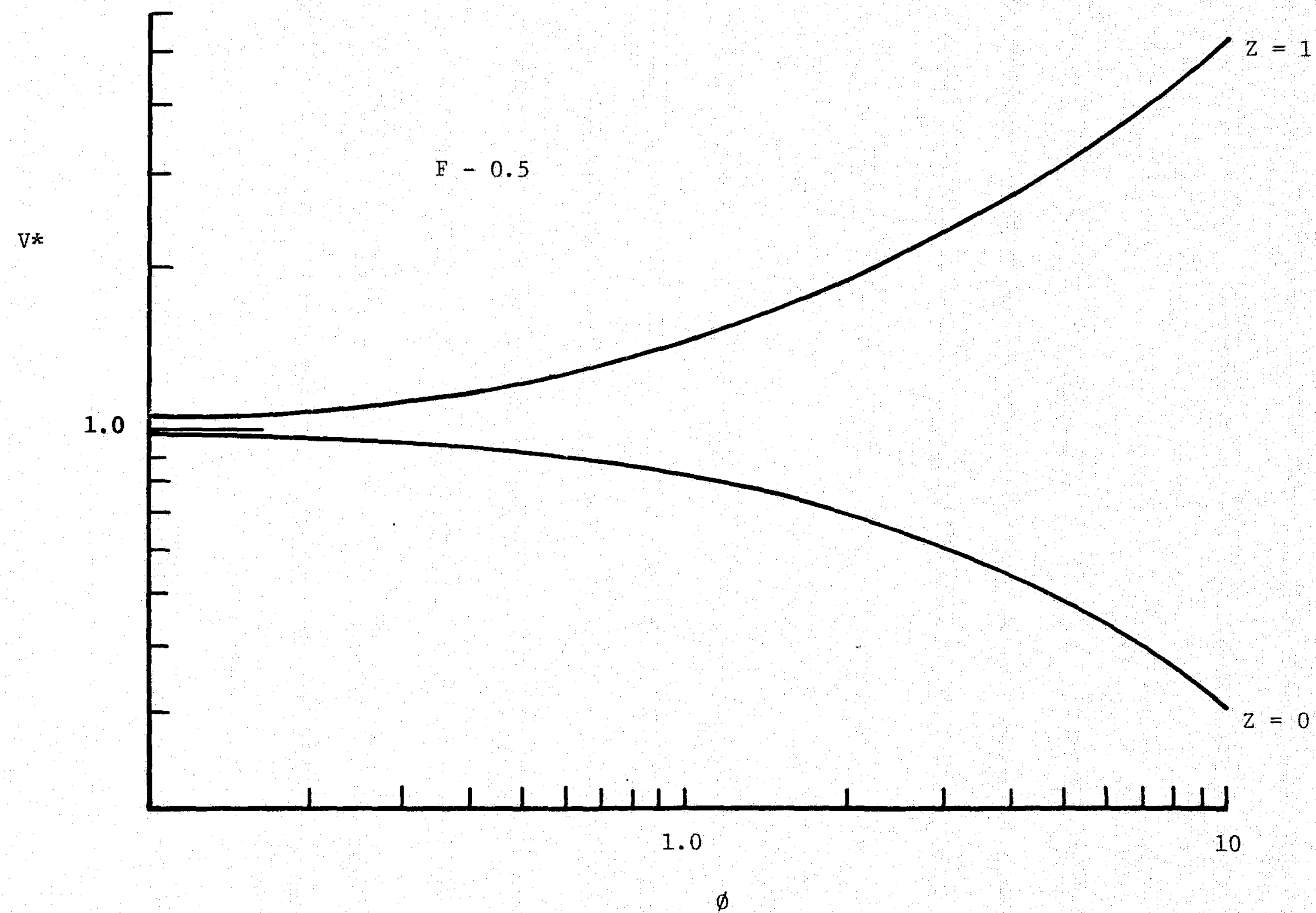

Figure B-4

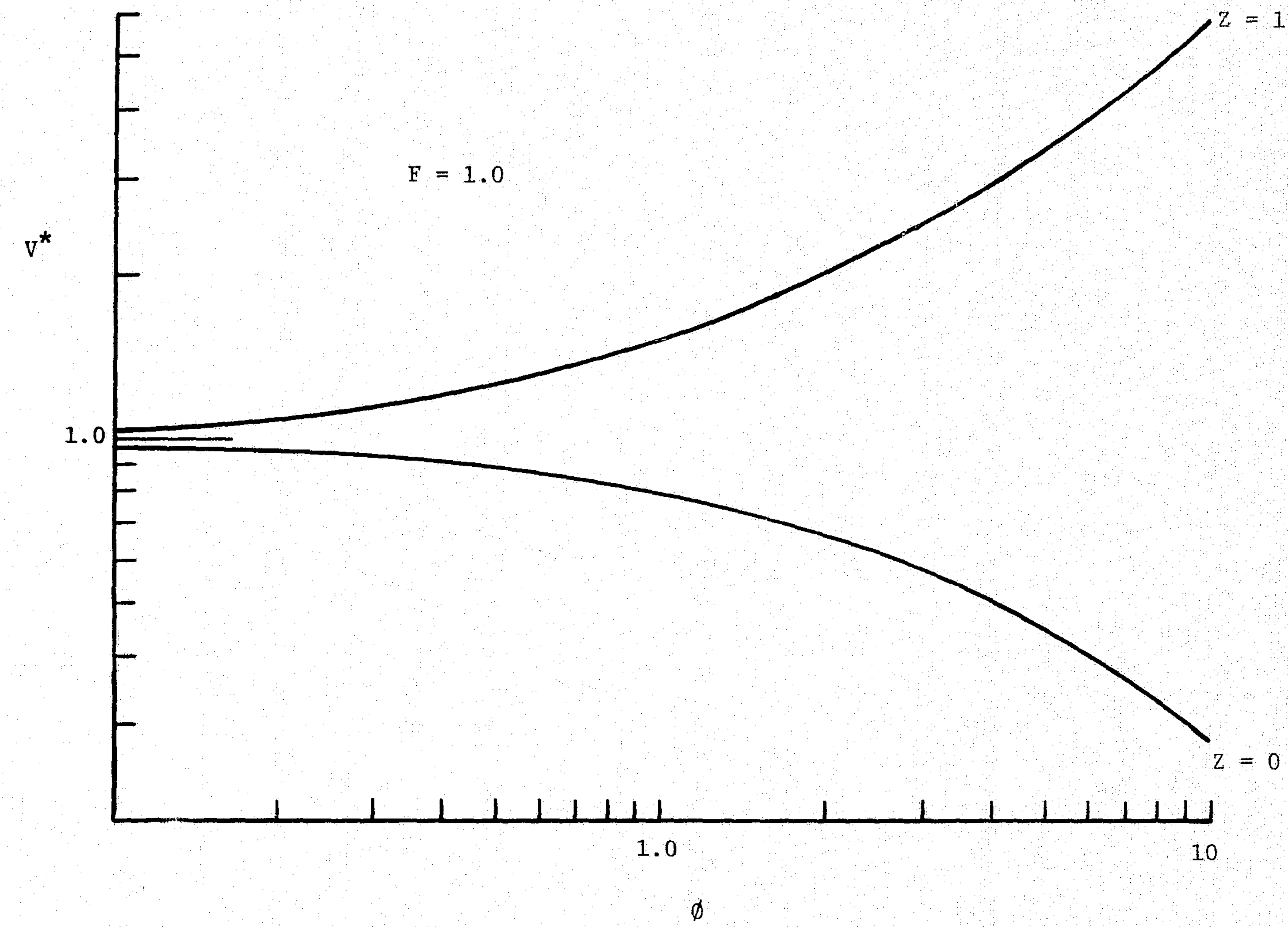

Figure B-5

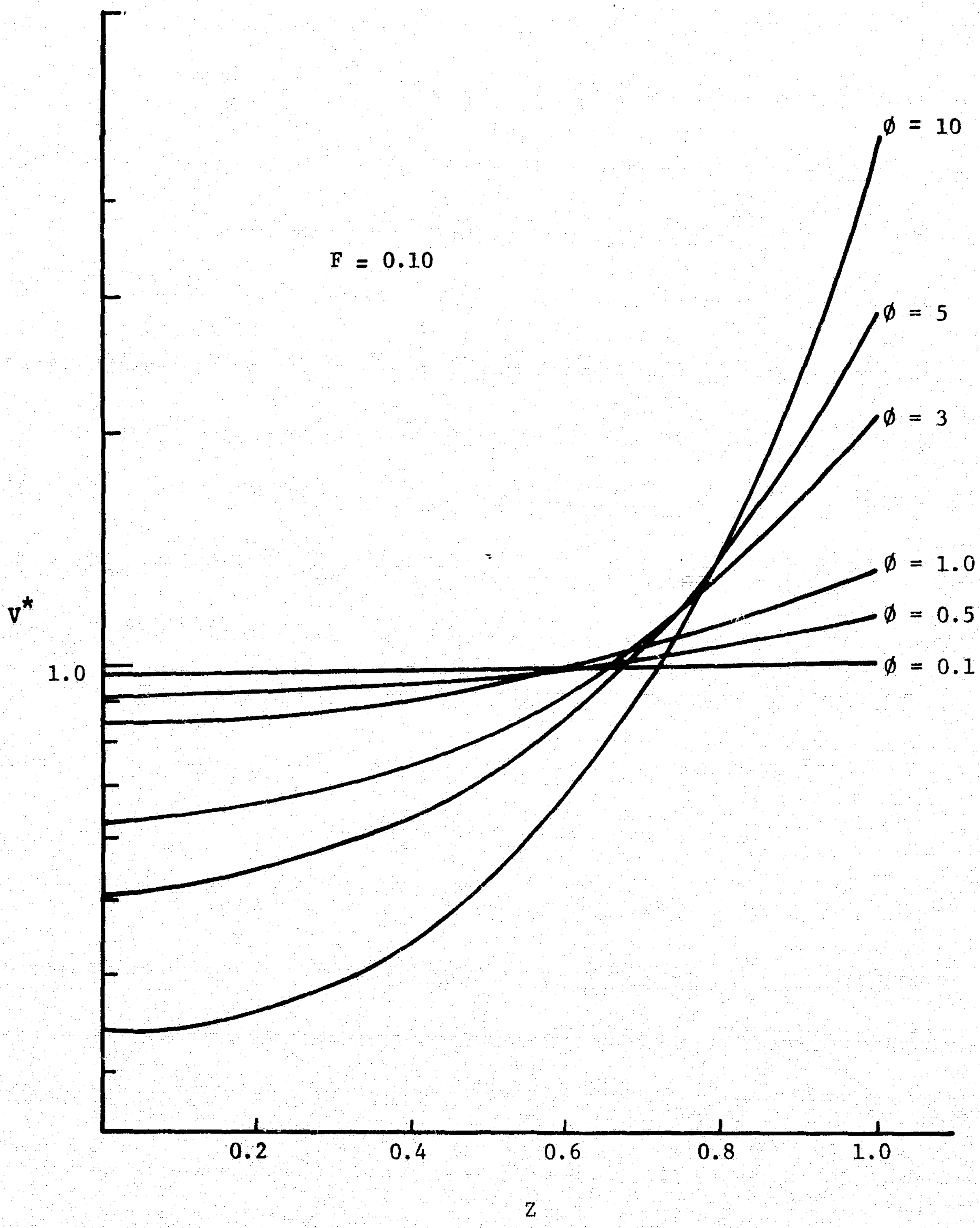

Figure B-6

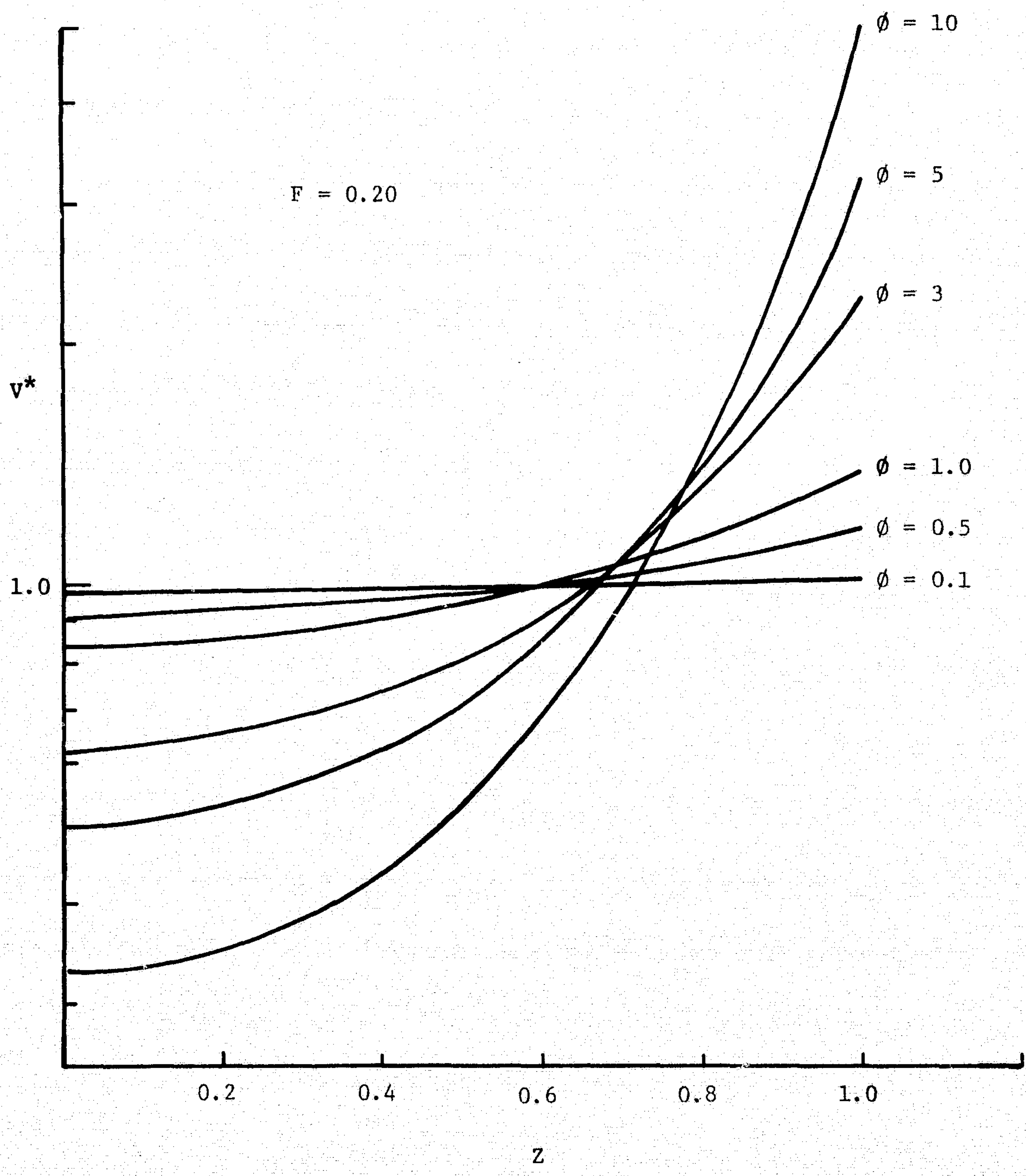

Figure B-7

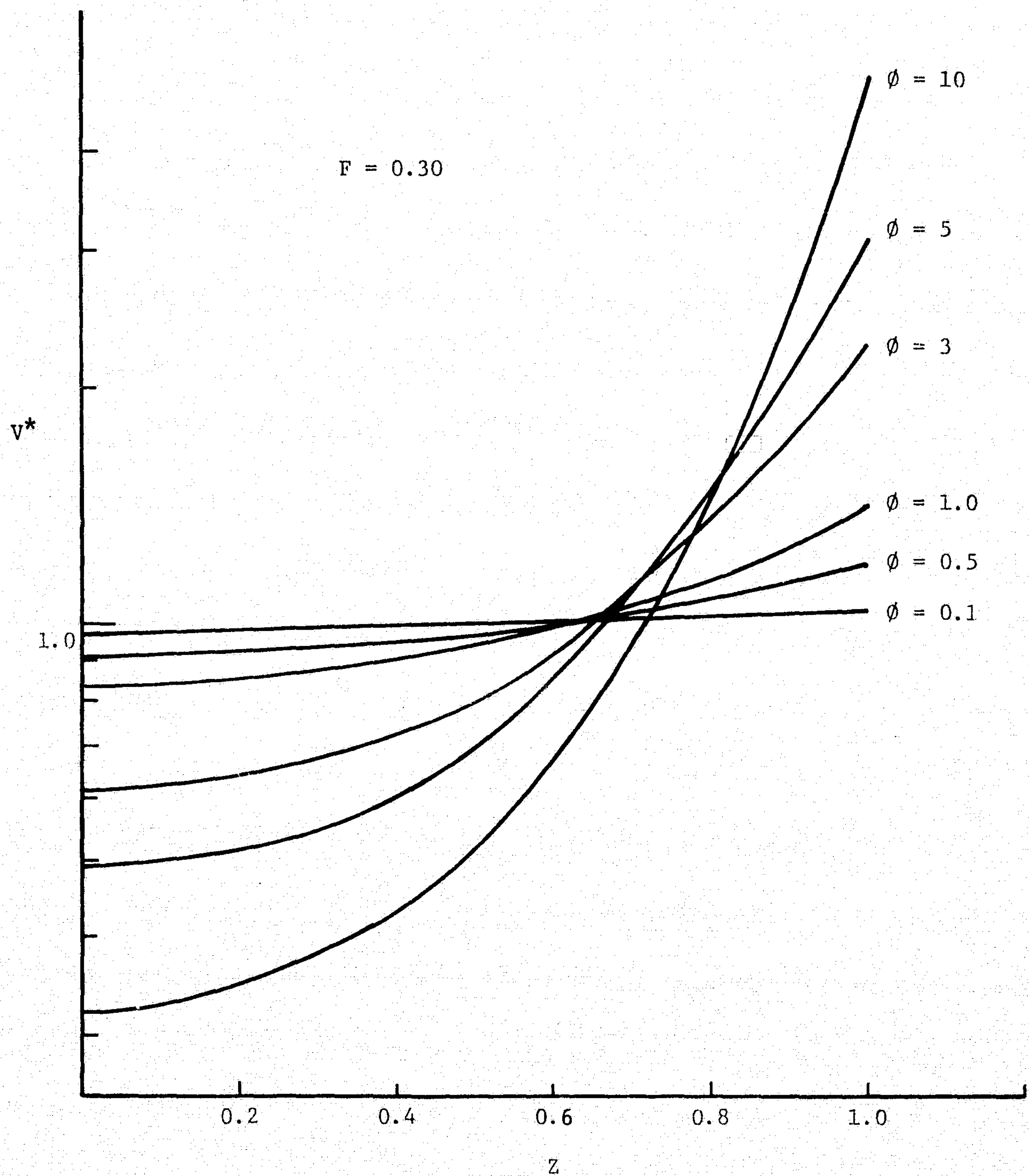

Figure B-8

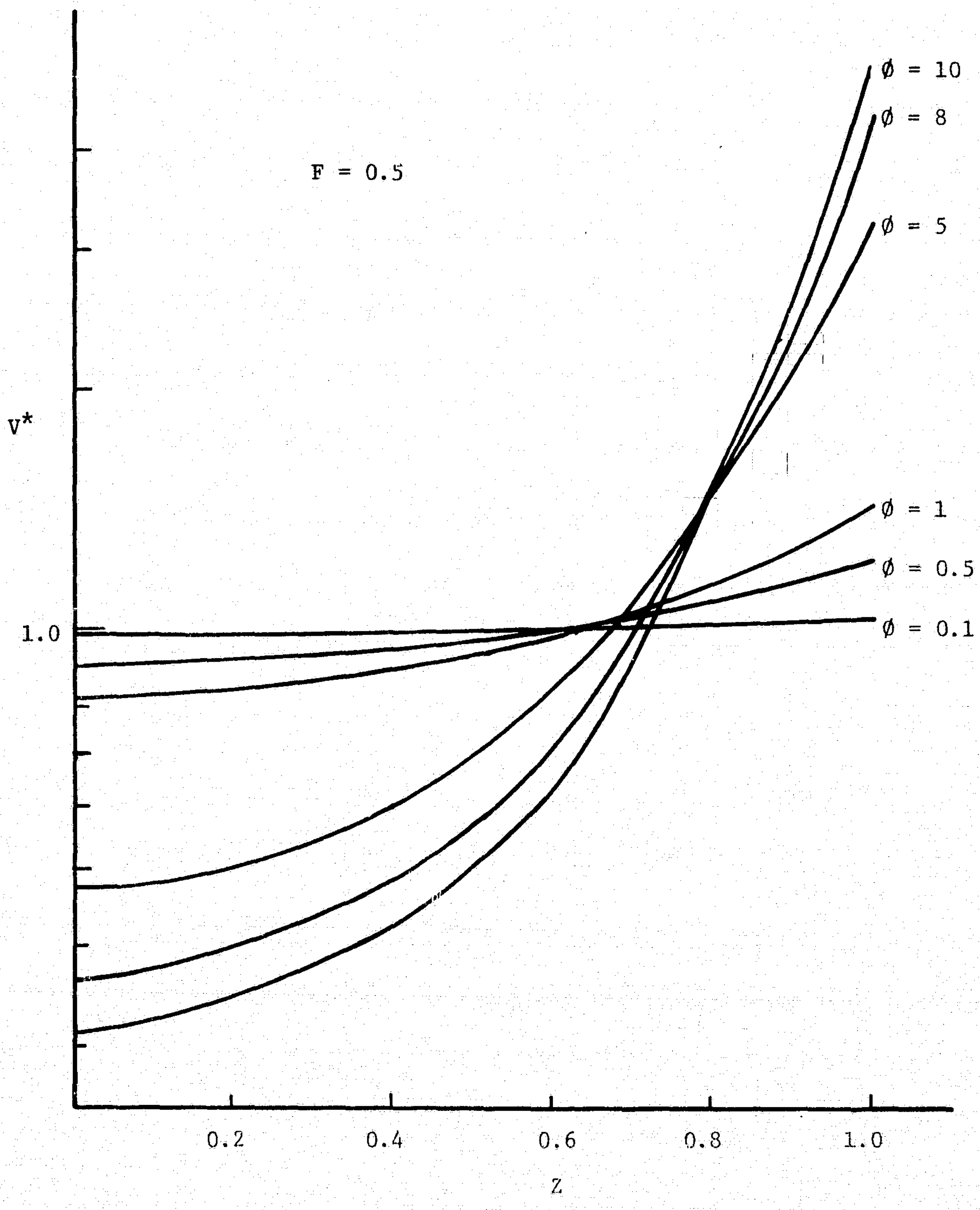

Figure B-9

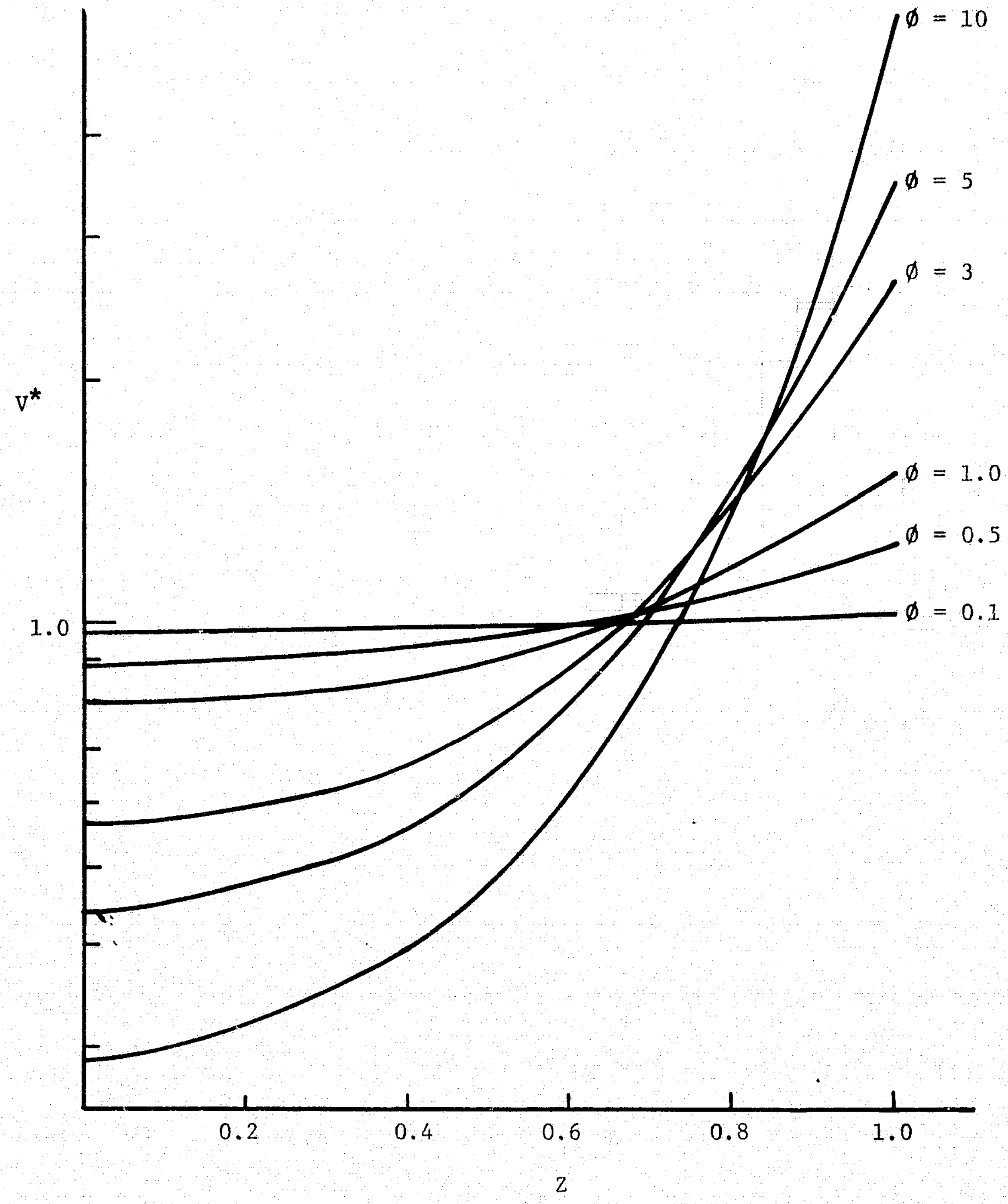

Figure B-10

CHAPTER II

INTRODUCTION

The experimental program mentioned in Chapter I is continued in Chapter II with slight modifications of the experimental system. The manifold system used in the earlier phase of the program had only four three-way stopcocks whereas the new manifold system used seven two-way stopcocks. This improvement facilitated in collecting the pressure drop data across the channel length at seven locations without disturbing the experimental setup. Several precautions were taken especially to eliminate airbubbles and to minimize the turbulence in the tank to obtain better and more accurate readings. Also two new screens (Dutch twill 200 x 200 and 325 x 325) were used during this phase of the project to investigate the pressure drop across the channel length. Three channel depths, namely 2.2, 2.85 and 3.5 cm, were used with the flow rates varying from 345 cc/sec to 65 cc/sec.

The second chapter of this portion of the report contains the theoretical consideration flow patterns in a rectangular channel followed by the summary of the experimental results.

SECTION 1
THEORETICAL CONSIDERATIONS

The fundamental physical laws of conservation of mass, momentum and energy, when applied to a continua, in most cases yield sufficient equations for evaluation of the flow parameters. These flow parameters are velocity, pressure and forces developed at a given region inside the continua. For our analysis we chose a control volume fixed in space and evaluated the flow parameters in an averaged integrated fashion. The choice of the control volume is arbitrary. However, in order to extract maximum information it is essential for the boundaries of the surface of the control volume to pass through regions where information is known and also where it is required. In most problems, several control volumes may be necessary for the formulation of a determinate set of equations. For clarity in presentation, we express the vector quantities, velocity, momentum and forces in their component form using the rectangular cartesian system (an appropriate system for our flow geometry). Hence, all the equations are scalar in nature.

1-1 Equations of Motion

The channel is shown in Fig. (1) and the dimensions are also marked on it. The control volume is shown in Figure (2). Figure (2) shows the mass flows, momenta and forces acting on the control volume as follows:

1-2 Conservation of Mass

Let u and v denote the x and y components of the velocity vector and p the density of the fluid flowing through the control

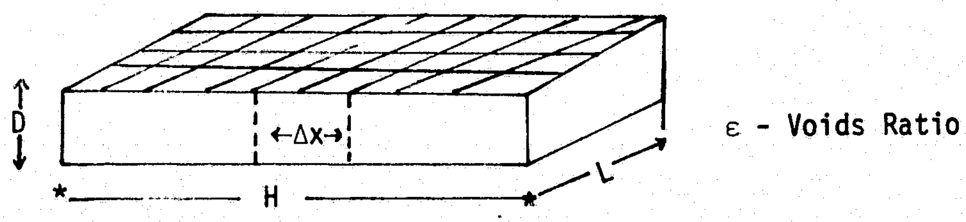

Figure 1. The Channel with the Screen

Consider the control volume shown in Figure 2.

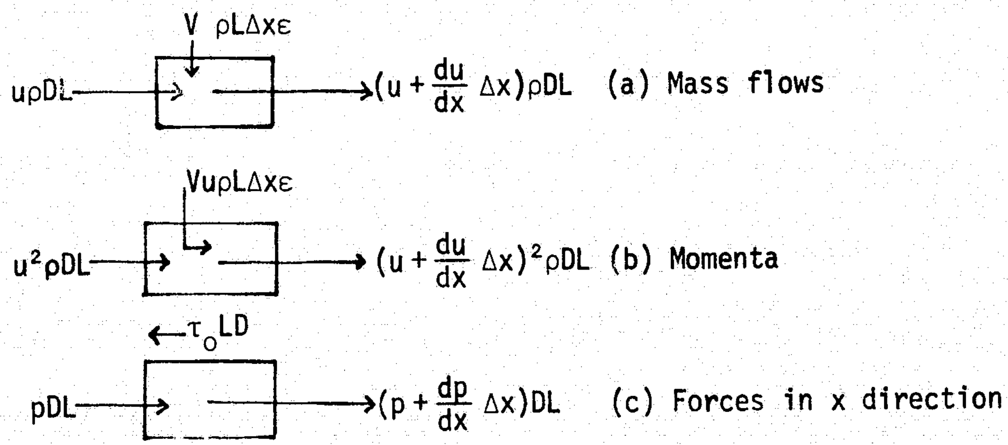

Figure 2. The Control Volume

volume. The control volume is a rectangular, parallelopiped with the dimensions of Δx, D and H in the x, y and z directions of the rectangular cartesian system. The voids ratio ε is introduced to calculate the actual area available for flow due to the pressure of the screen.

From Sketch (a):

Mass flow in = Mass flow out

$$v \rho L \Delta x \varepsilon + u \rho D L = u \rho D L + \frac{du}{dx} \Delta x \rho D L$$

or

$$v = \frac{D}{\varepsilon} \frac{du}{dx} . \tag{1}$$

In arriving at this result, we make the assumption that the velocity component u is a function of x only. This is approximately true because below the screen the velocity is predominately in the x direction.

1-3 Conservation of Momentum

We apply the law of conservation of momentum in component form in the x direction. In other words, we have to calculate the net efflux of x-momentum and equate it to the sum of the x-forces acting on the control volume. Since the forces in general can act in either direction, we adopt the sign convention that forces acting to the right are positive, whereas those acting to the left are negative.

The forces on the control volume are due to the pressure, p, of the fluid and also due to the shear stress, τ_o, acting on the control surface. Evaluation of the shear stress is not obvious; therefore, we have to adopt a suitable representation to do so. A conventional method is to introduce a friction factor, f, and to evaluate the losses in energy due to friction forces, as a fraction of the unit kinetic energy, $u^2/2g$. Several representations are therefore possible for relating the quantities

τ_o, f and u. One such formula for calculating the wall shear stress, τ_o, is to take the corresponding force acting opposite the direction of the flow, as $\tau_o L D$, thus the momentum equation becomes:

$$\Sigma F_x = (\text{momentum out} - \text{momentum in})\ \text{x-direction}$$

$$pDL - (p + \frac{dp}{dx}\Delta x)\ DL - \tau_o L D = (u + \frac{du}{dx}\Delta x)^2 \rho DL$$
$$- [u^2 \rho DL + v_u \rho L \Delta x \varepsilon] \tag{2}$$

since, $\tau_o = \dfrac{\rho f u^2}{2}$. (3)

By substituting equation (3) in equation (2) and neglecting terms containing Δx^2 and the simplified momentum equation we obtain:

$$\rho u \frac{du}{dx} + \frac{dp}{dx} + \frac{\rho f}{2D} u^2 = 0 \tag{4}$$

The purpose of the analysis is to solve for the flow parameters u, v and p. Equations (1) and (4) are insufficient since we have three unknowns. Therefore, we must obtain one more equation containing any or all of the terms (u, v, p).

There is no unique way to generate one more independent equation containing u, v and p. We will discuss two different methods, outlined as follows.

Method 1 - A successful method of relating p and v is to involve an experimentally determined constant, K (or parameter). Thus, the approach becomes quasi-analytical. Let us assume that

$$K_o V = p_o - p \tag{5}$$

The quantity p_o is a reference pressure introduced for ease in rendering the equations dimensionless at a later stage. In differentiating equation

(5) with respect to the independent variable x, we obtain,

$$- \frac{dp}{dx} = K_o \frac{dv}{dx} . \tag{6}$$

The term $\frac{dv}{dx}$ can be evaluated from equation (1) by simply obtaining the derivative with respect to x; thus,

$$\frac{dv}{dx} = \frac{D}{\varepsilon} \frac{d^2u}{dx^2} . \tag{7}$$

Substituting equation (7) in equation (5), we get

$$- \frac{dp}{dx} = K_o \frac{D}{\varepsilon} \frac{d^2u}{dx^2} . \tag{8}$$

Equation (8) facilitates elimination of the pressure gradient term, dp/dx, in equation (4) and thus yields a single ordinary non-linear differential equation for u. This equation is written as

$$K_o \frac{D}{\varepsilon} \frac{d^2u}{dx^2} - \rho u \frac{du}{dx} - \frac{\rho f}{2D} u^2 = 0. \tag{9}$$

If it is possible to solve this equation by using equation (1) and (5), we can determine v and p at any x location inside the control volume, as the solution for u from equation (9) is already known.

Alternatively, a totally different method is proposed here which obviates the necessity of the introduction of any new constants (e.g., K_o as in the method just discussed).

Method 2

Consider the control volume shown in figure (2). Applying the momentum equation in the Y direction, we obtain

$$\Sigma f_y = (\text{momentum out - momentum in}) \text{ Y-direction}$$

or

$$p_o L\Delta x - pL\Delta x + \rho g L\Delta x D = v^2 \rho L\Delta x.$$

Differentiating with respect to x we obtain

$$- \frac{dp}{dx} = 2\rho\varepsilon\, v \frac{dv}{dx} . \tag{10}$$

Substituting equation (1) and (7) for v and $\frac{dv}{dx}$ respectively in (10) yields

$$- \frac{dp}{dx} = 2\rho \frac{D^2}{\varepsilon} \frac{du}{dx} \frac{d^2u}{dx^2} \tag{11}$$

Now equation (11) for the pressure gradient can be employed in the x direction momentum equation to obtain an equation for u, namely,

$$2\rho \frac{D^2}{\varepsilon} \frac{d^2u}{dx^2} \frac{du}{dx} - \rho u \frac{du}{dx} - \frac{\rho f}{2D} u^2 = 0. \tag{12}$$

It is obvious that these two methods give slightly different governing equations for u in terms of the geometry (L, D, H, ε) and the independent variable x. A very useful conclusion can be drawn at this early stage if we compare equations (9) and (12). These equations become identical if K_o in equation (9) is chosen as being equal to $2\rho D \frac{du}{dx}$. This suggests that K_o is not an absolute constant but dependent on the velocity gradient du/dx. However, it will be a constant if the variation of u in the direction of x is linear (not a constant). As it will be seen later, the flow rate through the channel has a significant effect on K_o.

2-1 Solution for the Equations of Motion

In the previous section we discussed the formulation of the equations of motion. Two different representations for the variation of the u component of velocity were obtained. We consider the detailed solution for the equation (9) which is rewritten as,

$$K_o \frac{D}{\varepsilon} \frac{d^2u}{dx^2} - \rho u \frac{du}{dx} - \frac{\rho f}{2D} u^2 = 0 \tag{9}$$

To keep the solution general, we have to render equation (9) and other related equations dimensionless. For achieving this we use the following scheme:

$$u = \frac{Q}{\rho DL} u^*$$

$$v = \frac{Q}{\rho LH\varepsilon} v^*$$

$$x = H Z$$

$$\frac{p_o - p}{K_o} = \frac{Q}{\rho LH\varepsilon} \Delta p^*$$

Here Q is the flow rate through the control volume and u^*, v^* and Δp^* are the dimensionless velocity components and pressure differences, respectively. The quantity Z represents the dimensionless x co-ordinate. All other quantities have been defined earlier.

On substituting these variables into equation (9), we obtain

$$\frac{d^2u^*}{dz^2} - \phi u^* \frac{du^*}{dz} - \phi F u^{*2} = 0 \tag{13}$$

The terms Φ and F are termed the flow and friction analogs respectively, and are defined as:

$$\phi = \frac{H Q}{K_o D^2 L} \varepsilon,$$

$$F = \frac{f}{2D} .$$

The nonlinear equation (13) is solved by means of the Crank-Nicholson method on a digital computer. (A detailed listing of the program is included in Appendix A.)

The flow domain is subdivided into equal intervals of length Δz between two subsequent stations i and i + 1 or i and i - 1. The solution for the differential equation is thus a set of finite values u_i ($i \to 1$, N) and $u_i \to u$ as $\Delta z \to 0$.

The derivatives $\frac{d^2u^*}{dz^2}$ and $\frac{du^*}{dz}$ of (13) are replaced by the following equations:

$$\frac{d^2u^*}{dz^2} = \frac{u_{i+1} - 2u_i + u_{i-1}}{\Delta z^2}$$

$$\frac{du^*}{dz} = \frac{u_{i+1} - u_{i-1}}{2\Delta z} \; . \tag{14}$$

The resulting algebraic equation, derived from equation (13) by substituting equation (14) into it, is linearized by an interlue scheme as

$$A_1\, u_{i-1}^{\nu} + A_2\, u_i^{\nu} + A_3\, u_{i+1}^{\nu} = D_n \tag{15}$$

where

$$A_1 = \frac{1}{\Delta z^2} + \frac{\phi\, u_i^{\nu-1}}{2\Delta z}$$

$$A_2 = \frac{-2}{\Delta z^2} - F\,\Phi\, u_i^{\nu-1}$$

$$A_3 = \frac{1}{\Delta z^2} \quad \frac{\Phi u_i^{\nu-1}}{2\Delta z} \; ,$$

where

$D_n = 0$

ν = no of iteration

ν-1 = previous iteration.

The boundary conditions are $u_1 = 0$ at $z = 1$ and $u_1 = 1.0$ at $z = 1.0$. The calculation is initiated by arbitrarily choosing values for all the u_i^ν ($\nu = 1$) and then calculating A_1, A_2 and A_3. Since the boundary condition at $u_N = 1$ is known, a back substitution is necessary for evaluating the u_{i-1}^ν from u_i^ν based on the previous iterant. The procedure is repeated until a residue (arbitrarily fixed) of 1×10^{-4} or less is attained for the corresponding improvement in the value for u_i for each progressing ν. Here we used $\Delta z = 10^{-2}$.

3. EXPERIMENTAL RESULTS

Experimental data with the modified manifold system with seven stopcocks were collected for 200 x 200 and 325 x 325 dutch twill screens using tap water. The volumetric flow rates were varied from 345 cc/sec to 65cc/sec. Three different depths of the channel, namely 3.5, 2.85 and 2.5 cm were used to collect the data for various flow rates. The pressure drops across the screen along the channel length at fourteen locations were measured by changing the manifold system only once.

Figures 3 to 8 present the data on pressure drop across the screen along the channel length as a function of dimensionless length z for various flow rates and channel depths of 3.5, 2.85 and 2.2 cm. Examination of figures 3 to 8 show the following characteristics of the pressure drop across the screen length.

1. The pressure along the channel length across the screen is dependent on the volumetric flow rates. At smaller flow rates the pressure drop between the two extreme ends of the channel length is small whereas at large flow rates the pressure drop between the two extreme ends of the channel length are largest. In otherwords, larger the flow rate, larger the pressure drop between the extreme ends of the channel length.

2. Pressure drop across is the screen along the channel length is also a function of the channel depth. At the smallest depth 2.2 cm, the pressure drop between the two extreme ends of the channel is large compared to the pressure drop observed between the extreme ends of the channel at larger channel depths of 2.85 and 3.5.

The experimental results obtained in the second phase of the program are an improvement over the data collected in the first phase of the program and are in general agreement with the conclusions drawn in the first phase of the program.

APPENDIX

Computer Program

Using Crank Nicolson type iteration:

$$\frac{d^2u}{dz^2} = \frac{u_{i+1} - 2\,u_i + u_{i-1}}{\Delta z^2}$$

$$\frac{du^*}{dz} = \frac{u_{i+1} - u_{i-1}}{2\Delta z}$$

The equation becomes

$$\frac{u_{i+1}^{\nu} - 2u_i^{\nu} + u_{i-1}^{\nu}}{\Delta t^2} - \Phi\, u_i^{\nu-1}\; \frac{u_{i+1}^{\nu} - u_{i-1}^{\nu}}{2\Delta t} - \Phi F\, u_i^{\nu}\, u_i^{\nu-1} = 0$$

Or,

$$A_1\, u_{i-1}^{\nu} + A_2\, u_i^{\nu} + A_3\, u_{i+1}^{\nu} = D_n$$ Computational Alogrithem

$$A_1 = \frac{1}{\Delta z^2} + \frac{\Phi u_i^{\nu-1}}{2\Delta z}$$

$$A_2 = -\frac{2}{\Delta z^2} - F\,\Phi u_i^{\nu-1}$$

$$A_3 = \frac{1}{\Delta z^2} - \frac{\Phi\, u_i^{\nu-1}}{2\Delta z}$$

$D_n = 0.0$

$\nu \rightarrow$ no. of iteration

$\nu\text{-}1 \rightarrow$ previous iteration

Iteration Residue = 1.0×10^{-4}

In the program $\Delta z = 1/100 = 0.01$

Then, $u = \dfrac{Qu^*}{\rho DL}$ $\quad v = \dfrac{Qv^*}{\rho LH\varepsilon}$ $\quad \dfrac{d\Delta p^*}{dz} = \dfrac{dv^*}{dz}$

Substituting these variables we get

$$V^* = \frac{du^*}{dz} = \Delta p^*$$

$$\frac{d^2u^*}{dz^2} - \Phi u^* \frac{du^*}{dz} - \Phi F\ u^{2*} = 0 \qquad (1)$$

$$\Phi = \frac{HQ}{K_o D^2 L}\ \varepsilon \qquad F = \frac{f}{2D}$$

From method 2 we obtain,

$$\frac{d^2u^*}{dz}\ \frac{du^*}{dz} - \Phi\ u^* \frac{du^*}{dz} - \Phi F\ u^{*2} = 0$$

$$\Phi = \frac{\varepsilon H^3}{2D^2} \qquad F = \frac{f}{2D}$$

$$v^* = \frac{du^*}{dz} \qquad (2)$$

$$\Delta p^* = \frac{(p_o - p)}{Q^2}\ \rho\ L^2\ H^2\ \varepsilon = v^{*2} = \frac{du^*}{dz}^{\,2}$$

If model (2) of the analysis is adopted, we can estimate K_o from the following equations,

$$K_o = 2\rho D\ \frac{du}{dx} = \frac{2\rho D}{H}\ \frac{Q}{\rho DL}\ \frac{du^*}{dz} = \frac{2Q}{LH}\ \frac{du^*}{dz}$$

For a given q, Φ can be evaluated from

$\Phi\ \dfrac{\varepsilon H^3}{2D^2}$ for that Φ and some constant f the corresponding

$\frac{du}{dz}$, or simply Δp^*, can be read from the graph and therefore K_o can be computed theoretically. This can be compared with the value obtained from earlier type of calculation.

Hence to compare Δp^* from the program (Equation 1) (1) calculate $z = \frac{x}{H}$ for each tap location. Then $\tilde{\Delta p}^* = \frac{p_o - p}{K_o} \left(\frac{\rho L H \varepsilon}{Q}\right)$, K_o is experimentally determined.

Method 2 Procedure

The equations are

$$\frac{d^2u^*}{dz^2}\,\frac{du^*}{dz} - \Phi\, u^* \frac{du^*}{dz} - \Phi F\, u^{*2} = 0$$

$$F = \frac{f}{2D} \qquad \Phi = \frac{\varepsilon H^3}{2D^2}$$

Here u^* is independent of Q for a constant 'f'.

In turbulent flow, 'f' remains constant. Therefore for high flow rates a channel of given dimensions have a unique flow distribution. However, Δp^* will be different since, Δp^* does involve Q in calculations.

$$\Delta p^* = \frac{p_o - p}{Q^2}\ \rho L^2 H^2 \varepsilon$$

Figures 9, 10, 11 and 12 show the variation of u^* and Δp^* along z the non-dimensional variables for two sets of f and ϕ. Their effect is obvious as only the extreme values are chosen. Also plots for Δp^* at $z = 0$ and $z = 1$ into f as the parameter are plotted with respect to the flow analog ϕ. The effect of increasing f is opposite on Δp^* at these two locations.

Experimental Verification

Since only the pressure is measured the most useful graph would be that shows the variation of $(p_o - p) \leftarrow$ the dimensionless measured difference on the manometer taps.

Procedure

(1) Calculate K_o as follows:

$$K_o = \frac{(p_o - p)}{\Delta p^*} \left(\frac{\rho L H \varepsilon}{Q}\right)$$

here $(p_o - p) \leftarrow$ measured pressure drop

$\Delta p^* \leftarrow$ calculated from computer program on read off the graph.

ρ, L, H, ε, Q are parameters known.

(2) Hence, for a given screen ε and flow rate Q, K_o can be found.

Also

$$K_o V = p_o - p$$

or

$$V = \frac{p_o - p}{K_o}$$

Therefore V can be calculated.

Validity of the analysis can be established as follows:

(a) For small ϕ and f, u^* V_s z is a st. line

$u \quad \frac{du^*}{dz}$ = slope is constant, or $\frac{du}{dx}$ is constant,

$$V = \frac{D}{\varepsilon}\frac{du}{dx}$$ = constant from above. Hence for a series of Q's small but slightly different each other the test for the constant of v proves that the analysis is good for that range. It should start deviating after some Q because du^*/dz is not linear θ eq. at $\phi = 10.1$, $f = 0.6$ as shown by the figures.

(3) These calculations should reveal the nature of K_o variation.

(4) If model (2) of the analysis is adopted, we can estimate K_o from the following equations:

$$K_o = 2\rho D \frac{du}{dx} = \frac{2\rho D}{H} \frac{Q}{\rho DL} \frac{du^*}{dz} = \frac{2Q}{LH} \frac{du^*}{dz} .$$

For a given Q, ϕ can be evaluated from $\phi = \frac{\varepsilon H^3}{2D^2}$ for that ϕ and some constant f the corresponding $\frac{du^*}{dz}$ or simply Δp^* can be read and therefore K_o can be computed theoretically and compared with the value obtained from earlier types of calculations.

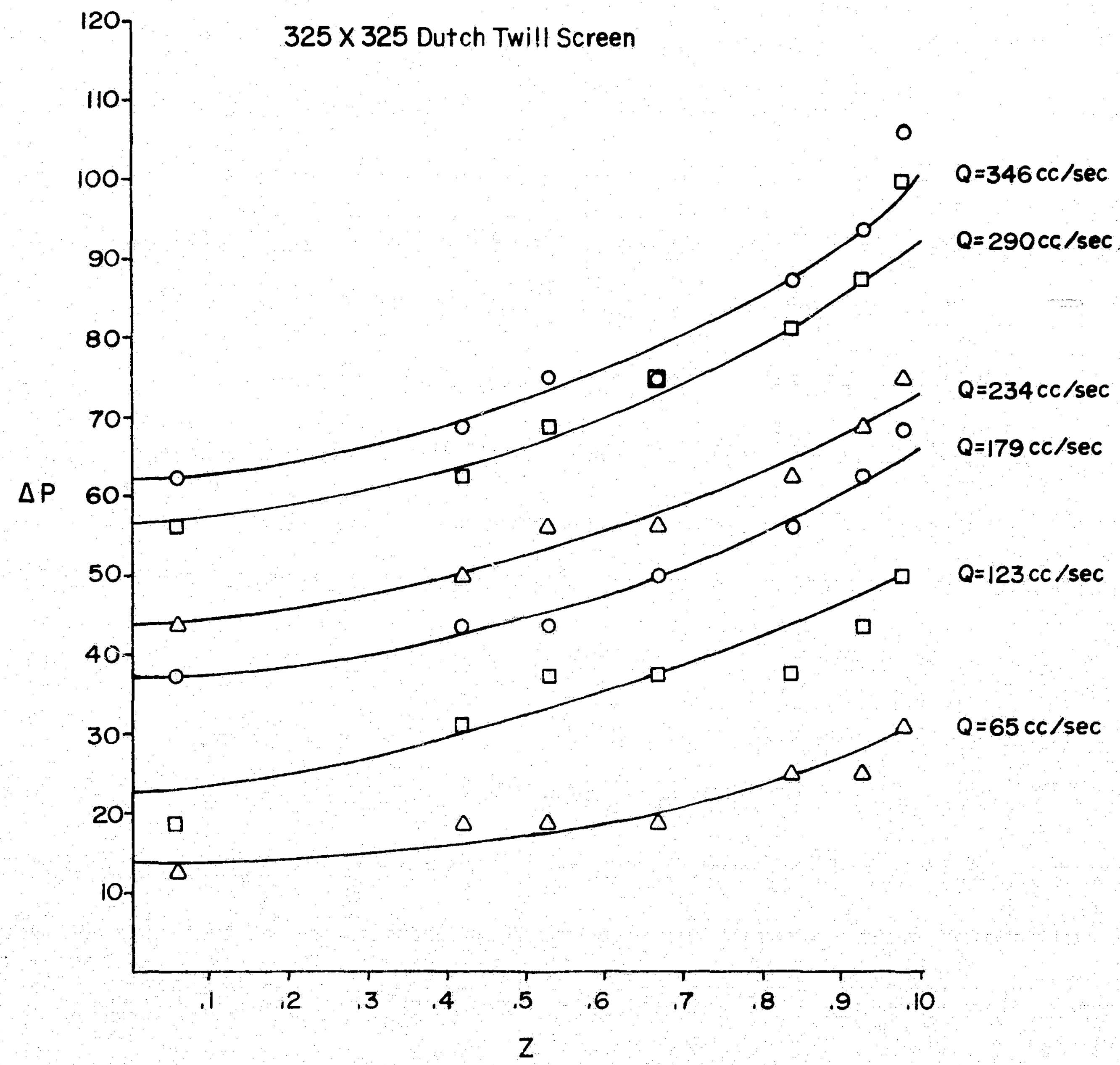

325 X 325 Dutch Twill Screen
120
110
100
90
80
70
ΔP
60
50
40
30
20
10
.1
.2
.3
.4
.5
.6
.7
.8
.9
.10
Z
Q=346 cc/sec
Q=290 cc/sec
Q=234 cc/sec
Q=179 cc/sec
Q=123 cc/sec
Q=65 cc/sec

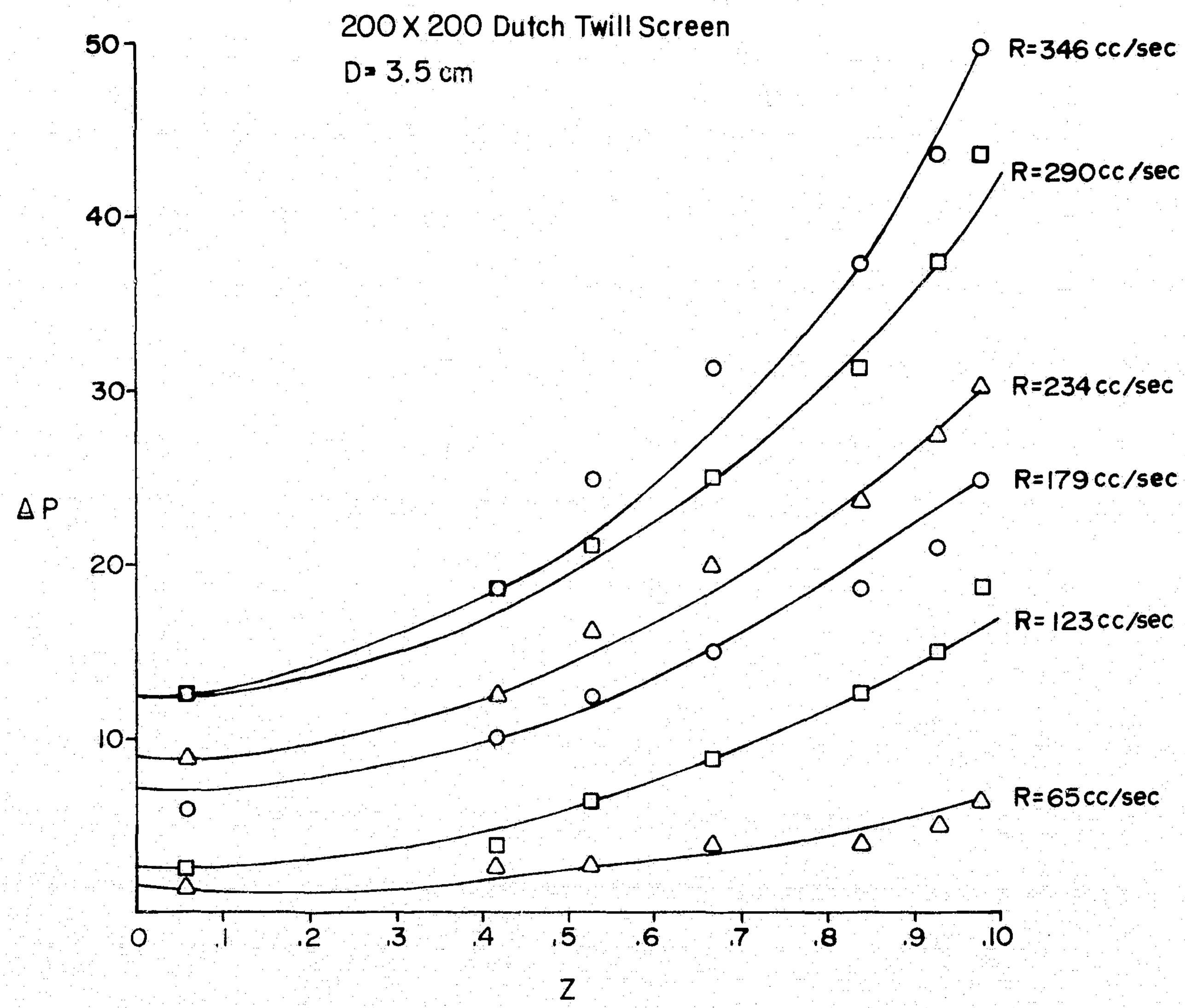
200 X 200 Dutch Twill Screen
D= 3.5 cm
R=346 cc/sec
R=290cc/sec
R=234 cc/sec
R=179 cc/sec
R= 123 cc/sec
R=65 cc/sec
ΔP
50
40
30
20
10
0
.1
.2
.3
.4
.5
.6
.7
.8
.9
.10
Z

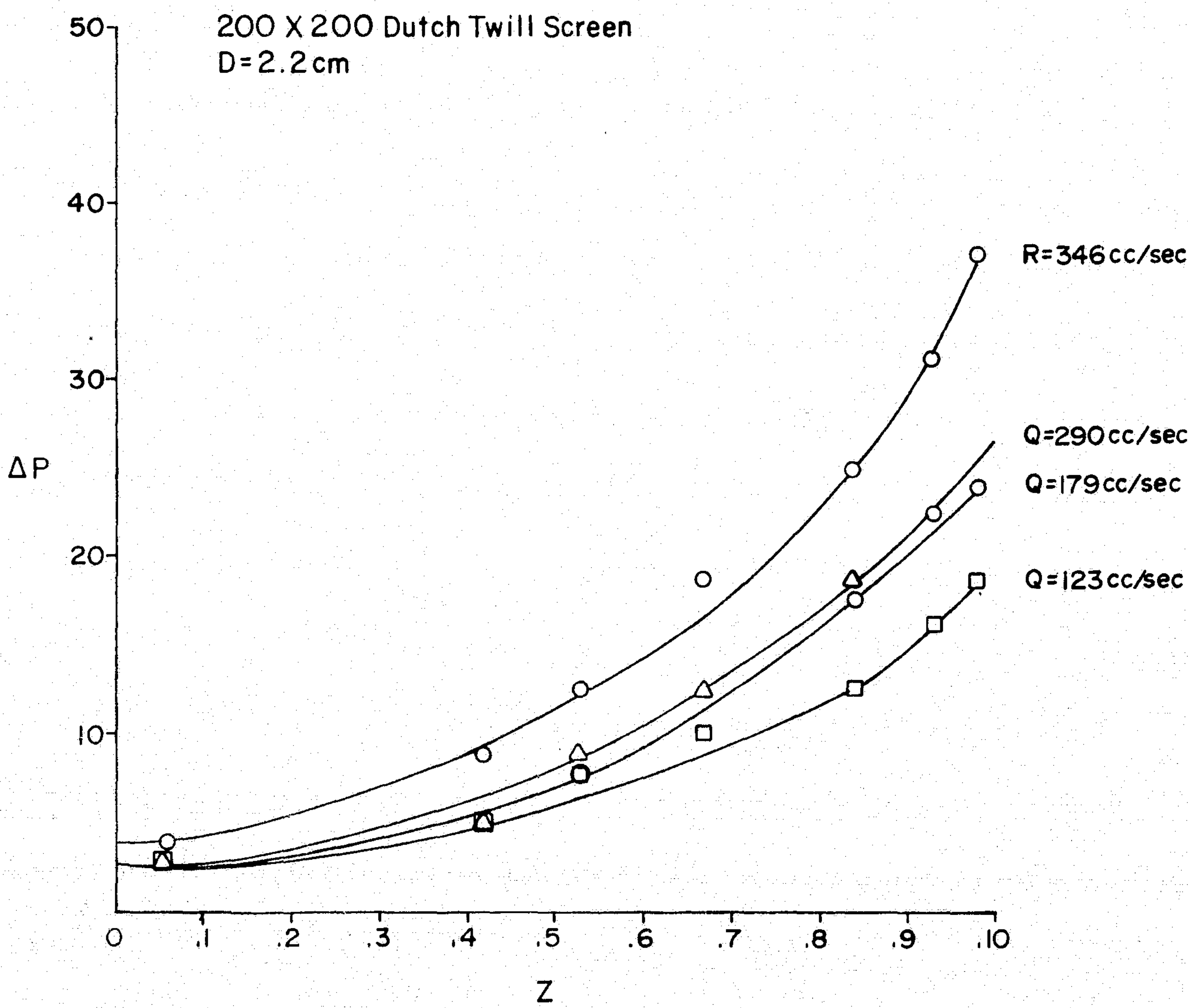
200 X 200 Dutch Twill Screen
D=2.2cm
R=346cc/sec
Q=290cc/sec
Q=179cc/sec
Q=123cc/sec
ΔP
Z
50
40
30
20
10
0
.1
.2
.3
.4
.5
.6
.7
.8
.9
.10

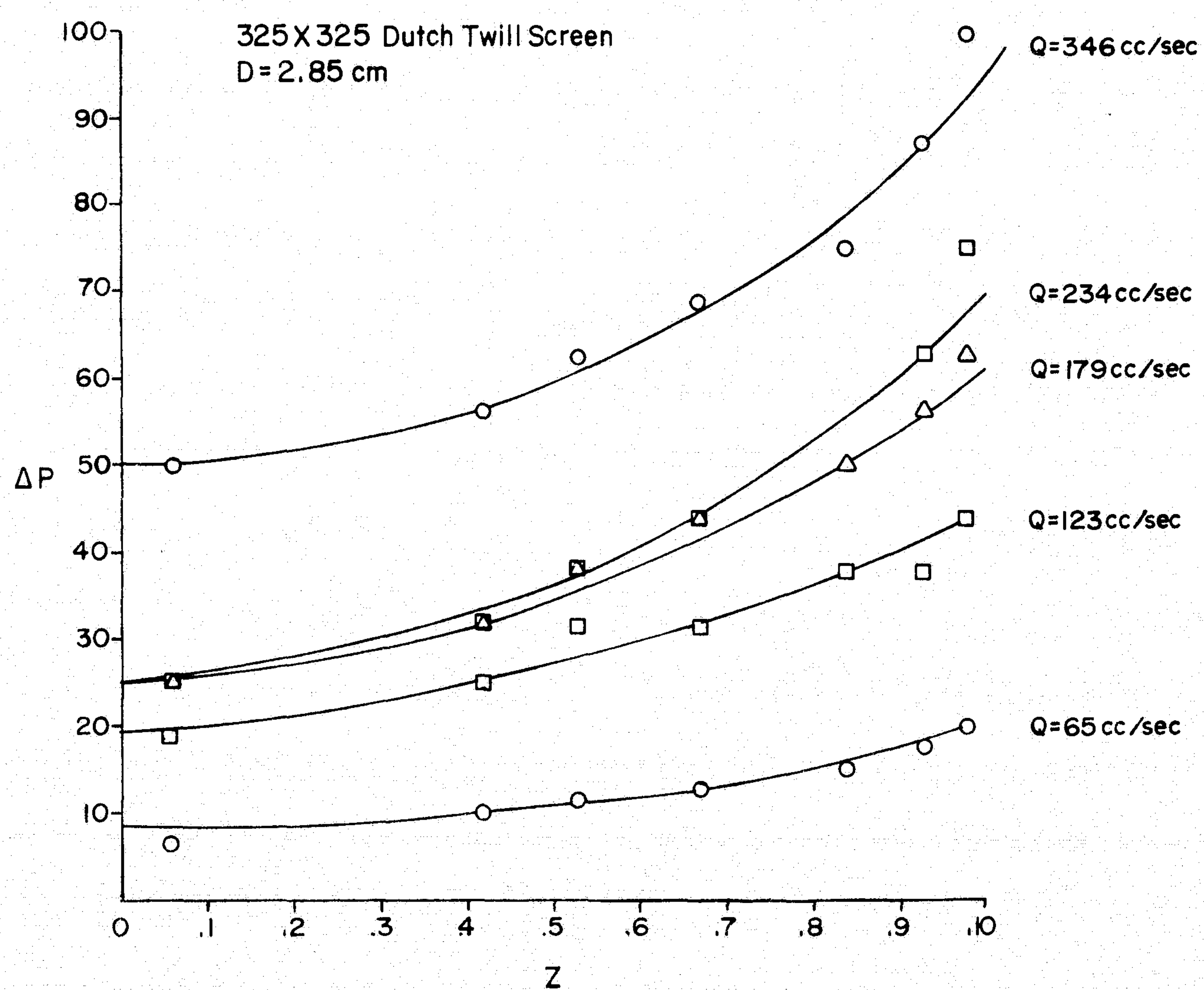

325 X 325 Dutch Twill Screen
D = 2.85 cm
Q=346 cc/sec
Q=234 cc/sec
Q=179 cc/sec
Q=123 cc/sec
Q=65 cc/sec
ΔP
Z
100
90
80
70
60
50
40
30
20
10
0
.1
.2
.3
.4
.5
.6
.7
.8
.9
.10

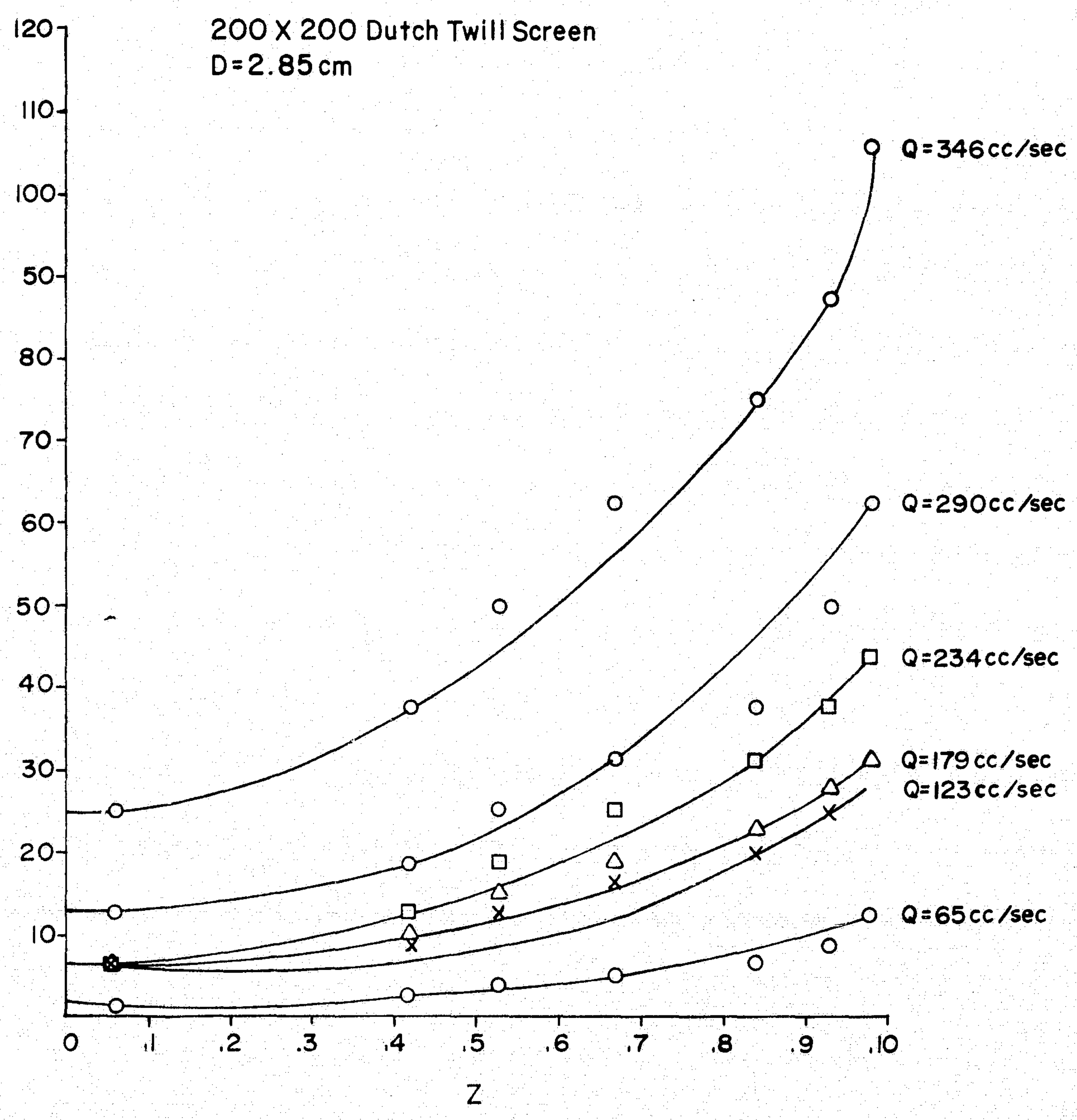
200 X 200 Dutch Twill Screen
D=2.85 cm
120
110
100
50
80
70
60
50
40
30
20
10
0
.1
.2
.3
.4
.5
.6
.7
.8
.9
.10
Z
Q=346 cc/sec
Q=290 cc/sec
Q=234 cc/sec
Q=179 cc/sec
Q=123 cc/sec
Q=65 cc/sec

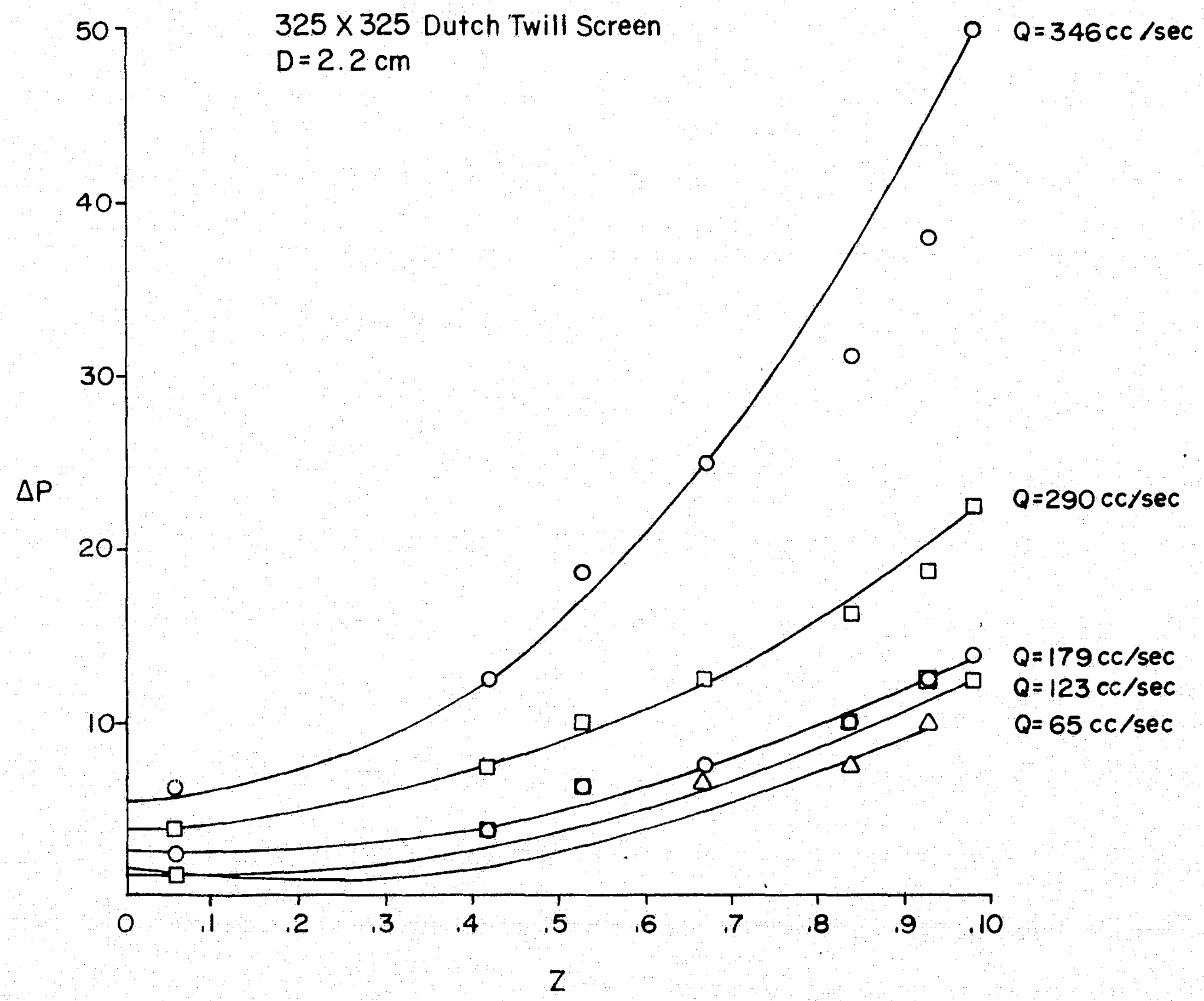
325 X 325 Dutch Twill Screen
D=2.2 cm
Q=346 cc/sec
Q=290 cc/sec
Q=179 cc/sec
Q=123 cc/sec
Q=65 cc/sec
ΔP
Z
50
40
30
20
10
0
.1
.2
.3
.4
.5
.6
.7
.8
.9
.10

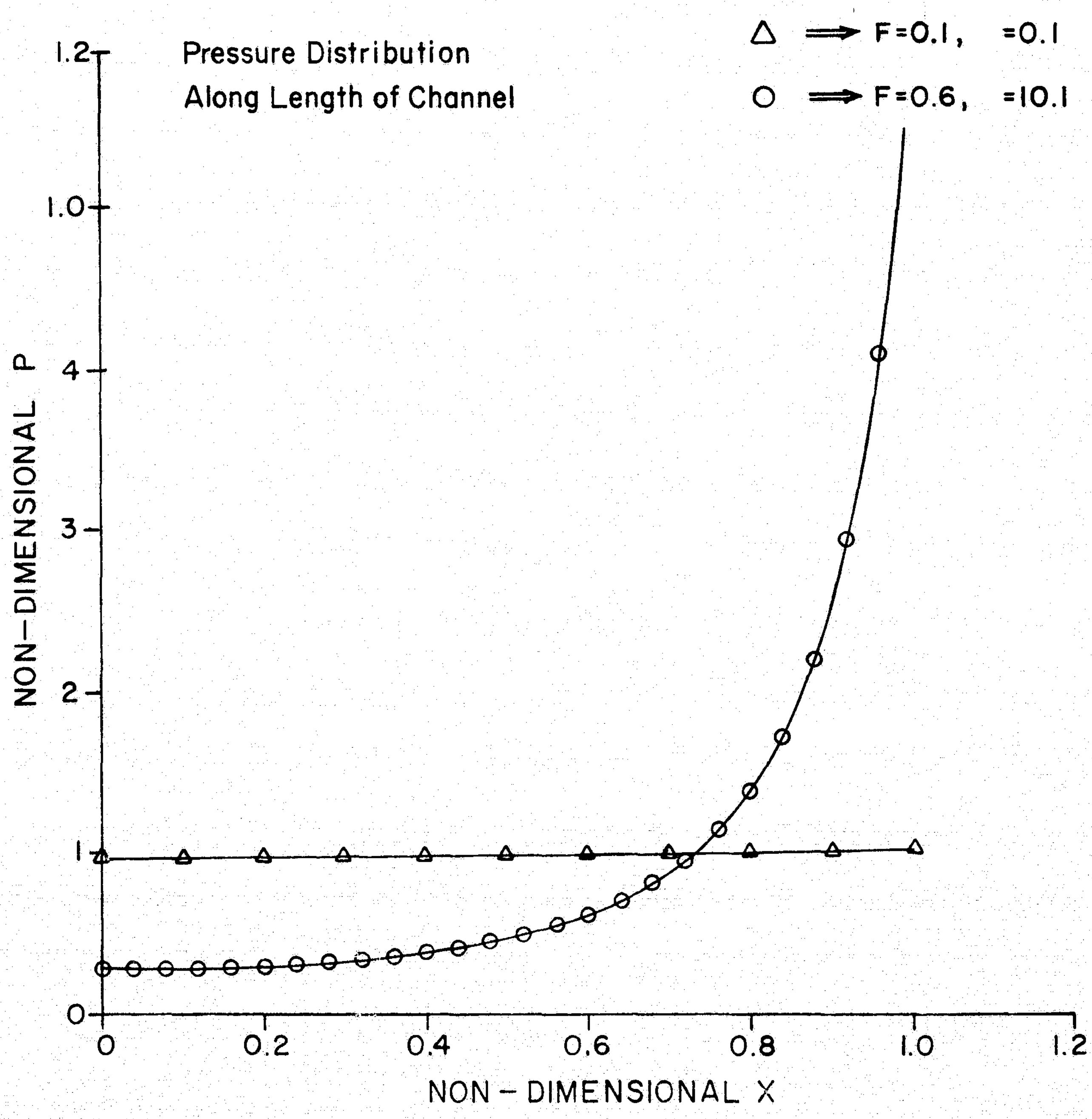
Pressure Distribution
Along Length of Channel
△ ⟹ F=0.1, =0.1
○ ⟹ F=0.6, =10.1
NON-DIMENSIONAL P
NON - DIMENSIONAL X
0
1
2
3
4
1.0
1.2
0
0.2
0.4
0.6
0.8
1.0
1.2

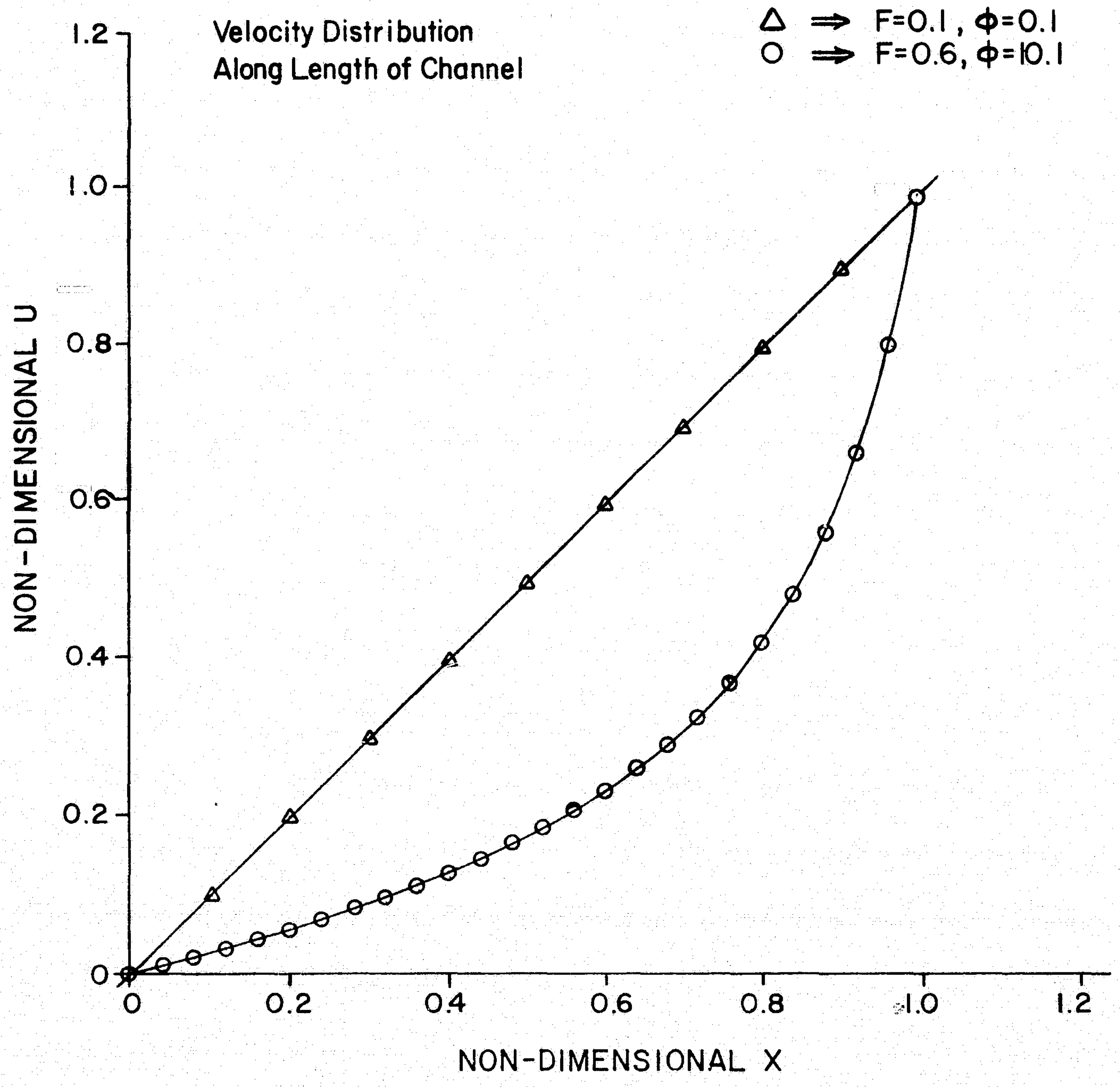
1.2
1.0
0.8
0.6
0.4
0.2
0
Velocity Distribution
Along Length of Channel
Δ ⇒ F=0.1 , Φ=0.1
O ⇒ F=0.6, Φ=10.1
NON-DIMENSIONAL U
0
0.2
0.4
0.6
0.8
1.0
1.2
NON-DIMENSIONAL X

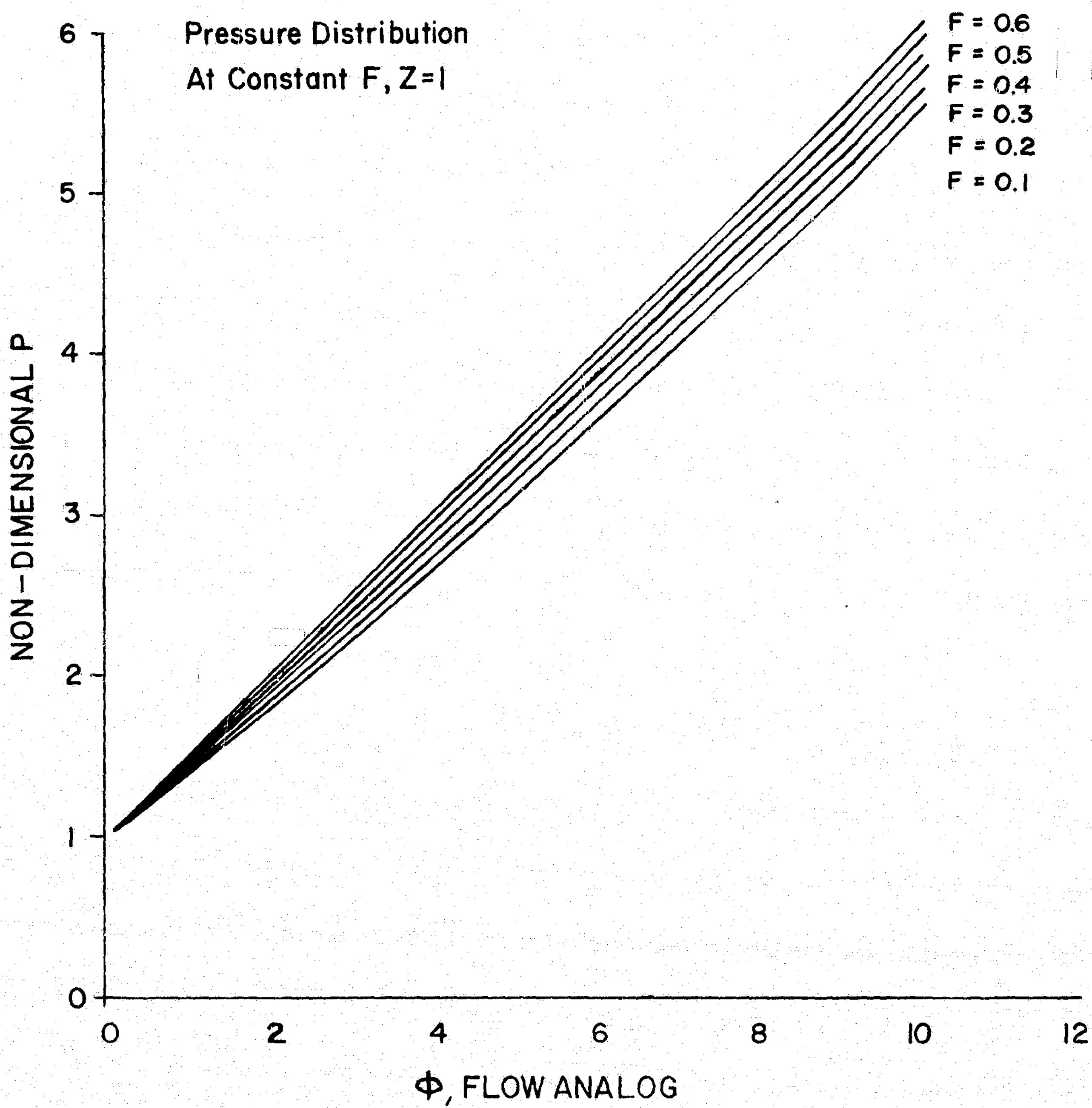

Pressure Distribution
At Constant F, Z=1
F = 0.6
F = 0.5
F = 0.4
F = 0.3
F = 0.2
F = 0.1
NON-DIMENSIONAL P
Φ, FLOW ANALOG
0
1
2
3
4
5
6
0
2
4
6
8
10
12

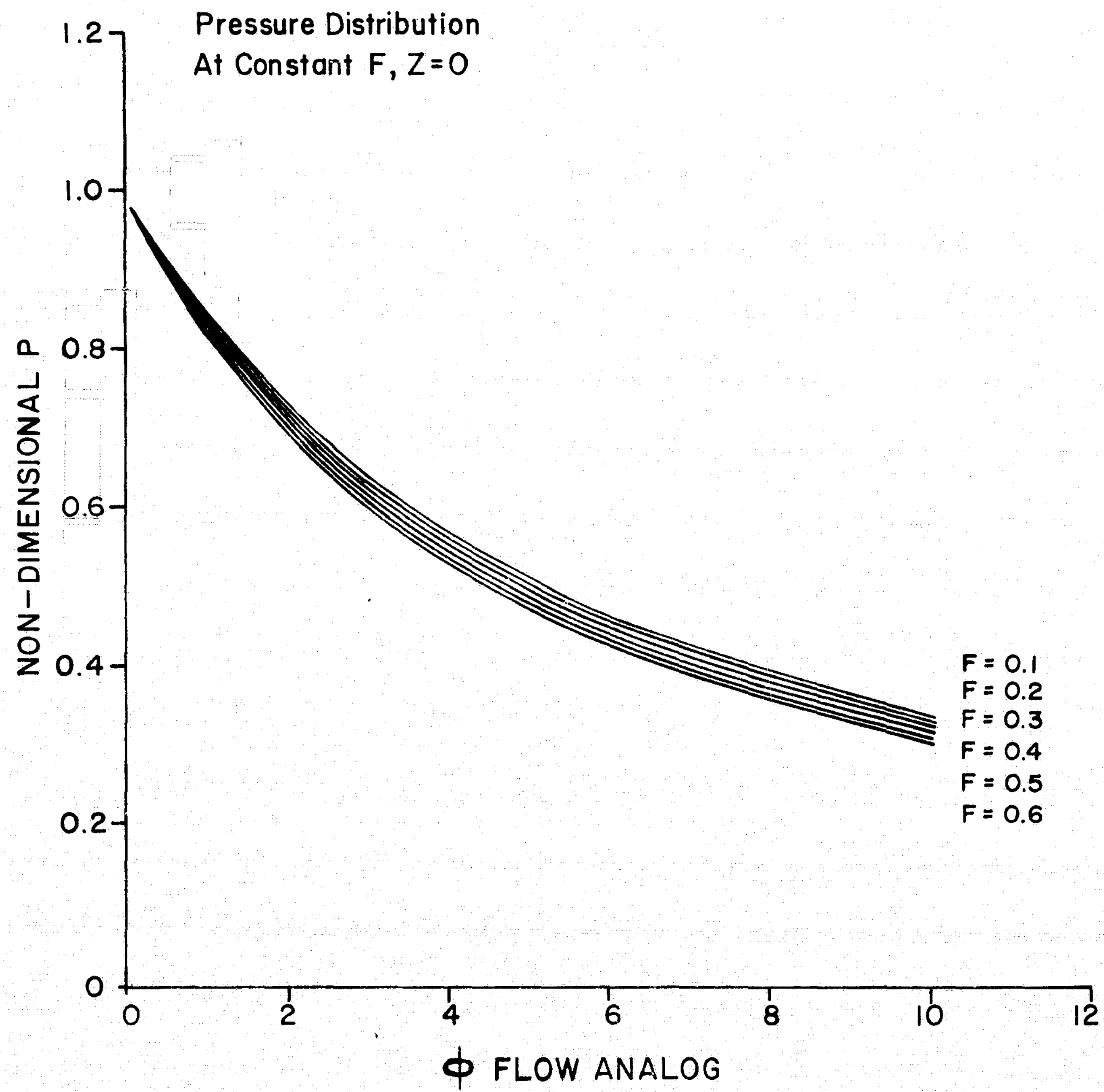
Pressure Distribution
At Constant F, Z=0
NON-DIMENSIONAL P
1.2
1.0
0.8
0.6
0.4
0.2
0
2
4
6
8
10
12
F = 0.1
F = 0.2
F = 0.3
F = 0.4
F = 0.5
F = 0.6
Φ FLOW ANALOG